THE EUROPEAN
PHYSICAL JOURNAL C

CrossMark

A search for new phenomena in pp collisions at $\sqrt{s} = 13$ TeV in final states with missing transverse momentum and at least one jet using the α_T variable

CMS Collaboration*

CERN, 1211 Geneva 23, Switzerland

Abstract A search for new phenomena is performed in final states containing one or more jets and an imbalance in transverse momentum in pp collisions at a centre-of-mass energy of 13 TeV. The analysed data sample, recorded with the CMS detector at the CERN LHC, corresponds to an integrated luminosity of 2.3 fb^{-1}. Several kinematic variables are employed to suppress the dominant background, multijet production, as well as to discriminate between other standard model and new physics processes. The search provides sensitivity to a broad range of new-physics models that yield a stable weakly interacting massive particle. The number of observed candidate events is found to agree with the expected contributions from standard model processes, and the result is interpreted in the mass parameter space of fourteen simplified supersymmetric models that assume the pair production of gluinos or squarks and a range of decay modes. For models that assume gluino pair production, masses up to 1575 and 975 GeV are excluded for gluinos and neutralinos, respectively. For models involving the pair production of top squarks and compressed mass spectra, top squark masses up to 400 GeV are excluded.

1 Introduction

The standard model (SM) of particle physics is successful in describing a wide range of phenomena, although it is widely believed to be only an effective approximation of a more complete theory that supersedes it at a higher energy scale. Supersymmetry (SUSY) [1–4] is a modification to the SM that extends its underlying space-time symmetry group. For each boson (fermion) in the SM, a fermionic (bosonic) superpartner, which differs in spin by one-half unit, is introduced.

Experimentally, SUSY is testable through the prediction of an extensive array of new observable states (of unknown masses) [5,6]. In the minimal supersymmetric extension to the SM [6], the gluinos $\widetilde{g}$, light- and heavy-flavour squarks $\widetilde{q}$, $\widetilde{b}$, $\widetilde{t}$, and sleptons $\widetilde{\ell}$ are, respectively, the superpartners to gluons, quarks, and leptons. An extended Higgs sector is also predicted, as well as four neutralino $\widetilde{\chi}^0_{1,2,3,4}$ and two chargino $\widetilde{\chi}^\pm_{1,2}$ states that arise from mixing between the higgsino and gaugino states, which are the superpartners of the Higgs and electroweak gauge bosons. The assumption of R-parity conservation [7] has important consequences for cosmology and collider phenomenology. Supersymmetric particles are expected to be produced in pairs at the LHC, with heavy coloured states decaying, potentially via intermediate SUSY states, to the stable lightest SUSY particle (LSP). The LSP is generally assumed to be the $\widetilde{\chi}^0_1$, which is weakly interacting and massive. This SUSY particle is considered to be a candidate for dark matter (DM) [8], the existence of which is supported by astrophysical data [9]. Hence, a characteristic signature of R-parity-conserving coloured SUSY production at the LHC is a final state containing an abundance of jets, possibly originating from top or bottom quarks, accompanied by a significant transverse momentum imbalance, $\vec{p}_\mathrm{T}^{\text{miss}}$.

The proposed supersymmetric extension of the SM is also compelling from a theoretical perspective, as the addition of superpartners to SM particles can modify the running of the gauge coupling constants such that their unification can be achieved at a high energy scale [10–12]. A more topical perspective, given the recently discovered Higgs boson [13–15], is the possibility that scale-dependent radiative corrections to the Higgs boson mass from loop processes can be largely cancelled through the introduction of superpartners, thus alleviating the gauge hierarchy problem [16,17]. Alternatively, these radiative corrections can be accommodated through an extreme level of fine tuning of the bare Higgs boson mass. A "natural" solution from SUSY, with minimal fine-tuning, implies that the masses of the $\widetilde{\chi}^0_1$, third-generation squarks, and the gluino are at or near the electroweak scale [18].

The lack of evidence to date for SUSY has also focused attention on regions of the natural parameter space with

* e-mail: cms-publication-committee-chair@cern.ch

Springer

sparse experimental coverage, such as phenomenologically well motivated models for which both the $\widetilde{t}$ and the $\widetilde{\chi}_1^0$ are light and nearly degenerate in mass [19–27]. This class of models, with "compressed" mass spectra, typically yield SM particles with low transverse momenta (p_T) from the decays of SUSY particles. Hence, searches rely on the associated production of jets, often resulting from initial-state radiation (ISR), to achieve experimental acceptance.

This paper presents an inclusive search for new-physics phenomena in hadronic final states with one or more energetic jets and an imbalance in $\vec{p}_T^{\,\text{miss}}$, performed in proton–proton (pp) collisions at a centre-of-mass energy $\sqrt{s} = 13$ TeV. The analysed data sample corresponds to an integrated luminosity of $2.3 \pm 0.1\,\text{fb}^{-1}$ collected by the CMS experiment. Earlier searches using the same technique have been performed in pp collisions at both $\sqrt{s} = 7$ [28–30] and 8 TeV [31,32] by the CMS Collaboration. The increase in the centre-of-mass energy of the LHC, from $\sqrt{s} = 8$ to 13 TeV, provides a unique opportunity to search for the characteristic signatures of new physics at the TeV scale. For example, the increase in $\sqrt{s}$ leads to a factor $\gtrsim 35$ increase in the parton luminosity [33] for the pair production of coloured SUSY particles, each of mass 1.5 TeV, which were beyond the reach of searches performed at $\sqrt{s} = 8$ TeV by the ATLAS [34,35] (and references therein) and CMS [36–43] Collaborations. Several searches in this final state, interpreted within the context of SUSY, have already provided results with the first data at this new energy frontier [44–50].

Two important features of this search are the application of selection criteria with low thresholds, in order to maximise signal acceptance, and the categorisation of candidate signal events according to multiple discriminating variables for optimal signal extraction over a broad range of models. The search is based on an examination of the number of reconstructed jets per event, the number of these jets identified as originating from bottom quarks, and the scalar and vector p_T sums of these jets. These variables provide sensitivity to the different production mechanisms (squark–squark, squark–gluino, and gluino–gluino) of massive coloured SUSY particles at hadron colliders, third-generation squark signatures, and both large and small mass splittings between the parent SUSY particle and the LSP. However, the search is sufficiently generic and inclusive to provide sensitivity to a wide range of SUSY and non-SUSY models that postulate the existence of a stable, only weakly interacting, massive particle. In addition to the jets+$\vec{p}_T^{\,\text{miss}}$ topology, the search considers final states containing a "monojet" topology, which is expected to improve the sensitivity to DM particle production in pp collisions [51,52].

The dominant background process for a search in all-jet final states is multijet production, a manifestation of quantum chromodynamics (QCD). An accurate estimate of this background is difficult to achieve, given the lack of precise

theoretical predictions for the multijet production cross section and kinematic properties. Hence, this search adopts a strategy that employs several variables to reduce the multijet contribution to a low level with respect to other SM backgrounds, rather than estimate a significant contribution with high precision.

The search is built around two variables that are designed to provide robust discrimination against multijet events. A dimensionless kinematic variable α_T [28,53] is constructed from jet-based quantities and provides discrimination between genuine sources of $\vec{p}_T^{\,\text{miss}}$ from stable, weakly interacting particles such as neutrinos or neutralinos that escape the detector, and instrumental sources such as the mismeasurements of jet energies. The $\Delta\phi_{\min}^*$ [28] variable exploits azimuthal angular information and also provides strong rejection power against multijet events, including rare energetic events in which neutrinos carry a significant fraction of the energy of a jet due to semileptonic decays of heavy-flavour mesons. Very restrictive requirements on the α_T and $\Delta\phi_{\min}^*$ variables are employed in this search to ensure a low level of contamination from the multijet background.

The organisation of this paper is as follows. Sections 2 and 3 describe, respectively, the CMS apparatus and the simulated event samples. Sections 4 and 5 describe the event reconstruction and selection criteria used to identify candidate signal events and control region samples. Section 6 provides details on the estimation of the multijet and all other SM backgrounds. Finally, the search results and interpretations, in terms of simplified SUSY models, are described in Sects. 7 and 8, and summarised in Sect. 9.

2 The CMS detector

The central feature of the CMS apparatus is a superconducting solenoid of 6 m internal diameter, providing an axial magnetic field of 3.8 T. The bore of the solenoid is instrumented with several particle detection systems. A silicon pixel and strip tracker measures charged particles within the pseudorapidity range $|\eta| < 2.5$. A lead tungstate crystal electromagnetic calorimeter (ECAL), and a brass and scintillator hadron calorimeter (HCAL), each composed of a barrel and two endcap sections, extend over a range $|\eta| < 3.0$. Outside the bore of the solenoid, forward calorimeters extend the coverage to $|\eta| < 5.0$, and muons are measured within $|\eta| < 2.4$ by gasionisation detectors embedded in the steel flux-return yoke outside the solenoid. A two-tier trigger system selects pp collision events of interest. The first level of the trigger system, composed of custom hardware processors, uses information from the calorimeters and muon detectors to select the most interesting events in a fixed time interval of less than 4 μs. The high-level trigger processor farm further decreases the event rate from around 100 kHz to less than 1 kHz, before

data storage. The CMS detector is nearly hermetic, which allows for momentum balance measurements in the plane transverse to the beam axis. A more detailed description of the CMS detector, together with a definition of the coordinate system used and the relevant kinematic variables, can be found in Ref. [54].

3 Simulated event samples

The search relies on multiple event samples, in data or generated from Monte Carlo (MC) simulations, to estimate the contributions from SM backgrounds, as described in Sect. 5. The SM backgrounds for the search are QCD multijet, top quark-antiquark ($t\bar{t}$), and single top production, and the associated production of jets and a vector boson (W, $Z \rightarrow \nu\bar{\nu}$). Residual contributions from other processes, such as WW, WZ, ZZ (diboson) production and the associated production of $t\bar{t}$ and a W or Z boson, are also considered. Other processes, such as Drell–Yan ($q\bar{q} \rightarrow Z/\gamma^* \rightarrow \ell^+\ell^-$) and γ + jets production, are also relevant for some control regions, defined in Sect. 5.5.

The MADGRAPH5_aMC@NLO 2.2.2 [55] event generator code is used at leading-order (LO) accuracy to produce samples of W + jets, Z + jets, γ + jets, $t\bar{t}$, and multijet events. The same code is used at next-to-leading-order (NLO) accuracy to generate samples of single top quarks (both s- and t-channel production), WZ, ZZ, $t\bar{t}$W, and $t\bar{t}$Z events. The NLO POWHEG v2 [56,57] generator is used to describe WW events and the tW-channel production of single top quark events. The simulated samples are normalised according to production cross sections that are calculated with NLO and next-to-NLO precision [55,57–62], or with LO precision in the case of multijet and γ + jets production. The GEANT4 [63] package is used to simulate the detector response.

Event samples for signal models involving gluino or squark pair production in association with up to two additional partons are generated at LO with MADGRAPH5_aMC@NLO, and the decay of the SUSY particles is performed with PYTHIA 8.205 [64]. Inclusive, process-dependent, signal production cross sections are calculated with NLO plus next-to-leading-logarithmic (NLL) accuracy [33,65–69]. The theoretical systematic uncertainties are typically dominated by the parton density function (PDF) uncertainties, evaluated using the CTEQ6.6 [70] and MSTW2008 [71] PDFs. The detector response for signal models is provided by the CMS fast simulation package [72].

The NNPDF3.0 LO and NLO [73] parton distribution functions (PDFs) are used, respectively, with the LO and NLO generators described above. The PYTHIA program with the CUETP8M1 underlying event tune [74] is used to describe parton showering and hadronisation for all simulated samples. To model the effects of multiple pp collisions within the same or neighbouring bunch crossings (pileup), all simulated events are generated with a nominal distribution of pp interactions per bunch crossing and then reweighted to match the pileup distribution as measured in data. On average, approximately fifteen different pp collisions, identifiable via their primary interaction vertex, are reconstructed per event. Finally, (near-unity) corrections to the normalisation of the simulated samples for the γ + jets, W($\rightarrow \mu\nu$)+jets, $t\bar{t}$, Z($\rightarrow \mu\mu$) + jets, and Z($\rightarrow \nu\bar{\nu}$) + jets processes are derived using data sidebands to the control regions.

4 Event reconstruction

Global event reconstruction is provided by the particle flow (PF) algorithm [75,76], designed to identify each particle using an optimised combination of information from all detector systems. In this process, the identification of the particle type (photon, electron, muon, charged hadron, neutral hadron) plays an important role in the determination of the particle direction and energy.

Among the vertices reconstructed within 24 (2) cm of the detector centre parallel (perpendicular) to the beam axis, the primary vertex (PV) is assigned to be the one with the largest sum of charged particle (track) p_T^2 values. Charged-particle tracks associated with reconstructed vertices from pileup events are not considered by the PF algorithm as part of the global event reconstruction.

Photon candidates [77] are identified as ECAL energy clusters not linked to the extrapolation of any track to the ECAL. The energy of photons is directly obtained from the ECAL measurement, corrected for contributions from pileup events. Various quality-related criteria must be satisfied in order to identify photons with high efficiency while minimising the misidentification of electrons and associated bremsstrahlung, jets, or ECAL noise as photons. The criteria include the following: the shower shape of the energy deposition in the ECAL must be consistent with that expected from a photon, the energy detected in the HCAL behind the photon shower must not exceed 5% of the photon energy, and no matched hits in the pixel tracker must be found.

Electron candidates [78] are identified as a track associated with an ECAL cluster compatible with the track trajectory, as well as additional ECAL energy clusters from potential bremsstrahlung photons emitted as the electron traverses material of the silicon tracker. The energy of electrons is determined from a combination of the track momentum at the main interaction vertex, the corresponding ECAL cluster energy, and the energy sum of all bremsstrahlung photons associated with the track. The quality criteria required for electrons are similar to those for photons, with regards to the ECAL shower shape and the relative contributions to the total energy deposited in the ECAL and HCAL. Additional

requirements are also made on the associated track, which consider the track quality, energy-momentum matching, and compatibility with the PV in terms of the transverse and longitudinal impact parameters.

Muon candidates [79] are identified as a track in the silicon tracker consistent with either a track or several hits in the muon system. The track and hit parameters must satisfy various quality-related criteria, described in Ref. [79]. The energy of muons is obtained from the corresponding track momentum.

Charged hadrons are identified as tracks not classified as either electrons or muons. The energy of charged hadrons is determined from a combination of the track momentum and the corresponding ECAL and HCAL energies, corrected for contributions from pileup events and the response function of the calorimeters to hadronic showers. Neutral hadrons are identified as HCAL energy clusters not linked to any charged-hadron trajectory, or as ECAL and HCAL energy excesses with respect to the expected charged-hadron energy deposit. The energy of neutral hadrons is obtained from the corresponding corrected ECAL and HCAL energy.

Photons are required to be isolated from other activity in the event, such as charged and neutral hadrons, within a cone $\Delta R = \sqrt{(\Delta\phi)^2 + (\Delta\eta)^2} = 0.3$ around the photon trajectory, corrected for contributions from pileup events and the photon itself. Electrons and muons are also required to be isolated from other reconstructed particles in the event, primarily to suppress background contributions from semileptonic heavy-flavour decays in multijet events. The isolation I_{rel}^{mini} is defined as the scalar p_T sum of all charged and neutral hadrons, and photons, within a cone around the lepton direction, divided by the lepton p_T. The "mini" cone radius is dependent on the lepton p_T, primarily to identify with high efficiency the collimated daughter particles of semileptonically decaying Lorentz-boosted top quarks, according to the following: $R = 0.2$ and 0.05 for, respectively, $p_T < 50$ GeV and $p_T > 200$ GeV, and $R = 10$ GeV$/p_T$ for $50 < p_T < 200$ GeV. The variable I_{rel}^{mini} excludes contributions from the lepton itself and pileup events. The isolation for electrons and muons is required to satisfy, respectively, $I_{rel}^{mini} < 0.1$ and 0.2 for the signal region and nonleptonic control sample selection criteria. A tighter definition of muon isolation I_{rel}^{μ} is used for the definition of control regions that are required to contain at least one muon. The variable I_{rel}^{μ} is determined identically to I_{rel}^{mini} except that a cone of fixed radius $R = 0.4$ is assumed.

Electron and muon candidates identified by the PF algorithm that do not satisfy the quality criteria or the I_{rel}^{mini} isolation requirements described above, as well as charged hadrons, are collectively labelled as "single isolated tracks" if they are isolated from neighbouring tracks associated to the PV. The isolation I_{rel}^{track} is defined as the scalar p_T sum of tracks (excluding the track under consideration) within a cone $\Delta R < 0.3$ around the track direction, divided by the track p_T. The requirement $I_{rel}^{track} < 0.1$ is imposed.

Jets are clustered from the PF candidate particles with the infrared- and collinear-safe anti-k_t algorithm [80], operated with a distance parameter of 0.4. The jet momentum is determined as the vectorial sum of all particle momenta in the jet, and is found in the simulation to be within 5–10% of its true momentum over the whole p_T spectrum and detector acceptance. Jet energy corrections, to account for pileup [81] and to establish a uniform relative response in η and a calibrated absolute response in p_T, are derived from the simulation, and are confirmed with in situ measurements using the energy balance in dijet and photon+jet events [82]. The jet energy resolution is typically 15% at 10 GeV, 8% at 100 GeV, and 4% at 1 TeV, compared to about 40, 12, and 5% obtained when the calorimeters alone are used for jet clustering. All jets are required to satisfy loose requirements on the relative composition of their particle constituents to reject noise in the calorimeter systems or failures in event reconstruction.

Jets are identified as originating from b quarks using the combined secondary vertex algorithm [83]. Control regions in data [84] are used to measure the probability of correctly identifying jets as originating from b quarks (b tagging efficiency), and the probability of misidentifying jets originating from light-flavour partons (u, d, s quarks or gluons) or a charm quark as a b-tagged jet (the light-flavour and charm mistag probabilities). A working point is employed that yields a b tagging efficiency of 65%, and charm and light-flavour mistag probabilities of approximately 12 and 1%, respectively, for jets with p_T that is typical of $t\bar{t}$ events.

An estimator of $\vec{p}_T^{miss}$ is given by the projection on the plane perpendicular to the beams of the negative vector sum of the momenta of all candidate particles in an event [85], as determined by the PF algorithm. Its magnitude is referred to as E_T^{miss}.

5 Event selection

The kinematic selection criteria used to define the signal region, containing a sample of candidate signal events, as well as a number of control regions in data, are described below. The criteria are based on the particle candidates defined by the event reconstruction algorithms described in Sect. 4.

5.1 Common preselection criteria

A number of beam- and detector-related effects, such as beam halo, reconstruction failures, spurious detector noise, or event misreconstruction due to detector inefficiencies, can lead to events with anomalous levels of activity. These rare events,

which can exhibit large values of E_T^{miss}, are rejected with high efficiency by applying a range of dedicated vetoes [85,86].

In order to suppress SM processes with genuine $\vec{p}_T^{miss}$ from neutrinos, events containing an isolated electron or muon that satisfies $p_T > 10\,\text{GeV}$ and $|\eta| < 2.5$ are vetoed. Events containing an isolated photon with $p_T > 25\,\text{GeV}$ and $|\eta| < 2.5$ are also vetoed, in order to select only multijet final states. Furthermore, events containing a single isolated track satisfying $p_T > 10\,\text{GeV}$ and $|\eta| < 2.5$ are vetoed in order to reduce the background contribution from final states containing hadronically decaying tau leptons.

Each jet j_i considered by this search is required to satisfy $p_T^{j_i} > 40\,\text{GeV}$ and $|\eta^{j_i}| < 3$. The number of jets within this experimental acceptance is labelled henceforth as n_{jet}. The highest p_T jet in the event is required to have $p_T^{j_1} > 100\,\text{GeV}$ and $|\eta^{j_1}| < 2.5$. The second-highest p_T jet in the event is used to categorise events, as described in Sect. 5.2. If the jet satisfies $p_T^{j_2} > 100\,\text{GeV}$, then this category of events is labelled "symmetric" and targets primarily topologies resulting from pair-produced SUSY particles. If the jet satisfies $40 < p_T^{j_2} < 100\,\text{GeV}$ then the event is labelled as "asymmetric," and if there exists no second jet with $p_T^{j_2} > 40\,\text{GeV}$, the event is labelled monojet. The asymmetric and monojet topologies target models involving the direct production of stable, weakly interacting, massive particles. The mass scale of the physics processes being probed is characterised by the scalar p_T sum of the jets, defined as $H_T = \sum_{i=1}^{n_{jet}} p_T^{j_i}$. The magnitude of the vector $\vec{p}_T$ sum of these jets, defined by $H_T^{miss} = |\sum_{i=1}^{n_{jet}} \vec{p}_T^{j_i}|$, is used to identify events with significant imbalance in $\vec{p}_T^{miss}$. Events are vetoed if any jet satisfies $p_T > 40\,\text{GeV}$ and $|\eta| > 3$ to ensure that jets reconstructed in the forward regions of the detector do not contribute significantly to H_T^{miss}.

The dimensionless variable H_T^{miss}/E_T^{miss} is used to remove events that contain several jets with transverse momenta below the jet p_T thresholds but an appreciable vector p_T sum so as to contribute significantly to H_T^{miss} relative to E_T^{miss}. This background is typical of multijet events, which is suppressed by requiring $H_T^{miss}/E_T^{miss} < 1.25$. The requirement is imposed as part of the common preselection criteria used to define all control samples to minimise potential systematic biases associated with the simulation modelling for this variable. A high efficiency is maintained for SM or new-physics processes that produce unobserved particles, which are characterised by large values of $\vec{p}_T^{miss}$ and values of H_T^{miss}/E_T^{miss} close to unity.

Significant jet activity and $\vec{p}_T^{miss}$ in the event is ensured by requiring $H_T > 200\,\text{GeV}$ and $H_T^{miss} > 130\,\text{GeV}$, respectively. These requirements complete the common preselection criteria, summarised in Table 1, used to define a sample of all-jet events characterised by high jet activity and appreciable $\vec{p}_T^{miss}$.

5.2 Event categorisation

Events selected by the common preselection criteria are categorised according to n_{jet}, the number of b-tagged jets n_b, and H_T. Nine categories in n_{jet} are employed: the mono-jet topology ($n_{jet} = 1$) and four n_{jet} bins (2, 3, 4, ≥ 5) for each of the asymmetric and symmetric topologies. Events are also categorised by n_b (0, 1, 2, ≥ 3), where n_b is bounded from above by n_{jet}, resulting in 32 categories in terms of both n_{jet} and n_b. For each (n_{jet}, n_b) category, events are binned according to H_T: four 50 GeV bins at low jet activity in the range $200 < H_T < 400\,\text{GeV}$, two 100 GeV bins in the range $400 < H_T < 600\,\text{GeV}$, one bin covering the region $600 < H_T < 800\,\text{GeV}$, and a final open bin for $H_T > 800\,\text{GeV}$. These categorisations are summarised in Table 1. The H_T binning scheme is adapted independently per (n_{jet}, n_b) category by removing or merging bins to satisfy a threshold on the minimum number of data events in the control regions, which are used to estimate SM backgrounds, provide checks, and validate assumptions within the methods. The lower bounds of the first and final (open) bins in H_T are summarised in Table 2. In summary, the search employs a categorisation scheme for events that results in 191 bins, defined in terms of n_{jet}, n_b, and H_T.

5.3 Signal region

For events satisfying the common preselection criteria described above, the multijet background dominates over all other SM backgrounds. Several variables are employed to reduce the multijet contribution to a low level with respect to other SM backgrounds.

The dimensionless kinematic variable α_T [28,53], defined in Eq. (2) below, is used to provide discrimination against multijet events that do not contain significant $\vec{p}_T^{miss}$ or that contain large $\vec{p}_T^{miss}$ only because of p_T mismeasurements, while retaining sensitivity to new-physics events with significant $\vec{p}_T^{miss}$. The α_T variable depends solely on the transverse component of jet four-momenta and is intrinsically robust against the presence of jet energy mismeasurements in multijet systems. For events containing only two jets, α_T is defined as $\alpha_T = E_T^{j_2}/M_T$, where $E_T = E \sin\theta$, where E is the energy of the jet and θ is its polar angle with respect to the beam axis, $E_T^{j_2}$ is the transverse energy of the jet with smaller E_T, and M_T is the transverse mass of the dijet system, defined as:

$$M_T = \sqrt{\left(\sum_{i=1,2} E_T^{j_i}\right)^2 - \left(\sum_{i=1,2} p_x^{j_i}\right)^2 - \left(\sum_{i=1,2} p_y^{j_i}\right)^2},$$

$$(1)$$

Table 1 Summary of the event selection criteria and categorisation used to define the signal and control regions

Common preselection	
E_T^{miss} quality	Filters related to beam and instrumental effects, and reconstruction failures
Lepton/photon vetoes	$p_T > 10,\ 10,\ 25$ GeV for isolated tracks, leptons, photons (respectively) and $|\eta| < 2.5$
Jet j_i acceptance	Consider each jet j_i that satisfies $p_T^{j_i} > 40$ GeV and $|\eta^{j_1}| < 3$
Jet j_1 acceptance	$p_T^{j_1} > 100$ GeV and $|\eta^{j_1}| < 2.5$
Jet j_2 acceptance	$p_T^{j_2} < 40$ GeV (monojet), $40 < p_T^{j_2} < 100$ GeV (asymmetric), $p_T^{j_2} > 100$ GeV (symmetric)
Forward jet veto	Veto events containing a jet satisfying $p_T > 40$ GeV and $|\eta| > 3$
Jets below threshold	$H_T^{miss}/E_T^{miss} < 1.25$
Energy sums	$H_T > 200$ GeV and $H_T^{miss} > 130$ GeV
Event categorisation	
n_{jet}	1 (monojet), 2, 3, 4, ≥ 5 (asymmetric), 2, 3, 4, ≥ 5 (symmetric)
n_b	0, 1, 2, ≥ 3 ($n_b \leq n_{jet}$)
H_T (GeV)	200, 250, 300, 350, 400, 500, 600, >800 GeV (bins can be dropped/merged *vs.* n_{jet}, Table 2)
Signal region (SR)	Preselection +
QCD multijet rejection	$\alpha_T > 0.65, 0.60, 0.55, 0.53, 0.52, 0.52, 0.52$ (mapped to H_T bins in range $200 < H_T < 800$ GeV)
QCD multijet rejection	$\Delta\phi_{min}^* > 0.5$ ($n_{jet} \geq 2$) or $\Delta\phi_{min}^{*25} > 0.5$ ($n_{jet} = 1$)
Control regions (CR)	Preselection +
Multijet-enriched	SR + $H_T^{miss}/E_T^{miss} > 1.25$ (inverted)
γ + jets	1γ with $p_T > 200$ GeV, $|\eta| < 1.45$, $\Delta R(\gamma, j_i) > 1.0$, $H_T > 400$ GeV, same α_T req. as SR
μ + jets	1μ with $p_T > 30$ GeV, $|\eta| < 2.1$, $I_{rel}^{\mu} < 0.1$, $\Delta R(\mu, j_i) > 0.5$, $30 < m_T(\vec{p}_T^{\mu}, \vec{p}_T^{miss}) < 125$ GeV
$\mu^{\pm}\mu^{\mp}$ + jets	2μ with $p_T > 30$ GeV, $|\eta| < 2.1$, $I_{rel}^{\mu} < 0.1$, $\Delta R(\mu_{1,2}, j_i) > 0.5$, $|m_{\mu\mu} - m_Z| < 25$ GeV

Table 2 Summary of the lower bounds of the first and final bins in H_T [GeV] (the latter in parentheses) as a function of n_{jet} and n_b

$n_{jet} \backslash n_b$	0	1	2	≥ 3
Monojet				
1	200 (600)	200 (500)	–	–
Asymmetric				
2	200 (600)	200 (500)	200 (400)	–
3	200 (600)	200 (600)	200 (500)	200 (300)
4	200 (600)	200 (600)	200 (600)	250 (400)
≥ 5	250 (600)	250 (600)	250 (600)	300 (500)
Symmetric				
2	200 (800)	200 (800)	200 (600)	–
3	200 (800)	250 (800)	250 (800)	– (250)
4	300 (800)	300 (800)	300 (800)	300 (800)
≥ 5	350 (800)	350 (800)	350 (800)	350 (800)

where $E_T^{j_i}$, $p_x^{j_i}$, and $p_y^{j_i}$ are, respectively, the transverse energy, and the x and y components of the transverse momentum of jet j_i. For a perfectly measured dijet event with $E_T^{j_1} = E_T^{j_2}$ and back-to-back jets ($\Delta\phi = \pi$), and in the limit in which the momentum of each jet is large compared with its mass, the value of α_T is 0.5. For an imbalance in the E_T of back-to-back jets, α_T is reduced to a value <0.5, which gives the variable its intrinsic robustness. Values sig-

nificantly greater than 0.5 are observed when the two jets are not back-to-back and recoil against $\vec{p}_T^{miss}$ from weakly interacting particles that escape the detector.

The definition of the α_T variable can be generalised for events with more than two jets [28]. The mass scale for any process is characterised through the scalar sum of the jet transverse energies, defined as $\mathcal{E}_T = \sum_{i=1}^{N_{jet}} E_T^{j_i}$, where N_{jet} is the number of jets with E_T above a predefined threshold. (The definition of $\mathcal{E}_T$ should be contrasted with that of H_T, the scalar p_T sum of the jets.) For events with three or more jets, a pseudo-dijet system is formed by combining the jets in the event into two pseudo-jets. The $\mathcal{E}_T$ for each of the two pseudo-jets is given by the scalar E_T sum of its contributing jets. The combination chosen is the one that minimises $\Delta\mathcal{E}_T$, defined as the difference between these sums for the two pseudo-jets. This clustering criterion assumes a balanced-event hypothesis, which provides strong separation between SM multijet events and events with genuine $\vec{p}_T^{miss}$. The α_T definition can be generalised to:

$$\alpha_T = \frac{1}{2} \frac{\mathcal{E}_T - \Delta\mathcal{E}_T}{\sqrt{(\mathcal{E}_T)^2 - (H_T^{miss})^2}}. \qquad (2)$$

When jet energies are mismeasured, or there are neutrinos from heavy-flavour quark decays, the magnitudes of H_T^{miss} and $\Delta\mathcal{E}_T$ are highly correlated. This correlation is much

weaker for *R*-parity-conserving SUSY events, where each of the two decay chains produces an undetected LSP.

Multijet events populate the region $\alpha_T < 0.5$ and the α_T distribution is characterised by a sharp edge at 0.5, beyond which the multijet event yield falls by several orders of magnitude. Multijet events with extremely rare but large stochastic fluctuations in the calorimetric measurements of jet energies can lead to values of α_T slightly above 0.5. The edge at 0.5 sharpens with increasing H_T for events containing at least three jets, primarily due to a corresponding increase in the average jet energy and consequently a (relative) improvement in the jet energy resolution.

For events containing at least two jets, thresholds on the minimum allowed α_T values are applied independent of n_{jet} and n_b but dependent on H_T, for events that satisfy $200 < H_T < 800$ GeV. The α_T thresholds vary between 0.65 and 0.52 for, respectively, the regions $200 < H_T < 250$ GeV and $400 < H_T < 800$ GeV. No requirement on α_T is made for the region $H_T > 800$ GeV. The thresholds employed are summarised in Table 1. The α_T thresholds are motivated both by the trigger conditions used to record the candidate signal events, described below, and by simulation-based studies and estimates of the multijet background derived from data.

An additional variable is based on the minimum azimuthal separation between a jet and the negative vector $\vec{p}_T$ sum derived from all other jets in the event [28],

$$\Delta\phi^*_{\min} = \min_{\forall\, j_k \in [1, n_{jet}]} \Delta\phi\left(\vec{p}_T^{\,j_k},\ -\sum_{\substack{j_i=1 \\ j_i \neq j_k}}^{n_{jet}} \vec{p}_T^{\,j_i} \right). \qquad (3)$$

This variable discriminates between final states with genuine $\vec{p}_T^{\,miss}$, e.g. from the leptonic decay of the W boson, and energetic multijet events that have significant $\vec{p}_T^{\,miss}$ through jet energy mismeasurements or through the production of neutrinos, collinear with the axis of a jet, from semileptonic heavy-flavour decays. Multijet events populate the region $\Delta\phi^*_{\min} < 0.5$, with the multijet distribution peaking at a value of zero and falling approximately exponentially over five orders of magnitude to a single-event level at a value of $\Delta\phi^*_{\min} \approx 0.5$, which is close to the distance parameter value of 0.4 used by the anti-k_T jet clustering algorithm. Events with a genuine source of $\vec{p}_T^{\,miss}$ exhibit a long tail in $\Delta\phi^*_{\min}$ with values as large as π.

A requirement of $\Delta\phi^*_{\min} > 0.5$ is sufficient to effectively suppress the multijet background to a low level while maintaining high efficiency for new-physics signatures. The combined rejection power of the α_T and $\Delta\phi^*_{\min}$ requirements for the region $200 < H_T < 800$ GeV is sufficient to suppress multijet events to the few percent level (and always <10%) with respect to all other SM backgrounds in all H_T bins for all event categories of the signal region. For the region
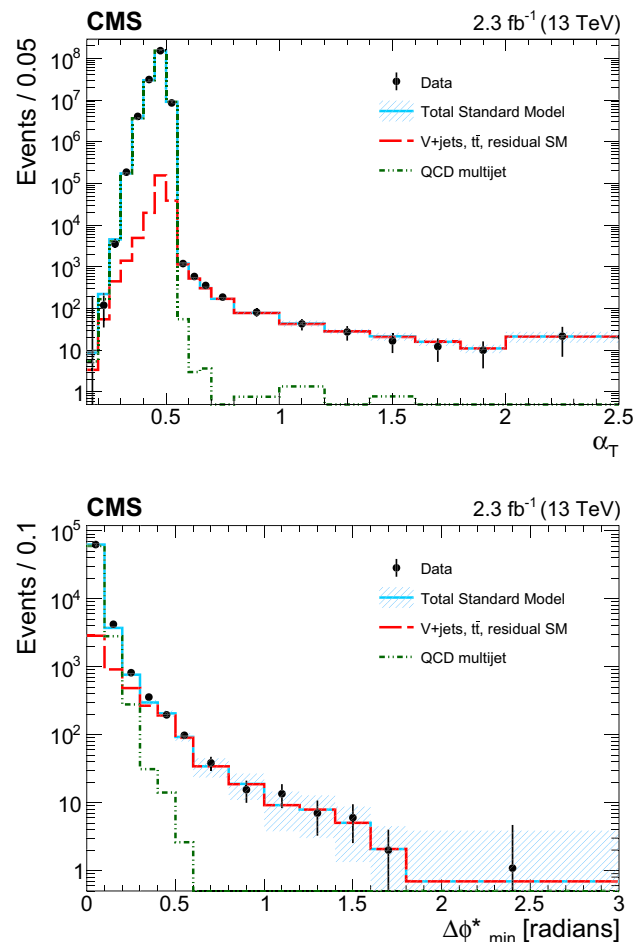

Fig. 1 The (*top*) α_T and (*bottom*) $\Delta\phi^*_{\min}$ distributions observed in data for events that satisfy the selection criteria defined in the text. The statistical uncertainties for the multijet and SM expectations are represented by the hatched areas (visible only for statistically limited bins). The final bin of each distribution contains the overflow events

$H_T > 800$ GeV, a similar control of the multijet background is achieved solely with the $\Delta\phi^*_{\min} > 0.5$ requirement.

Figure 1 shows the distributions of α_T and $\Delta\phi^*_{\min}$ observed in data for events that satisfy the full set of selection criteria used to define the signal region, summarised in Table 1, as well as the following modifications. The α_T and $\Delta\phi^*_{\min}$ distributions are constructed from events that satisfy $n_{jet} \geq 2$, $p_T^{j2} > 100$ GeV, and, respectively, $H_T > 300$ or 800 GeV. In the case of Fig. 1 (top), the events with α_T values greater than 0.55 must fulfill the full set of signal region criteria, including the $\Delta\phi^*_{\min} > 0.5$ requirement, while the events that satisfy $\alpha_T < 0.55$ are subject to the looser set of common preselection criteria defined in Table 1, excluding the $H_T^{miss} > 130$ GeV requirement. Hence, Fig. 1 (top) demonstrates the combined performance of several variables that are employed to suppress multijet events. For both distributions, the events are recorded with a set of inclusive trigger conditions that are independent of the α_T and $\Delta\phi^*_{\min}$ vari-

ables. The distributions for the QCD multijet background are determined from simulation while all other SM backgrounds (vector boson production in association with jets, $t\bar{t}$, and other residual contributions from rare SM processes) are estimated using a μ + jets data control sample, described in Sect. 6.2. The contribution from multijet events is observed to fall by more than five orders of magnitude for both variables.

The α_T and $\Delta\phi^*_{\min}$ requirements described above, in conjunction with the common preselection requirements $H_T^{\text{miss}} > 130$ GeV and $H_T^{\text{miss}}/E_T^{\text{miss}} < 1.25$, provide strong rejection power against the multijet background for events that satisfy $n_{\text{jet}} \geq 2$. For monojet events, a modification to the $\Delta\phi^*_{\min}$ variable, which considers soft jets with $p_T > 25$ GeV ($\Delta\phi^{*25}_{\min}$), is utilised. No α_T requirement is imposed, and $\Delta\phi^{*25}_{\min} > 0.5$ is sufficient to suppress contributions from multijet events to a negligible level. The aforementioned requirements complete the event selection criteria for the signal region.

Finally, $\Delta\phi^{*25}_{\min}$ is also used as a control variable for events that satisfy $n_{\text{jet}} \geq 2$ to identify multijet contributions arising from instrumental effects, such as inefficient detector elements or detector noise. The axis of any jet that satisfies $\Delta\phi^{*25}_{\min} < 0.5$ is used to identify localised behaviour in the (η, ϕ) plane, which may be indicative of instrumental defects. No significant anomalies are observed in the sample of candidate signal events following the application of the dedicated vetoes described in Sect. 5.1.

Multiple trigger conditions are employed in combination to record candidate signal events. A set of trigger conditions utilise calculations of both H_T and α_T to record events with two or more jets. An event is recorded if it satisfies any of the following pairs of (H_T [GeV], α_T) thresholds, (200, 0.57), (250, 0.55), (300, 0.53), (350, 0.52), or (400, 0.51), as well as a requirement on the mean value of the two highest p_T jets, $\langle p_T^{\text{j1}} + p_T^{\text{j2}} \rangle > 90$ GeV. These requirements are collectively labelled as the "H_T–α_T" triggers. In addition, candidate signal events with one or more jets are also recorded if they satisfy the requirements $H_T^{\text{miss}} > 90$ GeV and $E_T^{\text{miss}} > 90$ GeV. Finally, for events that satisfy $H_T > 800$ GeV, an additional trigger condition, defined by $H_T > 800$ GeV, is employed in addition to the H_T–α_T trigger requirements to record events characterised by high activity in the calorimeters with high efficiency. The trigger-level jet energies are corrected to account for energy scale and pileup effects. The aforementioned triggers are employed in combination to provide efficiencies at or near 100% for all bins in the signal region.

5.4 Using H_T^{miss} templates

Following the event selection criteria described above, which provide a sample of candidate signal events with a negligible contribution from multijet events, further discriminating

power is required to separate new-physics signatures from the remaining SM backgrounds, which are dominated by the production of $t\bar{t}$ or W($\rightarrow \ell\nu$) + jets and Z($\rightarrow \nu\bar{\nu}$) + jets events. As discussed in Sect. 1, the production of coloured SUSY particles with decays to a weakly interacting LSP typically gives rise to a final state with multiple jets and large $\vec{p}_T^{\text{miss}}$. The search therefore exploits the H_T^{miss} variable as an additional discriminant between new-physics and SM processes.

The search relies directly on simulation to determine a template for each (n_{jet}, n_b, H_T) bin that describes the expected distribution of events as a function of H_T^{miss}. These templates are used by the likelihood function as a model for the data, details of which can be found in Sect. 7. The templates are extensively validated against data in multiple control regions, and these studies are used to establish the uncertainty in the simulation modelling of the H_T^{miss} variable. The effects of theoretical and experimental uncertainties on the H_T^{miss} distributions are also studied. Further details can be found in Sect. 6.2.

5.5 Control regions

Four control regions in data are employed to estimate the background contributions from SM processes. The event selection criteria used to define the control regions comprise the common preselection requirements and additional sample-specific requirements, as summarised in Table 1. The first control region comprises a multijet-enriched sample of events, and is defined by the signal region selection criteria and the inverted requirement $H_T^{\text{miss}}/E_T^{\text{miss}} > 1.25$. The events are recorded with the signal triggers described above, and the sample is used to estimate the multijet background in the signal region. Three additional control regions, defined by inverting one of the photon or lepton vetoes to select samples of γ + jets, μ + jets, or $\mu\mu$ + jets events, are used to estimate the background contributions from SM processes with final states containing genuine $\vec{p}_T^{\text{miss}}$, which are primarily $t\bar{t}$, W($\rightarrow \ell\nu$) + jets, and Z($\rightarrow \nu\bar{\nu}$) + jets.

Additional kinematic requirements are employed to ensure the control samples are enriched in the same SM processes that contribute to background events in the signal region, and are depleted in contributions from multijet production or a wide variety of SUSY models (i.e. so-called signal contamination). The samples are defined, and their events are identically categorised and binned, such that the kinematic properties of events in the control regions and the candidate signal events resemble as closely as possible one another once the photon, muon, or dimuon system is ignored in the calculation of quantities such as H_T and H_T^{miss}. The selections are summarised in Table 1 and described below.

The γ + jets event sample is defined by the common preselection requirements, but the photon veto is inverted

and each event is required to contain a single isolated photon, as defined in Sect. 4, that satisfies $p_T > 200$ GeV and $|\eta| < 1.45$ and is well separated from each jet j_i in the event according to $\Delta R(\gamma, j_i) > 1.0$. In addition, events must satisfy $H_T > 400$ GeV, as well as the same H_T-dependent α_T requirements used to define the signal region. The events are recorded using a single-photon trigger condition and the selection criteria result in a trigger efficiency of $\gtrsim 99\%$.

The μ + jets event sample is defined by the common preselection requirements, but the muon veto is inverted and each event is required to contain a single isolated muon, as defined in Sect. 4, that satisfies $p_T > 30$ GeV and $|\eta| < 2.1$ and is well separated from each jet j_i in the event according to $\Delta R(\mu, j_i) > 0.5$. The transverse mass formed by the muon p_T and $\vec{p}_T^{\text{miss}}$ system must satisfy $30 < m_T < 125$ GeV to select a sample of events rich in W bosons, produced promptly or from the decay of top quarks. The $\mu\mu$ + jets sample uses a similar set of selection criteria as the μ + jets sample, but specifically requires two oppositely charged isolated muons that both satisfy $p_T > 30$ GeV and $|\eta| < 2.1$ and are well separated from the jets in the event ($\Delta R(\mu_{1,2}, j_i) > 0.5$). The muons are also required to have a dilepton invariant mass within a ± 25 GeV window around the nominal mass of the Z boson [9]. For both the muon and dimuon samples, no requirement is made on α_T in order to increase the statistical precision of the predictions from these samples. Both the μ + jets and $\mu\mu$ + jets samples are recorded using a trigger that requires an isolated muon. The selection criteria of the μ + jets and $\mu\mu$ + jets event samples are chosen so that the trigger is maximally efficient, with values of ~ 90 and $\sim 99\%$, respectively.

6 Estimation of backgrounds

6.1 Multijet background

The signal region is defined in a manner that suppresses the expected contribution from multijet production to a low level with respect to the total expected background from other SM processes for all signal region bins. This is achieved primarily through the application of very tight requirements on the variables α_T and $\Delta\phi_{\min}^*$, as described in Sect. 5.3, as well as the requirement $H_T^{\text{miss}}/E_T^{\text{miss}} < 1.25$. In this section, we discuss these requirements further, and present the estimate of the multijet background.

The contamination from multijet events in the signal region is estimated using a multijet-enriched data sideband to the signal region, defined by the (inverted) requirement $H_T^{\text{miss}}/E_T^{\text{miss}} > 1.25$. The observed counts in data, categorised according to n_{jet} and H_T, are corrected to account for contamination from nonmultijet SM processes, and the corrected counts $\mathcal{N}^{\text{data}}(n_{\text{jet}}, H_T)$ are assumed to arise solely

from QCD multijet production. The nonmultijet processes, which comprise vector boson and $t\bar{t}$ production and residual contributions from other SM processes, are estimated using the μ + jets control region, as described in Sect. 6.2.

Independent ratios $\mathcal{R}^{\text{QCD}}(n_{\text{jet}}, H_T)$ of the number of multijet events that satisfy the requirement $H_T^{\text{miss}}/E_T^{\text{miss}} < 1.25$ to the number that fail this requirement are determined from simulation for events categorised according to n_{jet} and H_T, and inclusively with respect to n_b and H_T^{miss}. The product of each ratio $\mathcal{R}^{\text{QCD}}(n_{\text{jet}}, H_T)$ and the corresponding corrected data count $\mathcal{N}^{\text{data}}(n_{\text{jet}}, H_T)$ provides the estimate of the multijet background $\mathcal{P}(n_{\text{jet}}, H_T)$. The estimates as a function of n_{jet}, H_T, n_b, and H_T^{miss} of the signal region are assumed to factorise as follows:

$$\mathcal{P}(n_{\text{jet}}, H_T) = \mathcal{N}^{\text{data}}(n_{\text{jet}}, H_T)\, \mathcal{R}^{\text{QCD}}(n_{\text{jet}}, H_T), \tag{4}$$

$$\mathcal{P}(n_{\text{jet}}, H_T, n_b, H_T^{\text{miss}}) = \mathcal{P}(n_{\text{jet}}, H_T)\, \mathcal{K}_{n_{\text{jet}}, H_T}(n_b, H_T^{\text{miss}}), \tag{5}$$

where $\mathcal{K}_{n_{\text{jet}}, H_T}(n_b, H_T^{\text{miss}})$ are multiplier terms that provide the estimated distribution of events as a function of n_b and H_T^{miss} while preserving the normalisation $\mathcal{P}(n_{\text{jet}}, H_T)$.

The use of simulation to determine $\mathcal{R}^{\text{QCD}}(n_{\text{jet}}, H_T)$ is validated using a multijet-enriched data sideband defined by $\Delta\phi_{\min}^* < 0.5$. Each ratio $\mathcal{R}^{\text{data}}(n_{\text{jet}}, H_T)$ is constructed from data counts, corrected to account for contributions from nonmultijet processes, and compared with the corresponding ratio $\mathcal{R}^{\text{QCD}}(n_{\text{jet}}, H_T)$, determined from simulation, through the double ratio $\mathcal{R}^{\text{data}}/\mathcal{R}^{\text{QCD}}$, as shown in Fig. 2. The double ratios are statistically compatible with unity across the full phase space of the signal region, including the bins at high H_T, which exhibit the highest statistical precision. In addition to statistical uncertainties as large as $\sim 100\%$, a systematic uncertainty of 100% in $\mathcal{R}^{\text{QCD}}$ is assumed to adequately cover the observed level of agreement for the full signal region phase space.

The distribution of multijet events as a function of n_b and H_T^{miss}, $\mathcal{K}_{n_{\text{jet}}, H_T}(n_b, H_T^{\text{miss}})$, is assumed to be identical to the distribution expected for the nonmultijet backgrounds. This final assumption is based on studies in simulation and is a valid approximation given the magnitude of this background contribution, as well as the magnitude of the statistical and systematic uncertainties in the ratios $\mathcal{R}^{\text{QCD}}(n_{\text{jet}}, H_T)$, as described above.

6.2 Backgrounds with genuine E_T^{miss}

Following the suppression of multijet events through the use of the α_T and $\Delta\phi_{\min}^*$ variables, the dominant nonmultijet backgrounds involve SM processes that produce high-p_T neutrinos in the final state. In events with few jets or few b quark jets, the associated production of W or Z bosons and jets, with the decays $W^\pm \to \ell\nu$ ($\ell = $ e, μ, τ) or $Z \to \nu\bar{\nu}$,

Fig. 2 Validation of the ratio $\mathcal{R}^{\mathrm{QCD}}$ determined from simulation in bins of n_{jet} and H_{T} [GeV] by comparing with an equivalent ratio $\mathcal{R}^{\mathrm{data}}$ constructed from data in a multijet-enriched sideband to the signal region. A value of unity is expected for the double ratio $\mathcal{R}^{\mathrm{data}}/\mathcal{R}^{\mathrm{QCD}}$, and the *grey shaded band* represents the assumed systematic uncertainty of 100% in $\mathcal{R}^{\mathrm{QCD}}$
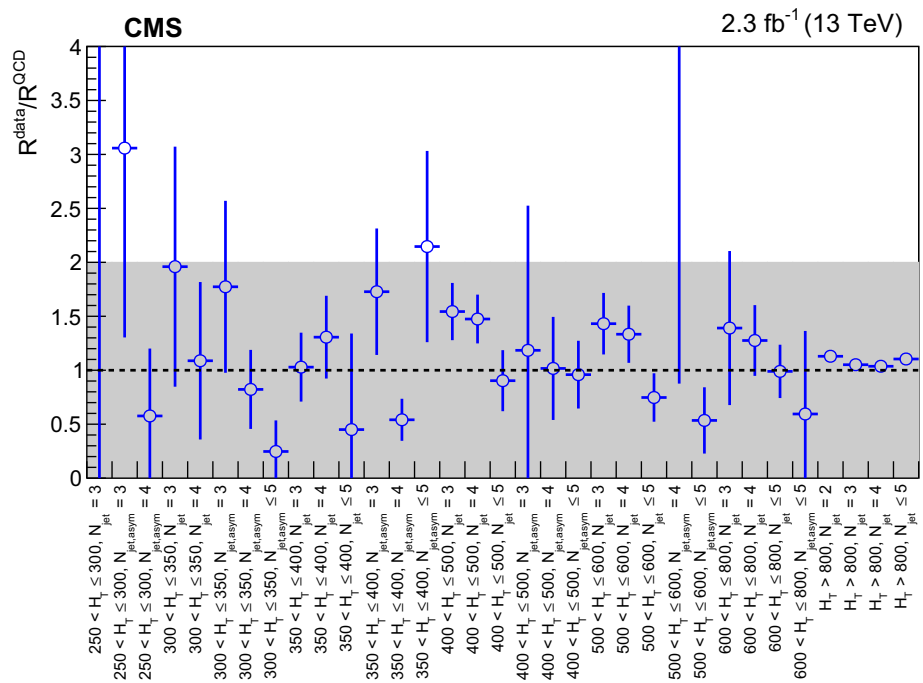
dominate the background counts. For W boson decays that yield an electron or muon (possibly originating from leptonic τ decays), the background contributions result from events containing an e or μ that are not rejected by the lepton vetoes. The veto of events containing at least one isolated track further suppresses these backgrounds, including those from single-prong τ-lepton decays. At higher jet or b-quark jet multiplicities, single top quark and $t\bar{t}$ production, followed by semileptonic top quark decay, also become an important source of background.

The method to estimate the nonmultijet backgrounds in the signal region relies on the use of a transfer ($\mathcal{T}$) factor determined from simulation that is constructed per bin (in terms of n_{jet}, n_{b}, and H_{T}) per control region. Each $\mathcal{T}$ factor is defined as the ratio of the expected yields in the same (n_{jet}, n_{b}, H_{T}) bins of the signal region $\mathcal{N}_{\mathrm{MC}}^{\mathrm{SR}}$ and one of the control regions $\mathcal{N}_{\mathrm{MC}}^{\mathrm{CR}}$. The $\mathcal{T}$ factors are used to extrapolate from the event yields observed in each bin of a data control sample $\mathcal{N}_{\mathrm{data}}^{\mathrm{CR}}$ to provide an estimate for the background, integrated over $H_{\mathrm{T}}^{\mathrm{miss}}$, from a particular SM process or processes in the corresponding bin of the signal region $\mathcal{N}_{\mathrm{data}}^{\mathrm{SR}}$. The superscript SR or CR refers to, respectively, the process or processes being estimated and one of the μ + jets, $\mu\mu$ + jets, and γ + jets control regions, described in Sect. 5.5. The subscript refers to whether the counts are obtained from data, simulation ("MC"), or an estimate ("pred").

The method aims to minimise the effects of simulation mismodelling, as many systematic biases in the simulation are expected to largely cancel in the $\mathcal{T}$ factors, given that the events in any given (n_{jet}, n_{b}, H_{T}) bin of the control regions closely mirror those in the corresponding bin in the signal

region in terms of the event energy scale, topology, and kinematics. In short, minimal extrapolations are made. Uncertainties in the $\mathcal{T}$ factors are determined from data, as described below.

Three independent estimates of the irreducible background of $Z \rightarrow \nu\bar{\nu}$ + jets events are determined from the γ + jets, $\mu\mu$ + jets, and μ + jets data control samples. The γ + jets and $Z \rightarrow \mu\mu$ + jets processes have similar kinematic properties when the photon or muons are ignored [87], albeit different acceptances. In addition, the γ + jets process has a larger production cross section than $Z \rightarrow \nu\bar{\nu}$ + jets events. The μ + jets data sample is used to provide an estimate for both the $Z \rightarrow \nu\bar{\nu}$ + jets background, as well as the other dominant SM processes, $t\bar{t}$ and W boson production (labelled collectively as W/$t\bar{t}$). Residual contributions from all other SM relevant processes, such as single top quark, diboson, and Drell–Yan production, are also included as part of the W/$t\bar{t}$ estimate from the μ + jets sample. The definition of the various $\mathcal{T}$ factors used in the search are given below:

$$\mathcal{N}_{\mathrm{pred}}^{\mathrm{W}/t\bar{t}} = \mathcal{T}_{\mu+\mathrm{jets}}^{\mathrm{W}/t\bar{t}} \, \mathcal{N}_{\mathrm{data}}^{\mu+\mathrm{jets}}, \qquad \mathcal{T}_{\mu+\mathrm{jets}}^{\mathrm{W}/t\bar{t}} = \left(\frac{\mathcal{N}_{\mathrm{MC}}^{\mathrm{W}/t\bar{t}}}{\mathcal{N}_{\mathrm{MC}}^{\mu+\mathrm{jets}}} \right);$$

(6)

$$\mathcal{N}_{\mathrm{pred}}^{Z\rightarrow\nu\bar{\nu}} = \mathcal{T}_{\mu+\mathrm{jets}}^{Z\rightarrow\nu\bar{\nu}} \, \mathcal{N}_{\mathrm{data}}^{\mu+\mathrm{jets}}, \qquad \mathcal{T}_{\mu+\mathrm{jets}}^{Z\rightarrow\nu\bar{\nu}} = \left(\frac{\mathcal{N}_{\mathrm{MC}}^{Z\rightarrow\nu\bar{\nu}}}{\mathcal{N}_{\mathrm{MC}}^{\mu+\mathrm{jets}}} \right);$$

(7)

$$\mathcal{N}_{\mathrm{pred}}^{Z\rightarrow\nu\bar{\nu}} = \mathcal{T}_{\mu\mu+\mathrm{jets}}^{Z\rightarrow\nu\bar{\nu}} \, \mathcal{N}_{\mathrm{data}}^{\mu\mu+\mathrm{jets}}, \quad \mathcal{T}_{\mu\mu+\mathrm{jets}}^{Z\rightarrow\nu\bar{\nu}} = \left(\frac{\mathcal{N}_{\mathrm{MC}}^{Z\rightarrow\nu\bar{\nu}}}{\mathcal{N}_{\mathrm{MC}}^{\mu\mu+\mathrm{jets}}} \right);$$

(8)

$$\mathcal{N}_{\mathrm{pred}}^{Z\to\nu\bar{\nu}} = \mathcal{T}_{\gamma+\mathrm{jets}}^{Z\to\nu\bar{\nu}}\,\mathcal{N}_{\mathrm{data}}^{\gamma+\mathrm{jets}}, \qquad \mathcal{T}_{\gamma+\mathrm{jets}}^{Z\to\nu\bar{\nu}} = \left(\frac{\mathcal{N}_{\mathrm{MC}}^{Z\to\nu\bar{\nu}}}{\mathcal{N}_{\mathrm{MC}}^{\gamma+\mathrm{jets}}}\right). \tag{9}$$

The likelihood function, described in Sect. 7, encodes the estimate via the $\mathcal{T}$ factors of the W/t$\bar{\mathrm{t}}$ background, as well as the three independent estimates of the $Z \to \nu\bar{\nu}$ background, which are considered simultaneously.

Several sources of uncertainty in the $\mathcal{T}$ factors are evaluated. The most relevant effects are discussed below, and generally fall into one of two categories. The first category concerns uncertainties in the "scale factor" corrections applied to simulation, which are determined using inclusive data samples that are defined by loose selection criteria, to account for the mismodelling of theoretical and experimental parameters. The second category concerns "closure tests" in data that probe various aspects of the accuracy of the simulation to model correctly the $\mathcal{T}$ factors in the phase space of this search.

The uncertainties in the $\mathcal{T}$ factors are studied for variations in scale factors related to the jet energy scale (that result in uncertainties in the $\mathcal{T}$ factors as large as $\sim 15\%$), the efficiency and misidentification probability of b quark jets (up to 5%), and the efficiency to identify well-reconstructed, isolated leptons (up to $\sim 5\%$). A 5% uncertainty in the total inelastic cross section, $\sigma_{\mathrm{in}} = 69.0 \pm 3.5$ mb [88], is assumed and propagated through to the reweighting procedure to account for differences between the simulated measured pileup, which results in changes of up to $\sim 10\%$. The modelling of the transverse momentum of top quarks ($p_{\mathrm{T}}^{\mathrm{t}}$) is evaluated by comparing the simulated and measured p_{T} spectra of reconstructed top quarks in t$\bar{\mathrm{t}}$ events [89]. Simulated events are reweighted according to scale factors that decrease from a value of ~ 1.2 to ~ 0.7, with uncertainties of ~ 10–20%, within the range $p_{\mathrm{T}}^{\mathrm{t}} < 400$ GeV. The systematic

uncertainties in $\mathcal{T}_{\mu+\mathrm{jets}}^{\mathrm{W}/\mathrm{t}\bar{\mathrm{t}}}$ arising from variations in the $p_{\mathrm{T}}^{\mathrm{t}}$ scale factors are typically small ($\lesssim 5\%$), due to the comparable phase space probed by the signal and control regions, while larger uncertainties ($\lesssim 20\%$) in $\mathcal{T}_{\mu+\mathrm{jets}}^{Z\to\nu\bar{\nu}}$ are observed due to the potential for significant contamination from t$\bar{\mathrm{t}}$ when using $\mathrm{W}(\to \ell\nu)$ + jets to predict $Z(\to \nu\bar{\nu})$ + jets.

The aforementioned systematic uncertainties, resulting from variations in scale factors, are summarised in Table 3, along with representative magnitudes. These sources of uncertainty are each assumed to originate from a unique underlying source and so the effect of each source is varied assuming a fully correlated behaviour across the full phase space of the signal and control regions.

The second category of uncertainty is determined from sets of closure tests based on data control samples [31]. Each set uses the observed event counts in up to eight bins in H_{T} for each of the nine n_{jet} event categories in one of the three independent data control regions. These counts are used with the corresponding $\mathcal{T}$ factors, determined from simulation, to obtain a prediction $\mathcal{N}^{\mathrm{pred}}(n_{\mathrm{jet}}, H_{\mathrm{T}})$ of the observed yields $\mathcal{N}^{\mathrm{obs}}(n_{\mathrm{jet}}, H_{\mathrm{T}})$ in another control sample (or, in one case, n_{b} event category).

Each set of tests targets a specific (potential) source of bias in the simulation modelling that may introduce an n_{jet}- or H_{T}-dependent source of systematic bias in the $\mathcal{T}$ factors [31]. Several sets of tests are performed. The Z/γ ratio determined from simulation is tested against the same ratio measured using $Z(\to \mu\mu)$ + jets events and the γ + jets sample. The W/Z ratio is also probed using the μ+jets and $\mu\mu$+jets samples, which directly tests the simulation modelling of vector boson production, as well as the modelling of t$\bar{\mathrm{t}}$ contamination in the μ+jets sample. A further set probes the modelling of the relative composition between $\mathrm{W}(\to \ell\nu)$ + jets and t$\bar{\mathrm{t}}$ events using μ + jets events containing exactly zero or one or more b-tagged jets, which represents a larger extrapolation in

Table 3 Systematic uncertainties (in percent) in the transfer ($\mathcal{T}$) factors used in the method to estimate the SM backgrounds with genuine $\vec{p}_{\mathrm{T}}^{\mathrm{miss}}$ in the signal region. The quoted ranges provide representative values of the observed variations as a function of n_{jet} and H_{T}

Systematic source	Uncertainty in $\mathcal{T}$ factor [%]			
	$\mathcal{T}_{\mu+\mathrm{jets}}^{\mathrm{W}/\mathrm{t}\bar{\mathrm{t}}}$	$\mathcal{T}_{\mu+\mathrm{jets}}^{Z\to\nu\bar{\nu}}$	$\mathcal{T}_{\mu\mu+\mathrm{jets}}^{Z\to\nu\bar{\nu}}$	$\mathcal{T}_{\gamma+\mathrm{jets}}^{Z\to\nu\bar{\nu}}$
Scale factors (applied to simulation)				
Jet energy scale	<15	<15	<10	<15
b tagging eff and mistag rate	<5	<5	<2	<2
Lepton identification	2–5	2–5	2–5	–
Pileup	<10	<6	<4	<3
Top quark p_{T}	<5	<20	<4	–
Closure tests				
W/Z ratio	–	10–30	–	–
Z/γ ratio	–	–	–	10–30
W/t$\bar{\mathrm{t}}$ composition	10–100	–	–	–
W polarisation	5–50	5–50	–	–
$\alpha_{\mathrm{T}}/\Delta\phi_{\mathrm{min}}^{*}$	5–80	5–80	50–80	–

relative composition than used in the search. The effects of W polarisation are probed by using $\mu + \text{jets}$ events with a positively charged muon to predict those containing a negatively charged muon. Finally, the accuracy of the modelling of the efficiencies of the α_T and $\Delta\phi^*_\text{min}$ requirements are estimated using the $\mu + \text{jets}$ sample.

For each set of tests, the level of closure, $(\mathcal{N}^\text{obs} - \mathcal{N}^\text{pred})/\mathcal{N}^\text{obs}$, which considers only statistical uncertainties, is inspected to ensure no statistically significant biases are observed as a function of the nine n_jet categories or the eight H_T bins. In the absence of such a bias, the level of closure is recomputed by integrating over either all monojet and asymmetric n_jet categories, or the symmetric n_jet categories. The level of closure and its statistical uncertainty are combined in quadrature to determine additional contributions to the uncertainties in the $\mathcal{T}$ factors. These uncertainties are considered to be fully correlated between the monojet and asymmetric n_jet categories or the symmetric n_jet categories, and fully uncorrelated between these two regions in n_jet and H_T bins. If the closure tests use the $\mu\mu + \text{jets}$ sample, the level of closure is determined by additionally integrating over pairs of adjacent H_T bins. These uncertainties, derived from the closure tests in data, are summarised in Table 3, along with representative magnitudes. These uncertainties are the dominant contribution to the total uncertainty in the $\mathcal{T}$ factors, due to the limited number of events in the data control regions.

As introduced in Sect. 5.4, templates are derived from simulation to predict the H_T^miss distributions of the background. The uncertainties in the $\mathcal{T}$ factors are used to constrain the normalisation of the H_T^miss templates. The uncertainties in the H_T^miss shape are discussed below.

The accuracy to which the simulation describes the H_T^miss distributions is evaluated with respect to data in each (n_jet, n_b, H_T) bin in each of the $\mu + \text{jets}$, $\mu\mu + \text{jets}$, and $\gamma + \text{jets}$ data control regions. The level of agreement between data and simulation, defined in terms of the ratio of observed and expected counts (from simulation) as a function of H_T^miss, is parameterised using an orthogonal first-order polynomial, $f(x) = p_0 + p_1(\bar{x} - x)$, and described by two uncorrelated parameters, p_0 and p_1. A binned likelihood fit is performed in each (n_jet, n_b, H_T) bin of each control region, and the best fit value p_1 and its uncertainty is used to determine the presence of biases dependent on H_T^miss. The pull of p_1 from a value of zero is defined as the best fit value over its standard deviation, considering only statistical uncertainties associated with the finite size of the data and simulated samples.

The lower bound of the final (open) bin in H_T^miss is not more than 800 GeV and is bounded from above by the upper bound of the H_T bin in question. The lower bound of the final H_T^miss bin is merged with lower bins if fewer than ten events in the data control regions are observed. If a bin in (n_jet, n_b, H_T) contains fewer than ten events, the H_T^miss template is not used and the background estimates are determined inclu-

sively with respect to H_T^miss. The merging of bins is typically only relevant for event categories that satisfy $n_\text{b} \geq 2$.

The presence of systematic biases is evaluated at a statistical level by considering the distribution of pulls obtained from each control region, which are consistent with statistical fluctuations, with no indication of trends across the full phase space of each control region. The p-values obtained from the fits are uniformly distributed.

The uncertainty in the H_T^miss modelling is extracted under the hypothesis of no bias. This is done using the maximum likelihood (ML) values of the fit parameters to determine the statistical precision to which this hypothesis can be confirmed. The quadrature sum of the ML value and its uncertainty for p_1 from each fit is used to define alternative templates that represent $\pm 1\sigma$ variations to the nominal H_T^miss template. These alternative templates are encoded in the likelihood function, as described in Sect. 7. The observed variations are compatible with the expected values obtained from studies relying only on simulated event samples. The uncertainties in the final H_T^miss bin of the templates depend on the event category and H_T bin, and are typically found to be in the range $\sim$10–100%.

The effect on the H_T^miss templates is determined under $\pm 1\sigma$ variations in the jet energy scale, the efficiency and misidentification probability of b-quark jets, the efficiency to identify well-reconstructed, isolated leptons, the pileup reweighting, and the modelling of the top quark p_T. These effects are easily covered by the uncertainties determined from data, as described above, across the full phase space of the control regions, which mirror closely that of the signal region.

7 Results

A model of the observations in all data samples, described by a likelihood function, is used to obtain a prediction of the SM backgrounds and to test for the presence of new-physics signals if the signal region is included in the ML fit. The observation in each bin defined by the n_jet, n_b, H_T, and H_T^miss variables is modelled as a Poisson-distributed variable around the SM expectation and a potential signal contribution (assumed to be zero in the following discussion), where the SM expectation is the sum over the estimated contributions from all background processes according to the methods described in Sect. 6.

The nonmultijet backgrounds are related to the expected yields in the $\mu + \text{jets}$, $\mu\mu + \text{jets}$, and $\gamma + \text{jets}$ control samples via the transfer factors derived from simulation, as described in Sect. 5.5. Estimates of the contribution from multijet events in the signal region are determined according to the method described in Sect. 6.1, and are included in the likelihood function.
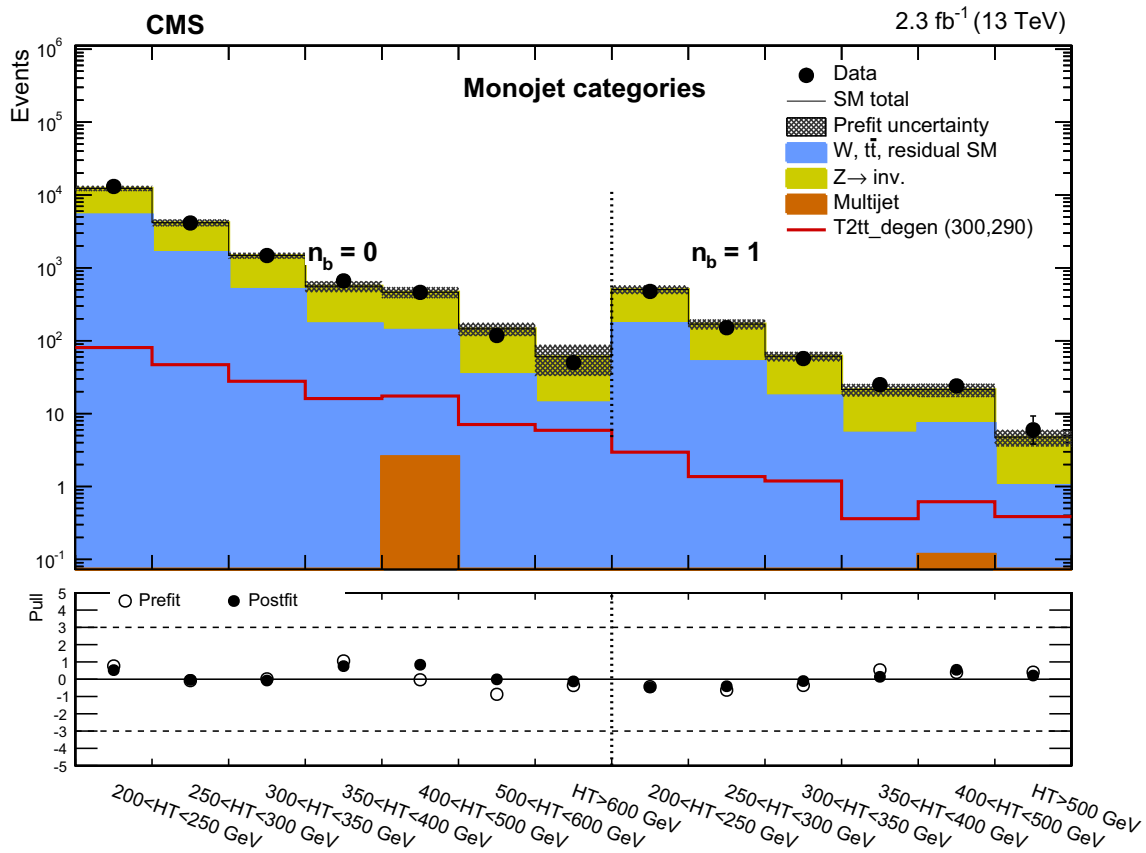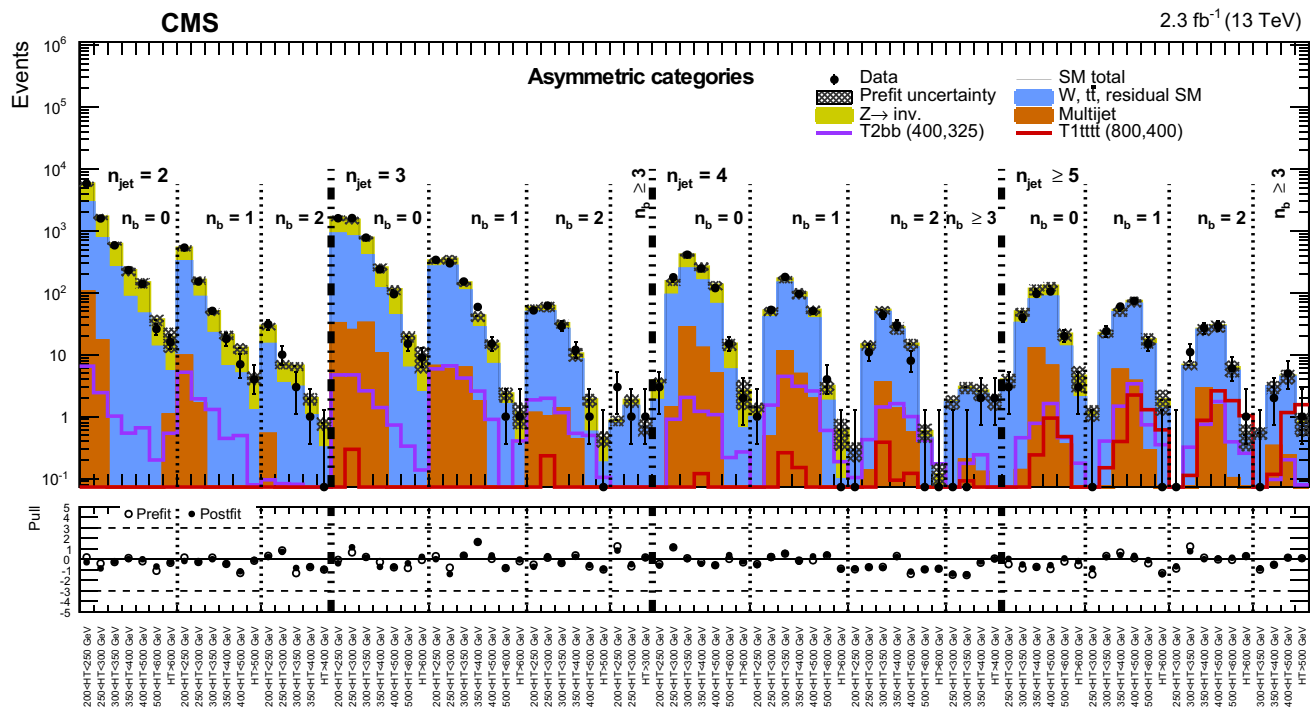
Fig. 3 (*Upper panel*) Event yields observed in data (*solid circles*) and pre-fit SM expectations with their associated uncertainties (*black histogram with shaded band*), integrated over H_T^{miss}, as a function of n_b and H_T for the monojet category ($n_{jet} = 1$) in the signal region. For illustration only, the expectations for a benchmark model (`T2tt_degen` with $m_{\tilde{t}} = 300$ GeV and $m_{\tilde{\chi}_1^0} = 290$ GeV) are superimposed on the SM-only expectations. (*Lower panel*) The significance of deviations (pulls) observed in data with respect to the pre-fit (*open circles*) and post-fit (*closed circles*) SM expectations, expressed in terms of the total uncertainty in the SM expectations. The pulls cannot be considered independently due to inter-bin correlations

The systematic uncertainties summarised in Table 3 are accommodated in the likelihood function through the use of nuisance parameters, the measurements of which are assumed to follow a log-normal distribution. Alternative templates are used to describe the uncertainties in the modelling of the H_T^{miss} variable. A vertical template morphing scheme [90] is used to interpolate between the nominal and alternative H_T^{miss} templates. A nuisance parameter controls the interpolation, which is Gaussian distributed with a mean of zero and a standard deviation of one, where ± 1 corresponds to the alternative templates for a $\pm 1\sigma$ variation in the uncertainty. Each template is interpolated quadratically between $\pm 1\sigma$, and a linear extrapolation is employed beyond these bounds.

The data are inspected to ascertain whether they are well described by the null (SM-only) hypothesis. This is done by considering the "pre-fit" SM background estimates, which are determined from observed data counts in the control regions only. The pre-fit result of this search is summarised in Figs. 3, 4 and 5 for, respectively, the monojet, asymmetric,

and symmetric topologies. The figures also show the significance of deviations observed in data with respect to the pre-fit SM expectations expressed in terms of the total uncertainty in the SM expectations ("pull"). The data are well described by the background-only hypothesis. Figures 3, 4 and 5 also summarise the pulls from the post-fit result, which is based on a ML fit to observations in the signal region as well as the control regions.

A quantitative statement on the degree of compatibility between the observed yields and the SM expectations under the background-only hypothesis is obtained from a goodness-of-fit test based on a log likelihood ratio. The alternative hypothesis is defined by a "saturated" model [91], for which the background expectation is set equal to the observed number of events, and provides a reference for the largest value that the likelihood can take for any model for the given data set. Hence, this reference can be used as a reasonable normalisation for the maximum value observed for a more constraining model. A p-value of 0.20 is observed for the fit over the full signal region, and p-values in the range 0.04–1.00,
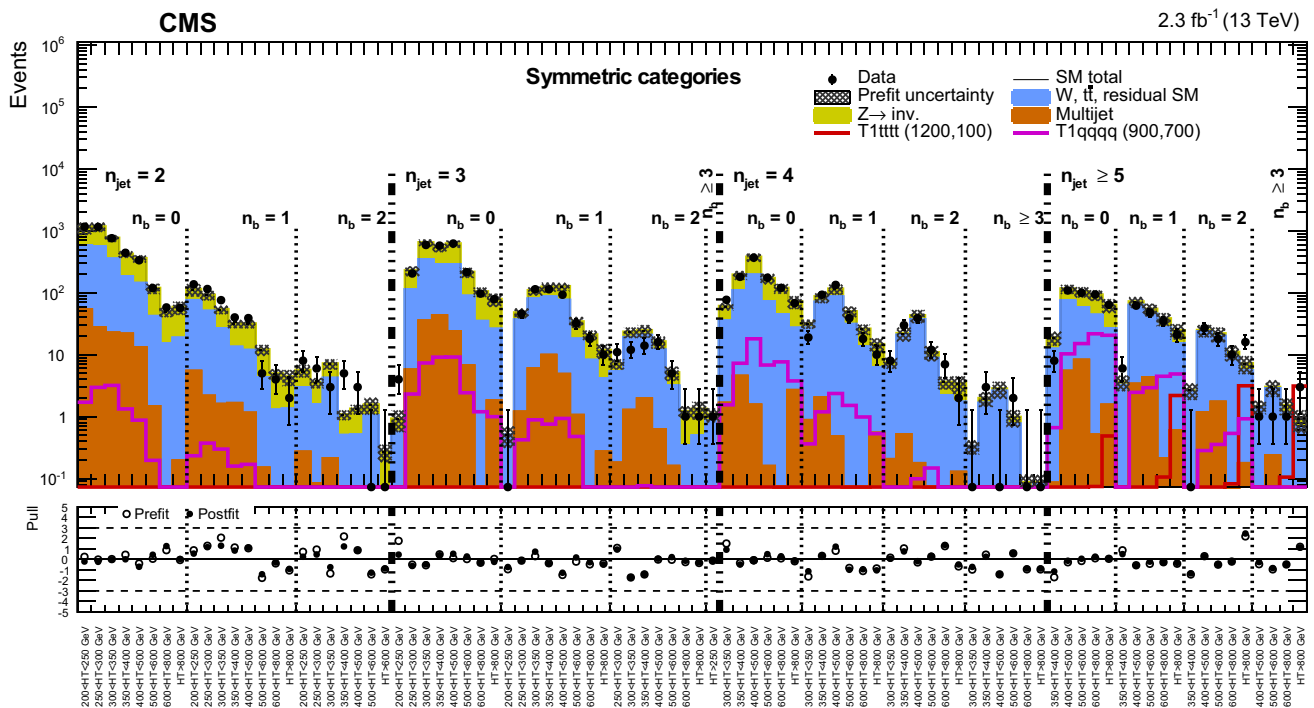
Fig. 4 (*Upper panel*) Event yields observed in data (*solid circles*) and pre-fit SM expectations with their associated uncertainties (*black histogram with shaded band*), integrated over H_T^{miss}, as a function of n_{jet}, n_b, and H_T for the asymmetric n_{jet} categories in the signal region. For illustration only, the expectations for two benchmark models (T2bb with $m_{\tilde{b}} = 400$ GeV and $m_{\tilde{\chi}_1^0} = 325$ GeV, T1tttt with $m_{\tilde{g}} = 800$ GeV and $m_{\tilde{\chi}_1^0} = 400$ GeV) are superimposed on the SM-only expectations. (*Lower panel*) The significance of deviations (pulls) observed in data with respect to the pre-fit (*open circles*) and post-fit (*closed circles*) SM expectations, expressed in terms of the total uncertainty in the SM expectations. The pulls cannot be considered independently due to inter-bin correlations

consistent with a uniform distribution, are obtained when considering events categorised according to n_{jet}.

The covariance and correlation matrices for the pre-fit SM expectations in all bins of the signal region, defined by n_{jet}, n_b, H_T, and integrated over H_T^{miss}, are determined from 500 pseudo-experiments by sampling the pre-fit nuisance parameters under the background-only hypothesis. The SM expectations for different n_{jet} and n_b categories exhibit a nonnegligible level of covariance within the same H_T bin, primarily as a result of the systematic uncertainties evaluated from closure tests, described in Sect. 6.2, that integrate yields over n_{jet} and n_b. Bins adjacent and next-to-adjacent in n_{jet} and/or n_b can have correlation coefficients in the range 0.2–0.4, and, infrequently, as large as ~0.5. Otherwise, the correlation coefficients are <0.2. Anticorrelation coefficients are typically not larger than ~0.2.

Figure 6 shows the event yields observed in data and pre-fit SM expectations with their associated uncertainties as a function of H_T^{miss} for two categories of candidate signal events, which provide good sensitivity to models with high-mass gluinos. For illustration only, the expected counts from benchmark signal models that assume the pair production and decay of gluinos, described further in Sect. 8, are also shown.

8 Interpretation

8.1 Specification for simplified models

The results of the search are used to constrain simplified SUSY models [92–94]. Each model assumes the pair production of gluinos or squarks and their subsequent prompt decays to SM particles and the LSP with a 100% branching fraction (unless indicated otherwise). The gluino decays contain intermediate on-shell SUSY particle states (such as the top squark or the chargino) for a subset of the models. All other SUSY particles are assumed to be too heavy ($m_{\tilde{g}}/m_{\tilde{q}} = 10$ TeV) to be produced directly. Three-body decays of gluinos are assumed to occur via off-shell squarks of light or heavy flavour. Off-shell decays are processed by PYTHIA in a single three- or four-body step, without taking into account the width or polarisation of the parent: this is true for the top-squark four-body decay ($\tilde{t} \to b f \bar{f}' \tilde{\chi}_1^0$), as well as the three-body decay of the chargino ($\tilde{\chi}_1^\pm \to f \bar{f}' \tilde{\chi}_1^0$), where f and f′ are fermions produced in the decay of an intermediate off-shell W boson.

Fourteen unique production and decay modes are considered, which yield a range of topologies and final states (with only the all-jet final state considered in this search). Each
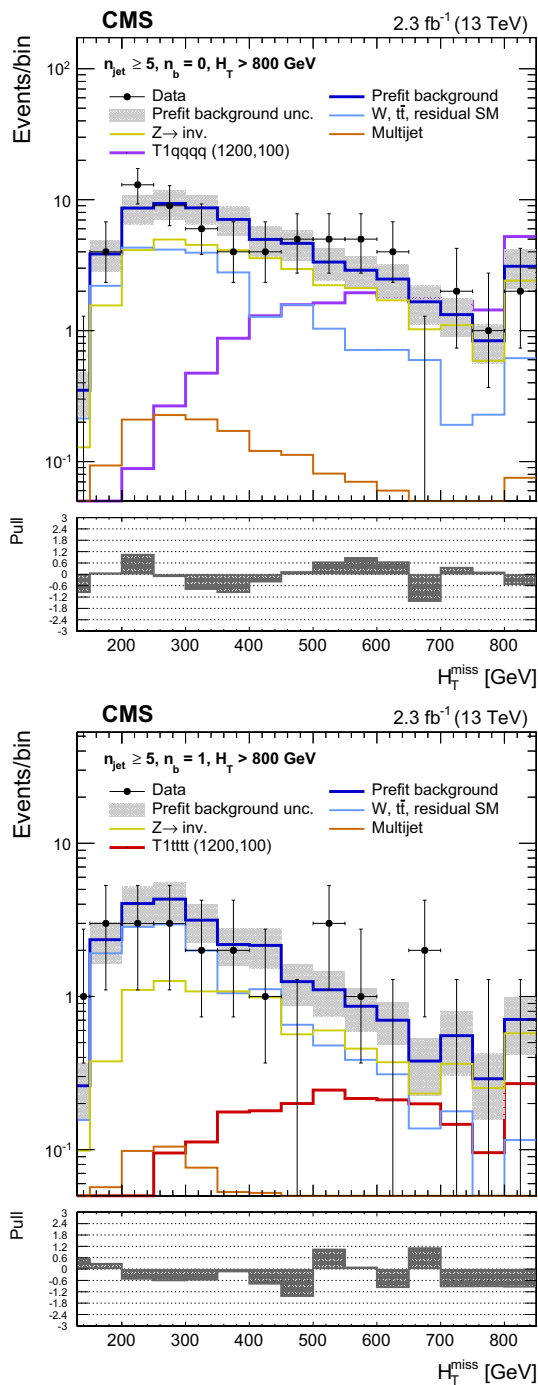
Fig. 5 (*Upper panel*) Event yields observed in data (*solid circles*) and pre-fit SM expectations with their associated uncertainties (*black histogram with shaded band*), integrated over H_T^{miss}, as a function of n_{jet}, n_b, and H_T for the symmetric n_{jet} categories in the signal region. For illustration only, the expectations for two benchmark models (T1tttt with $m_{\tilde{g}} = 1200\,\text{GeV}$ and $m_{\tilde{\chi}_1^0} = 100\,\text{GeV}$, T1qqqq with $m_{\tilde{g}} = 900\,\text{GeV}$ and $m_{\tilde{\chi}_1^0} = 700\,\text{GeV}$) are superimposed on the SM-only expectations. (*Lower panel*) The significance of deviations (pulls) observed in data with respect to the pre-fit (*open circles*) and post-fit (*closed circles*) SM expectations, expressed in terms of the total uncertainty in the SM expectations. The pulls cannot be considered independently due to inter-bin correlations

class of simplified model is identified by a label that indicates the topology and final state, and scans in the gluino or squark ($m_{\tilde{g}}/m_{\tilde{q}}$) and LSP ($m_{\tilde{\chi}_1^0}$) mass parameter space are performed. Table 4 summarises the production and decay modes, as well as any additional assumptions that define the simplified models. The models can be categorised according to the following descriptions: the gluino-mediated and direct production of light-flavour squarks, the gluino-mediated production of off-shell third-generation squarks, the natural gluino-mediated production of on-shell top squarks, and the direct production of on-shell third-generation squarks. In the case of direct pair production of light-flavour squarks, two different assumptions on the theoretical production cross section are made. For the "eightfold" scenario (T2qq_8fold), the scalar partners to left- and right-handed quarks of the u, d, s, and c flavours are assumed to be light and degenerate in mass, with other squark states decoupled to a high mass. For the "onefold" scenario (T2qq_1fold), only a single light squark is assumed to participate in the interaction and all other squarks are decoupled to a high mass.

Under the signal+background hypothesis, and in the presence of a nonzero signal contribution, a modified frequentist approach is used to determine upper limits at the 95% confidence level (CL) on the cross section, σ_{UL}, to produce pairs of

SUSY particles as a function of the parent SUSY particle and the LSP masses. The limits can be expressed in terms of the signal strength parameter, μ, which is determined relative to the theoretical cross section that is calculated at NLO + NLL accuracy. An Asimov data set [95] is used to determine the expected upper limit on the allowed cross section for a given model. The potential contributions from a new-physics signal to each of the signal and control regions are considered, even though the only significant contribution occurs in the signal region and not in the control regions (i.e. signal contamination). The approach is based on the one-sided (so called LHC-style) profile likelihood ratio as the test statistic [96] and the CL_s criterion [97,98]. Asymptotic formulae [95] are utilised to approximate the distributions of the test statistics under the SM background-only and signal+background hypotheses.

8.2 Acceptances and uncertainties

The experimental acceptance times efficiency ($\mathcal{A}\,\varepsilon$) and its uncertainty are evaluated independently for each model class as a function of (m_{SUSY}, m_{LSP}). Table 5 summarises $\mathcal{A}\,\varepsilon$ for a number of benchmark models for which the search yields an expected exclusion ($\mu \lesssim 1$). For each topology,

Fig. 6 Event yields observed in data (*solid circles*) and pre-fit SM expectations with their associated uncertainties (*blue histogram with shaded band*) as a function of H_T^{miss} for events in the signal region that satisfy $n_{jet} \geq 5$, $H_T > 800$ GeV, and (*top*) $n_b = 0$ or (*bottom*) $n_b = 1$. For illustration only, the expectations for one of two benchmark models (T1qqqq and T1tttt, both with $m_{\tilde{g}} = 1200$ GeV and $m_{\tilde{\chi}_1^0} = 100$ GeV) are superimposed on the SM-only expectations. The *lower panels* indicate the significance of deviations (pulls) observed in data with respect to both the pre-fit SM expectations, expressed in terms of the total uncertainty in the SM expectations. The pulls cannot be considered independently due to inter-bin correlations

typically two different pairs of parent SUSY particle and LSP masses (m_{SUSY}, m_{LSP}) are chosen that are characterised by a large and a small (i.e. compressed) difference in parent SUSY particle and LSP masses. The four most sensitive event categories, defined in terms of n_{jet}, are used to determine σ_{UL}. The categories used per benchmark model are listed in Table 5, along with $\mathcal{A}\varepsilon$ determined for these four categories.

The effects of several sources of uncertainty on $\mathcal{A}\varepsilon$, as well as the potential for event migration between bins of the signal region, are considered. The potential effect of each source of uncertainty is assessed by including in the likelihood function the alternative normalisations and shapes for the H_T^{miss} templates with respect to the nominal versions. The nominal and alternative templates are obtained from simulated event samples for the signal models, and the alternative templates effectively propagate the various input uncertainties to determine their effects on the n_{jet}, n_b, H_T, and H_T^{miss} distributions for the signal model.

In addition to the uncertainty in the integrated luminosity of 2.7% [99], the following sources of uncertainty are dominant: the statistical uncertainty arising from the finite size of simulated signal samples, the modelling of ISR, the jet energy corrections (JEC) evaluated in simulation, and the modelling of scale factors applied to simulated event samples that correct for differences in the efficiency and misidentification probability of b-quark jets ($SF_{b\text{-tag}}$). The magnitude of each contribution depends on the model and the masses of the parent SUSY particle and LSP.

The $\mathcal{A}\varepsilon$ for models with small mass splittings (e.g. $m_{\tilde{q}} - m_{\tilde{\chi}_1^0} \lesssim m_t$) is due largely to ISR, the modelling of which is evaluated by comparing the simulated and measured p_T spectra of the system recoiling against the ISR jets in $t\bar{t}$ events, using the technique described in Ref. [100]. The uncertainty can be as large as ∼30%, and is the dominant systematic uncertainty for systems with a compressed mass spectrum. Uncertainties in the jet energy scale, as large as ∼40%, can also be dominant for models characterised by high jet multiplicities in the final state. The uncertainties in $SF_{b\text{-tag}}$ can be as large as ∼25%. Table 5 summarises these dominant contributions to the uncertainty in $\mathcal{A}\varepsilon$ for a range of benchmark models. Characteristic values for each model are expressed in terms of a range that is representative of the values across all bins of the signal region. The upper bound for each range may be subject to moderate statistical fluctuations.

Further uncertainties with subdominant contributions are considered on a similar footing. The uncertainties in the efficiency of identifying well-reconstructed, isolated leptons are considered, with a typical magnitude of ∼5% and treated as anticorrelated between the signal and control regions. The uncertainty of 5% in σ_{in} is propagated through to the

Table 4 A summary of the simplified SUSY models used to interpret the results of this search. All on-shell SUSY particles in the decay are stated

Model class	Production	Decay	Additional assumptions
Gluino-mediated and direct production of light-flavour squarks			
T1qqqq	$pp \to \tilde{g}\tilde{g}$	$\tilde{g} \to \bar{q}q\tilde{\chi}_1^0$	–
T2qq_8fold	$pp \to \tilde{q}\bar{\tilde{q}}$	$\tilde{q} \to q\tilde{\chi}_1^0$	$m_{\tilde{q}} = m_{\tilde{q}_L} = m_{\tilde{q}_R}, \tilde{q} = \{\tilde{u}, \tilde{d}, \tilde{s}, \tilde{c}\}$
T2qq_1fold	$pp \to \tilde{q}\bar{\tilde{q}}$	$\tilde{q} \to q\tilde{\chi}_1^0$	$m_{\tilde{q}(\tilde{q} \neq \tilde{u}_L)} \gg m_{\tilde{u}_L}$
Gluino-mediated production of off-shell third-generation squarks			
T1bbbb	$pp \to \tilde{g}\tilde{g}$	$\tilde{g} \to \bar{b}b\tilde{\chi}_1^0$	–
T1tttt	$pp \to \tilde{g}\tilde{g}$	$\tilde{g} \to \tilde{t}\bar{t}^* \to \bar{t}t\tilde{\chi}_1^0$	–
T1ttbb	$pp \to \tilde{g}\tilde{g}$	$\tilde{g} \to \bar{t}b\tilde{\chi}_1^\pm \to \bar{t}bW^*\tilde{\chi}_1^0$	$m_{\tilde{\chi}_1^\pm} - m_{\tilde{\chi}_1^0} = 5\,\text{GeV}$
Natural gluino-mediated production of on-shell top squarks			
T5tttt_DM175	$pp \to \tilde{g}\tilde{g}$	$\tilde{g} \to \tilde{t}\bar{t} \to \bar{t}t\tilde{\chi}_1^0$	$m_{\tilde{t}} - m_{\tilde{\chi}_1^0} = 175\,\text{GeV}$
T5ttcc	$pp \to \tilde{g}\tilde{g}$	$\tilde{g} \to \tilde{t}\bar{t} \to \bar{t}c\tilde{\chi}_1^0$	$m_{\tilde{t}} - m_{\tilde{\chi}_1^0} = 20\,\text{GeV}$
Direct production of on-shell third-generation squarks			
T2bb	$pp \to \tilde{b}\bar{\tilde{b}}$	$\tilde{b} \to b\tilde{\chi}_1^0$	–
T2tb	$pp \to \tilde{t}\bar{\tilde{t}}$	$\tilde{t} \to t\tilde{\chi}_1^0$ or $b\tilde{\chi}_1^\pm \to bW^*\tilde{\chi}_1^0$	50/50%, $m_{\tilde{\chi}_1^\pm} - m_{\tilde{\chi}_1^0} = 5\,\text{GeV}$
T2tt	$pp \to \tilde{t}\bar{\tilde{t}}$	$\tilde{t} \to t\tilde{\chi}_1^0$	–
T2cc	$pp \to \tilde{t}\bar{\tilde{t}}$	$\tilde{t} \to c\tilde{\chi}_1^0$	$10 < m_{\tilde{t}} - m_{\tilde{\chi}_1^0} < 80\,\text{GeV}$
T2tt_degen	$pp \to \tilde{t}\bar{\tilde{t}}$	$\tilde{t} \to bW^*\tilde{\chi}_1^0$	$10 < m_{\tilde{t}} - m_{\tilde{\chi}_1^0} < 80\,\text{GeV}$
T2tt_mixed	$pp \to \tilde{t}\bar{\tilde{t}}$	$\tilde{t} \to c\tilde{\chi}_1^0$ or $bW^*\tilde{\chi}_1^0$	50/50%, $10 < m_{\tilde{t}} - m_{\tilde{\chi}_1^0} < 80\,\text{GeV}$

reweighting procedure to account for differences between the simulated and measured pileup. Finally, uncertainties in the simulation modelling of the efficiencies of the trigger strategy employed by the search are typically <10%.

The choice of PDF set, or variations therein, predominantly affects $\mathcal{A}\varepsilon$ through changes in the p_T spectrum of the system recoil, which is covered by the ISR uncertainty, hence no additional uncertainty is adopted. Uncertainties in $\mathcal{A}\varepsilon$ due to variations in the renormalisation and factorisation scales are determined to be ∼5%. In both cases, contributions to the uncertainty in the theoretical production cross section are considered.

8.3 Cross section and mass exclusions

Limits for each of the aforementioned benchmark models are summarised in Table 5, expressed in terms of μ. All benchmark models are expected to be excluded. The observed limits fluctuate around the expected μ values, with some models exhibiting a moderately weaker than expected limit.

Figures 7 and 8 summarise the disfavoured regions of the mass parameter space for the fourteen classes of simplified models. These regions are derived by comparing the upper limits on the measured fiducial cross section, corrected for the experimental $\mathcal{A}\varepsilon$, with the theoretical cross sections calculated at NLO+NLL accuracy in α_s [33]. The former cross section value is determined as a function of $m_{\tilde{g}}$ or $m_{\tilde{q}}$ and

$m_{\tilde{\chi}_1^0}$, while the latter has a dependence solely on $m_{\tilde{g}}$ or $m_{\tilde{q}}$. The exclusion of models is evaluated using observed data counts in the signal region (solid contours) and also expected counts based on an Asimov data set (dashed contours).

Figure 7 (upper) shows the excluded mass parameter space for models that assume the gluino-mediated or direct production of light-flavour squarks. The excluded region extends to higher masses for the gluino-mediated production of light-flavour squarks (T1qqqq), with respect to direct pair production when assuming an eightfold degeneracy in mass (T2qq_8fold), due to a combination of a higher gluino pair production cross section and a final state characterised by higher jet multiplicities, which are exploited to provide better signal-to-background separation. The excluded mass region is significantly reduced when assuming only a single light squark (T2qq_1fold), with limits weakening due to the lower production cross section, compounded by the reduced signal-to-background ratios achieved in the core of distributions in the discriminating variables.

Figure 7 (lower) shows the exclusion contours for models that assume the gluino-mediated pair production of off-shell third-generation squarks. For the topologies T1tttt and T1bbbb, each gluino is assumed to undergo a three-body decay via, respectively, an off-shell top or bottom squark to a quark-antiquark pair of the same flavour and the $\tilde{\chi}_1^0$. In the case of T1ttbb, each gluino is assumed to undergo a three-body decay to an on-shell chargino, $\tilde{\chi}_1^\pm$, a bottom quark, and

Table 5 A summary of benchmark simplified models, the most sensitive n_{jet} categories, and representative values for the corresponding experimental acceptance times efficiency ($\mathcal{A}\varepsilon$), the dominant system- atic uncertainties, the theoretical production cross section (σ_{theory}), and the expected and observed upper limits on the production cross section, expressed in terms of the signal strength parameter (μ)

Benchmark models		Most sensitive	$\mathcal{A}\varepsilon$	Systematic uncertainties [%]				σ_{theory}	μ (95% CL)	
$(m_{\text{SUSY}}, m_{\text{LSP}})$ [GeV]		n_{jet} categories	[%]	MC stat.	ISR	JEC	$SF_{b-\text{tag}}$	[fb]	Exp.	Obs.
T1qqqq	(1300, 100)	$\geq 5, 4, 3, 2$	21.2	7–30	~2	4–21	2–14	46.1	0.79	0.76
	(900, 700)	$\geq 5, \geq 5a, 4, 4a$	12.8	10–33	1–13	1–26	1–10	677	0.58	0.44
T2qq_8fold	(1050, 100)	$\geq 5, 3, 4, 2$	40.3	7–33	1–4	3–16	1–11	35.2	0.90	0.63
	(650, 550)	$\geq 5, 4, \geq 5a, 4a$	6.3	10–28	1–16	2–29	1–6	864	0.93	0.80
T2qq_1fold	(600, 50)	$5, 3, 2, 4$	30.2	5–33	1–5	1–30	1–8	177	0.78	0.84
	(400, 250)	$\geq 5, 4, \geq 5a, 3$	7.1	8–30	1–8	3–25	1–7	1849	0.73	0.71
T1bbbb	(1500, 100)	$\geq 5, 4, 3, 2$	22.7	5–17	1–2	1–12	2–22	14.2	0.81	0.79
	(1000, 800)	$\geq 5, 4, \geq 5a, 4a$	11.4	8–31	1–17	1–40	1–14	325	0.33	0.32
T1ttbb	(1300, 100)	$\geq 5, \geq 5a, 4, 3$	5.3	7–16	1–2	2–7	2–12	46.1	1.00	1.89
	(800, 400)	$\geq 5, \geq 5a, 4, 4a$	1.5	7–27	1–2	3–45	1–8	1490	0.56	1.03
T1ttbb	(1300, 100)	$\geq 5, 4, 3, \geq 5a$	8.5	9–32	1–2	3–16	2–19	46.1	0.60	0.91
	(1000, 700)	$\geq 5, \geq 5a, 4, 3$	7.7	9–30	1–9	3–65	1–14	325	0.51	0.70
T5tttt_DM175	(800, 100)	$\geq 5, \geq 5a, 3, 4$	0.5	12–20	2–4	3–5	1–6	1490	0.69	1.19
	(700, 400)	$\geq 5, \geq 5a, 4, 4a$	0.5	20–29	2–10	8–10	1–2	3530	1.00	1.35
T5ttcc	(1200, 200)	$\geq 5, 4, 3, \geq 5a$	11.0	6–25	5–25	3–21	1–24	85.6	0.58	0.87
	(750, 600)	$\geq 5, \geq 5a, 4, 4a$	2.2	9–23	1–4	5–21	1–3	2270	0.89	0.72
T2bb	(800, 50)	$2, 3, 4, \geq 5$	34.9	5–31	2–6	1–21	1–23	28.3	0.96	1.06
	(375, 300)	$\geq 5, 4, 3a, 3$	3.2	8–33	1–10	3–25	1–7	2610	0.67	0.87
T2tb	(600, 50)	$\geq 5, 4, 3, 2$	13.4	3–28	1–3	1–22	1–17	175	0.70	1.35
	(350, 225)	$\geq 5, 4, 3, 3a$	2.3	9–33	1–4	2–41	1–8	3790	0.79	0.88
T2tt	(700, 50)	$\geq 5, 4, 3, \geq 5a$	18.2	8–33	1–4	2–22	1–21	67.0	0.90	1.19
	(350, 100)	$\geq 5, \geq 5a, 4a, 4$	3.4	7–31	1–1	1–28	1–7	3790	0.44	0.50
T2cc	(325, 305)	$\geq 5, 4, 3, 2$	1.9	3–32	1–27	1–27	1–12	5600	0.92	0.68
T2tt_degen	(300, 290)	$3, 4, \geq 5, 2$	2.0	2–27	1–27	1–25	1–12	8520	0.56	0.41
T2tt_mixed	(300, 250)	$\geq 5, 4, \geq 5a, 4a$	1.0	3–33	1–27	1–33	1–13	8520	0.99	0.58

a top antiquark. The chargino mass is defined relative to the neutralino mass via the expression $m_{\widetilde{\chi}_1^{\pm}} - m_{\widetilde{\chi}_1^0} = 5\,\text{GeV}$. The chargino decays promptly to the $\widetilde{\chi}_1^0$ and an off-shell W boson. The excluded mass regions differ significantly for these topologies, primarily due to the different number of (on-shell) W bosons in their final states, resulting in the highest $\mathcal{A}\varepsilon$ for T1bbbb and lowest for T1tttt. Further, $\mathcal{A}\varepsilon$ has a strong dependence on jet multiplicity, which is highest for T1tttt, due to the $\Delta\phi_{\text{min}}^*$ variable. An additional feature for T1ttbb is the weakening of the mass limit at low values of $m_{\widetilde{\chi}_1^0}$, when $m_{\widetilde{\chi}_1^{\pm}} = m_{\widetilde{\chi}_1^0} + 5\,\text{GeV} \lesssim m_{\text{t}}$. In this scenario, the $\widetilde{\chi}_1^{\pm}$ (and hence $\widetilde{\chi}_1^0$) is not highly Lorentz boosted relative to the top quark resulting from the three-body decay of the gluino. Hence, two $\widetilde{\chi}_1^0$ SUSY particles do not carry away significant $\vec{p}_{\text{T}}^{\text{miss}}$, which is instead realised through W boson decays to neutrinos and "lost" leptons or τ leptons that decay to neutrinos and hadrons. The observed mass limits for these topologies are up to ~2 standard deviations weaker than the expected limits. These differences are due to upward fluctuations in data for two contiguous bins that satisfy the requirements $n_{\text{jet}} \geq 5$, $n_b \geq 2$, and $H_T > 800\,\text{GeV}$. This region has the highest sensitivity to models involving gluino production and decays to third-generation quarks (via on- or off-shell squarks). The observed counts are consistent with statistical fluctuations and the events do not exhibit anomalous nonphysical behaviour. The events are distributed in H_T^{miss} consistent with expectation, hence models characterised by high values of H_T^{miss}, such as T1bbbb with $m_{\widetilde{g}} \gg m_{\widetilde{\chi}_1^0}$ or $m_{\widetilde{g}} \approx m_{\widetilde{\chi}_1^0}$, are less compatible with the data counts in this high-n_{jet}, n_b, and H_T region.

Figure 8 (upper) shows exclusion contours for models that assume gluino pair production, with each gluino decaying to a top quark and an on-shell top squark, the latter of which decays to SM particles and the LSP. As discussed earlier, these models can be considered as representations of a natural solution to the little hierarchy problem. Two different scenarios are considered for the decay of the top squarks.
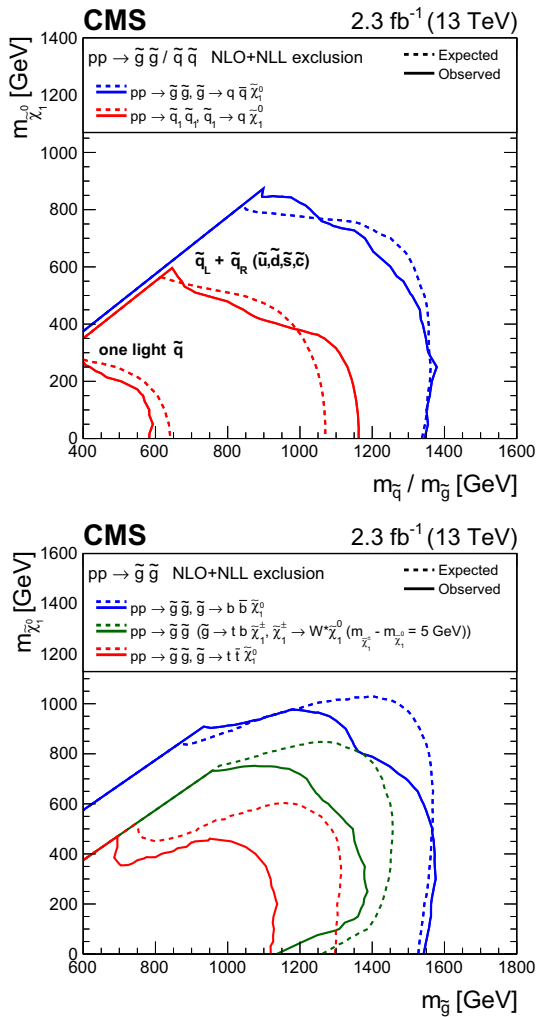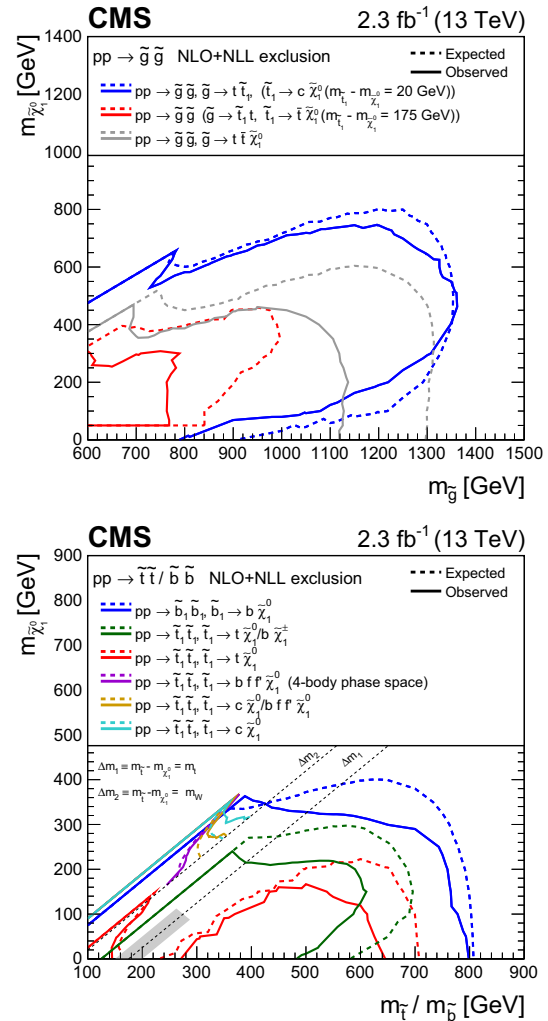
Fig. 7 Observed and expected mass exclusions at 95% CL (indicated, respectively, by *solid* and *dashed contours*) for various classes of simplified models. (*Top*) Gluino-mediated or direct pair production of light-flavour squarks. The two scenarios involve, respectively, the decay $\tilde{g} \to \bar{q}q\tilde{\chi}_1^0$ (T1qqqq) and $\tilde{q} \to q\tilde{\chi}_1^0$, and the latter involves two assumptions on the mass degeneracy of the squarks (T2qq_8fold and T2qq_1fold). (*Bottom*) Three scenarios involving the gluino-mediated pair production of off-shell third-generation squarks: $\tilde{g} \to \bar{b}b\tilde{\chi}_1^0$ (T1bbbb), $\tilde{g} \to \tilde{t}\tilde{t}^* \to \bar{t}t\tilde{\chi}_1^0$ (T1tttt), and $\tilde{g} \to \bar{t}b\tilde{\chi}_1^\pm \to \bar{t}bW^*\tilde{\chi}_1^0$ (T1ttbb)

Fig. 8 Observed and expected mass exclusions at 95% CL (indicated, respectively, by *solid* and *dashed contours*) for a number of simplified models. (*Top*) Two scenarios involving the gluino-mediated pair production of on-shell top squarks: $\tilde{g} \to \tilde{t}\tilde{t} \to \bar{t}t\tilde{\chi}_1^0$ with $m_{\tilde{t}} - m_{\tilde{\chi}_1^0} = 175$ GeV (T5tttt_DM175) and $\tilde{g} \to \tilde{t}\tilde{t} \to \bar{t}c\tilde{\chi}_1^0$ with $m_{\tilde{t}} - m_{\tilde{\chi}_1^0} = 20$ GeV (T5ttcc). Also shown, for comparison, is T1tttt. (*Bottom*) Six scenarios involving the direct pair production of third-generation squarks. The first scenario involves the pair production of bottom squarks, $\tilde{b} \to b\tilde{\chi}_1^0$ (T2bb). Two scenarios involve the decay of top squark pairs as follows: $\tilde{t} \to t\tilde{\chi}_1^0$ or $\tilde{t} \to b\tilde{\chi}_1^\pm \to bW^*\tilde{\chi}_1^0$ with $m_{\tilde{\chi}_1^\pm} - m_{\tilde{\chi}_1^0} = 5$ GeV and branching fractions 50/50% (T2tb), or $\tilde{t} \to t\tilde{\chi}_1^0$ (T2tt). The final three scenarios consider top squark decays under the assumption $10 < m_{\tilde{t}} - m_{\tilde{\chi}_1^0} < 80$ GeV: $\tilde{t} \to c\tilde{\chi}_1^0$ (T2cc), $\tilde{t} \to bW^*\tilde{\chi}_1^0$ (T2tt_degen), and $\tilde{t} \to c\tilde{\chi}_1^0$ or $\tilde{t} \to bW^*\tilde{\chi}_1^0$ with branching fractions 50/50% (T2tt_mixed). The *grey shaded region* denotes T2tt models that are not considered for interpretation

The T5tttt_DM175 models assume a two-body decay to a top quark and the $\tilde{\chi}_1^0$, with the top squark mass defined relative to the $\tilde{\chi}_1^0$ as $m_{\tilde{t}} - m_{\tilde{\chi}_1^0} = m_t$. Models that satisfy $m_{\tilde{\chi}_1^0} < 50$ GeV are not considered here, as the $\tilde{\chi}_1^0$ particles carry very little momentum. The T5ttcc models assume $m_{\tilde{t}} - m_{\tilde{\chi}_1^0} = 20$ GeV and two-body decays to a charm quark and the $\tilde{\chi}_1^0$.

Finally, Fig. 8 (lower) shows exclusion contours for models that assume the direct production of pairs of third-generation squarks. For the T2bb models, bottom squarks are pair produced and each decays to a bottom quark and the

$\tilde{\chi}_1^0$. The T2tt models assume top squarks are pair produced and each is assumed to undergo a two- or three-body decay to, respectively, a top quark and the $\tilde{\chi}_1^0$ when $m_{\tilde{t}} - m_{\tilde{\chi}_1^0} > m_t$ is satisfied, or a b quark, an on-shell W boson, and the $\tilde{\chi}_1^0$ for the condition $m_W < m_{\tilde{t}} - m_{\tilde{\chi}_1^0} < m_t$. Models that satisfy

Table 6 Summary of the mass limits obtained for the fourteen classes of simplified models. The limits indicate the strongest observed and expected (in parentheses) mass exclusions in $\widetilde{g}$, $\widetilde{q}$, $\widetilde{b}$, $\widetilde{t}$, and $\widetilde{\chi}_1^0$. The quoted values have uncertainties of ± 25 and ± 10 GeV for models involving the pair production of, respectively, gluinos and squarks

Model class	Parent SUSY particle	Best mass limit [GeV]	
		$\widetilde{g}/\widetilde{q}/\widetilde{b}/\widetilde{t}$	$\widetilde{\chi}_1^0$
T1qqqq	$\widetilde{g}$	1375 (1350)	875 (850)
T2qq_8fold	$\widetilde{q}$	1150 (1075)	600 (550)
T2qq_1fold	$\widetilde{q}$	575 (650)	275 (275)
T1bbbb	$\widetilde{g}$	1575 (1575)	975 (1025)
T1tttt	$\widetilde{g}$	1125 (1325)	475 (600)
T1ttbb	$\widetilde{g}$	1375 (1450)	750 (850)
T5tttt_DM175	$\widetilde{g}$	800 (1000)	300 (450)
T5ttcc	$\widetilde{g}$	1350 (1350)	700 (800)
T2bb	$\widetilde{b}$	800 (800)	360 (400)
T2tb	$\widetilde{t}$	610 (690)	240 (300)
T2tt (3-body)	$\widetilde{t}$	670 (720)	210 (240)
T2tt (2-body)	$\widetilde{t}$	280 (280)	200 (200)
T2cc	$\widetilde{t}$	400 (350)	310 (340)
T2tt_degen	$\widetilde{t}$	370 (360)	360 (350)
T2tt_mixed	$\widetilde{t}$	360 (350)	350 (340)

$|m_{\widetilde{t}} - m_t - m_{\widetilde{\chi}_1^0}| < 25$ GeV and $m_{\widetilde{t}} + m_{\widetilde{\chi}_1^0} < 375$ GeV are not considered here, as σ_{UL} is a strong function of $m_{\widetilde{t}} - m_{\widetilde{\chi}_1^0}$ in this low-$m_{\widetilde{t}}$ region due to the high levels of signal contamination found in the $\mu +$ jets control region for models that resemble the $t\bar{t}$ background in terms of their topological and kinematic properties. The T2tb models also assume the pair production of top squarks, with each undergoing a two-body decay to either a top quark and the $\widetilde{\chi}_1^0$, or a bottom quark and the $\widetilde{\chi}_1^\pm$, with equal branching fractions of 50%. As for the T1ttbb models, the chargino mass is defined relative to the neutralino mass via the expression $m_{\widetilde{\chi}_1^\pm} - m_{\widetilde{\chi}_1^0} = 5$ GeV, and the chargino decays promptly to the $\widetilde{\chi}_1^0$ and an off-shell W boson. The excluded mass regions differ significantly for the T2bb, T2tb, and T2tt topologies, in an analogous way to the T1bbbb, T1ttbb, and T1tttt models described above. The difference in the mass exclusions is due primarily to the different number of (on-shell) W bosons in the final states, which affects $\mathcal{A}\varepsilon$ through the presence of leptons from the decay of the W boson. An additional feature for T2tb is the weakening of the mass limit at low values of $m_{\widetilde{\chi}_1^0}$, when $m_{\widetilde{\chi}_1^\pm} = m_{\widetilde{\chi}_1^0} + 5$ GeV $\lesssim m_t$. Moderately weaker than expected mass limits are observed for all models involving two-body decays, which is traced to mild upward fluctuations in data for events satisfying $n_{jet} = 2$, $n_b = 2$, and $350 < H_T < 500$ GeV.

Figure 8 (lower) also shows exclusion contours for models that assume the pair production of top squarks but a near-mass-degenerate system that satisfies 10 GeV $< m_{\widetilde{t}} - m_{\widetilde{\chi}_1^0} < m_W$. Two decays of the top squark are considered. The T2cc and T2tt_degen models assume two- and four-body decays of the top squark to, respectively, a charm quark and the $\widetilde{\chi}_1^0$, or to $bff'\widetilde{\chi}_1^0$, where f and $\bar{f}'$ are fermions produced

in the decay of an intermediate off-shell W boson. A third class of models, T2tt_mixed, assumes both these decay modes with an equal branching fraction of 50%. For T2cc, the excluded mass region is relatively stable as a function of the mass splitting $\Delta m = m_{\widetilde{t}} - m_{\widetilde{\chi}_1^0}$, with $\widetilde{t}$ masses excluded up to 400 GeV. For T2tt_degen, the excluded mass region is strongly dependent on Δm, weakening considerably for increasing values of Δm due to the increased momentum phase space available to leptons produced in the four-body decay. The T2tt_mixed models exhibit an intermediate behaviour. Mass limits for all three model classes converge for the smallest mass splitting considered, $\Delta m = 10$ GeV, when the SM particles from the $\widetilde{t}$ decay are extremely soft and outside the experimental acceptance. An approximately contiguous mass exclusion limit is observed across the transition from the T2tt_degen four-body to the T2tt three-body decay of the $\widetilde{t}$, as the top quark moves on-shell. The excluded mass region weakens further as $\Delta m \to m_t$.

Table 6 summarises the strongest expected and observed mass limits for each class of simplified model.

9 Summary

An inclusive search for new-physics phenomena is reported, based on data from pp collisions at $\sqrt{s} = 13$ TeV. The data are recorded with the CMS detector and correspond to an integrated luminosity of 2.3 ± 0.1 fb^{-1}. The final states analysed contain one or more jets with large transverse momenta and a significant imbalance of transverse momentum, as expected from the production of massive coloured SUSY particles,

each decaying to SM particles and the lightest stable, weakly-interacting, SUSY particle.

The sums of the standard model backgrounds are estimated from a simultaneous binned likelihood fit to the observed yields for samples of events categorised according to the number of reconstructed jets, the number of jets identified as originating from b quarks, and the scalar and the magnitude of the vector sums of the transverse momenta of jets. In addition to the signal region, $\mu + \text{jets}$, $\mu\mu + \text{jets}$, and $\gamma + \text{jets}$ control regions are included in the likelihood fit. The observed yields are found to be in agreement with the expected contributions from standard model processes. The search result is interpreted in the mass parameter space of fourteen simplified SUSY models, which cover scenarios that involve the gluino-mediated or direct production of light- or heavy-flavour squarks, intermediate SUSY particle states, as well as natural and nearly mass-degenerate spectra.

The increase in the centre-of-mass energy of the LHC, from 8 to 13 TeV, provides a significant gain in sensitivity to heavy particle states such as gluinos. In the case of pair-produced gluinos, each decaying via an off-shell b squark to the b quark and the LSP, models with masses up to $\sim$1.6 and $\sim$1.0 TeV are excluded for, respectively, the gluino and LSP. These limits improve on those obtained at $\sqrt{s} = 8$ TeV by, respectively, $\sim$250 and $\sim$300 GeV. In the case of direct pair production, models with masses up to $\sim$800 and $\sim$350 GeV are excluded for, respectively, the b squark and LSP. These mass limits are sensitive to the assumptions on the squark flavour and the presence of intermediate states such as charginos.

Finally, a comprehensive study of nearly mass-degenerate models involving top squark pair production is performed. The two decay modes of the top squark are the loop-induced two-body decay to the neutralino and one c quark, and the four-body decay to the neutralino, one b quark, and an off-shell W boson. A third scenario is considered in which the two modes are simultaneously open, each with a branching fraction of 50%. Masses of the top squark and LSP up to, respectively, 400 and 360 GeV are excluded, depending on the decay modes considered.

In conclusion, the analysis provides sensitivity across a large region of the natural SUSY parameter space, as characterised by interpretations with several simplified models. In particular, these studies improve on existing limits for nearly mass-degenerate models involving the production of pairs of top squarks.

References

1. Y.A. Gol'fand, E.P. Likhtman, Extension of the algebra of Poincare group generators and violation of p invariance. JETP Lett. **13**, 323 (1971)
2. J. Wess, B. Zumino, Supergauge transformations in four dimensions. Nucl. Phys. B **70**, 39 (1974). doi:10.1016/0550-3213(74)90355-1
3. R. Barbieri, S. Ferrara, C.A. Savoy, Gauge models with spontaneously broken local supersymmetry. Phys. Lett. B **119**, 343 (1982). doi:10.1016/0370-2693(82)90685-2
4. H.P. Nilles, Supersymmetry, supergravity and particle physics. Phys. Rep. **110**, 1 (1984). doi:10.1016/0370-1573(84)90008-5
5. S. Dawson, E. Eichten, C. Quigg, Search for supersymmetric particles in hadron-hadron collisions. Phys. Rev. D **31**, 1581 (1985). doi:10.1103/PhysRevD.31.1581
6. H.E. Haber, G.L. Kane, The search for supersymmetry: probing physics beyond the standard model. Phys. Rep. **117**, 75 (1985). doi:10.1016/0370-1573(85)90051-1
7. G.R. Farrar, P. Fayet, Phenomenology of the production, decay, and detection of new hadronic states associated with supersymmetry. Phys. Lett. B **76**, 575 (1978). doi:10.1016/0370-2693(78)90858-4
8. G. Jungman, M. Kamionkowski, K. Griest, Supersymmetric dark matter. Phys. Rep. **267**, 195 (1996). doi:10.1016/0370-1573(95)00058-5. arXiv:hep-ph/9506380
9. Particle Data Group, K.A. Olive et al., Review of particle physics. Chin. Phys. C **38**, 090001 (2014). doi:10.1088/1674-1137/38/9/090001
10. S. Dimopoulos, S. Raby, F. Wilczek, Supersymmetry and the scale of unification. Phys. Rev. D **24**, 1681 (1981). doi:10.1103/PhysRevD.24.1681
11. L.E. Ibanez, G.G. Ross, Low-energy predictions in supersymmetric grand unified theories. Phys. Lett. B **105**, 439 (1981). doi:10.1016/0370-2693(81)91200-4
12. W.J. Marciano, G. Senjanović, Predictions of supersymmetric grand unified theories. Phys. Rev. D **25**, 3092 (1982). doi:10.1103/PhysRevD.25.3092
13. ATLAS Collaboration, Observation of a new particle in the search for the Standard Model Higgs boson with the ATLAS detector at the LHC. Phys. Lett. B **716**, 1 (2012). doi:10.1016/j.physletb.2012.08.020. arXiv:1207.7214
14. CMS Collaboration, Observation of a new boson at a mass of 125 GeV with the CMS experiment at the LHC. Phys. Lett. B **716**, 30 (2012). doi:10.1016/j.physletb.2012.08.021
15. CMS Collaboration, Observation of a new boson with mass near 125 GeV in pp collisions at $\sqrt{s} = 7$ and 8 TeV. JHEP **06**, 081 (2013). doi:10.1007/JHEP06(2013)081. arXiv:1303.4571
16. E. Witten, Dynamical breaking of supersymmetry. Nucl. Phys. B **188**, 513 (1981). doi:10.1016/0550-3213(81)90006-7
17. S. Dimopoulos, H. Georgi, Softly broken supersymmetry and SU(5). Nucl. Phys. B **193**, 150 (1981). doi:10.1016/0550-3213(81)90522-8
18. R. Barbieri, D. Pappadopulo, S-particles at their naturalness limits. JHEP **10**, 061 (2009). doi:10.1088/1126-6708/2009/10/061. arXiv:0906.4546
19. C. Boehm, A. Djouadi, M. Drees, Light scalar top quarks and supersymmetric dark matter. Phys. Rev. D **62**, 035012 (2000). doi:10.1103/PhysRevD.62.035012. arXiv:hep-ph/9911496
20. C. Boehm, A. Djouadi, Y. Mambrini, Decays of the lightest top squark. Phys. Rev. D **61**, 095006 (2000). doi:10.1103/PhysRevD.61.095006. arXiv:hep-ph/9907428
21. C. Balazs, M.S. Carena, C.E.M. Wagner, Dark matter, light stops and electroweak baryogenesis. Phys. Rev. D **70**, 015007 (2004). doi:10.1103/PhysRevD.70.015007. arXiv:hep-ph/0403224
22. S.P. Martin, Compressed supersymmetry and natural neutralino dark matter from top squark-mediated annihilation to top quarks. Phys. Rev. D **75**, 115005 (2007). doi:10.1103/PhysRevD.75.115005. arXiv:hep-ph/0703097
23. S.P. Martin, Top squark-mediated annihilation scenario and direct detection of dark matter in compressed supersymmetry. Phys. Rev. D **76**, 095005 (2007). doi:10.1103/PhysRevD.76.095005. arXiv:0707.2812
24. M. Carena, A. Freitas, C.E.M. Wagner, Light stop searches at the LHC in events with one hard photon or jet and missing energy. JHEP **10**, 109 (2008). doi:10.1088/1126-6708/2008/10/109. arXiv:0808.2298
25. A. Delgado et al., The light stop window. Eur. Phys. J. C **73**, 2370 (2013). doi:10.1140/epjc/s10052-013-2370-5. arXiv:1212.6847
26. R. Grober, M.M. Muhlleitner, E. Popenda, A. Wlotzka, Light stop decays: implications for LHC searches. Eur. Phys. J. C **75**, 420 (2015). doi:10.1140/epjc/s10052-015-3626-z. arXiv:1408.4662
27. R. Grober, M. Muhlleitner, E. Popenda, A. Wlotzka, Light stop decays into $Wb\tilde{\chi}_1^0$ near the kinematic threshold. Phys. Lett. B **747**, 144 (2015). doi:10.1016/j.physletb.2015.05.060. arXiv:1502.05935
28. CMS Collaboration, Search for supersymmetry in pp collisions at 7 TeV in events with jets and missing transverse energy. Phys. Lett. B **698**, 196 (2011). doi:10.1016/j.physletb.2011.03.021. arXiv:1101.1628
29. CMS Collaboration, Search for supersymmetry at the LHC in events with jets and missing transverse energy. Phys. Rev. Lett. **107**, 221804 (2011). doi:10.1103/PhysRevLett.107.221804
30. CMS Collaboration, Search for supersymmetry in final states with missing transverse energy and 0, 1, 2, or $\geq$3 b-quark jets in 7 TeV pp collisions using the variable α_T. JHEP **01**, 077 (2013). doi:10.1007/JHEP01(2013)077
31. CMS Collaboration, Search for supersymmetry in hadronic final states with missing transverse energy using the variables α_T and b-quark multiplicity in pp collisions at $\sqrt{s} = 8$ TeV. Eur. Phys. J. C **73**, 2568 (2013). doi:10.1140/epjc/s10052-013-2568-6. arXiv:1303.2985
32. CMS Collaboration, Search for top squark pair production in compressed-mass-spectrum scenarios in proton–proton collisions at $\sqrt{s} = 8$ TeV using the α_T variable (2016). arXiv:1605.08993 (Submitted to Phys. Lett. B)
33. C. Borschensky et al., Squark and gluino production cross sections in pp collisions at $\sqrt{s} = 13$, 14, 33 and 100 TeV. Eur. Phys. J. C **74**, 3174 (2014). doi:10.1140/epjc/s10052-014-3174-y. arXiv:1407.5066
34. ATLAS Collaboration, Summary of the searches for squarks and gluinos using $\sqrt{s} = 8$ TeV pp collisions with the ATLAS experiment at the LHC. JHEP **10**, 054 (2015). doi:10.1007/JHEP10(2015)054. arXiv:1507.05525

35. ATLAS Collaboration, ATLAS Run 1 searches for direct pair production of third-generation squarks at the Large Hadron Collider. Eur. Phys. J. C **75**, 510 (2015). doi:10.1140/epjc/s10052-015-3726-9. arXiv:1506.08616 [Erratum: Eur. Phys. J. C **76**, (2016) 153. doi:10.1140/epjc/s10052-016-3935-x]

36. CMS Collaboration, Searches for supersymmetry based on events with b jets and four W bosons in pp collisions at 8 TeV. Phys. Lett. B **745**, 5 (2015). doi:10.1016/j.physletb.2015.04.002. arXiv:1412.4109

37. CMS Collaboration, Searches for supersymmetry using the M_{T2} variable in hadronic events produced in pp collisions at 8 TeV. JHEP **05**, 078 (2015). doi:10.1007/JHEP05(2015)078

38. CMS Collaboration, Search for direct pair production of supersymmetric top quarks decaying to all-hadronic final states in pp collisions at $\sqrt{s} = 8$. Eur. Phys. J. C **76**, 460 (2016). doi:10.1140/epjc/s10052-016-4292-5. arXiv:1603.00765

39. CMS Collaboration, Search for gluino mediated bottom- and top-squark production in multijet final states in pp collisions at 8 TeV. Phys. Lett. B **725**, 243 (2013). doi:10.1016/j.physletb.2013.06.058. arXiv:1305.2390

40. CMS Collaboration, Search for new physics in the multijet and missing transverse momentum final state in proton–proton collisions at $\sqrt{s} = 8$. JHEP **06**, 055 (2014). doi:10.1007/JHEP06(2014)055. arXiv:1402.4770

41. CMS Collaboration, Search for supersymmetry using razor variables in events with b-tagged jets in pp collisions at $\sqrt{s} = 8$ TeV. Phys. Rev. D **91**, 052018 (2015). doi:10.1103/PhysRevD.91.052018. arXiv:1502.00300

42. CMS Collaboration, Searches for third-generation squark production in fully hadronic final states in proton–proton collisions at $\sqrt{s} = 8$ TeV. JHEP **06**, 116 (2015). doi:10.1007/JHEP06(2015)116. arXiv:1503.08037

43. CMS Collaboration, Search for supersymmetry in pp collisions at $\sqrt{s} = 8$ TeV in final states with boosted W bosons and b jets using razor variables. Phys. Rev. D **93**, 092009 (2016). doi:10.1103/PhysRevD.93.092009. arXiv:1602.02917

44. ATLAS Collaboration, Search for new phenomena in final states with large jet multiplicities and missing transverse momentum with ATLAS using $\sqrt{s} = 13$ TeV proton–proton collisions. Phys. Lett. B **757**, 334 (2016). doi:10.1016/j.physletb.2016.04.005. arXiv:1602.06194

45. ATLAS Collaboration, Search for new phenomena in final states with an energetic jet and large missing transverse momentum in pp collisions at $\sqrt{s} = 13$ TeV using the ATLAS detector (2016). arXiv:1604.07773 (Submitted to Phys. Rev. D)

46. ATLAS Collaboration, Search for squarks and gluinos in final states with jets and missing transverse momentum at $\sqrt{s} = 13$ TeV with the ATLAS detector. Eur. Phys. J. C **76**, 392 (2016). doi:10.1140/epjc/s10052-016-4184-8. arXiv:1605.03814

47. ATLAS Collaboration, Search for pair production of gluinos decaying via stop and sbottom in events with b-jets and large missing transverse momentum in pp collisions at $\sqrt{s} = 13$ TeV with the ATLAS detector. Phys. Rev. D **94**, 032003 (2016). doi:10.1103/PhysRevD.94.032003. arXiv:1605.09318

48. ATLAS Collaboration, Search for bottom squark pair production in proton–proton collisions at $\sqrt{s} = 13$ TeV with the ATLAS detector (2016). arXiv:1606.08772 (Submitted to Eur. Phys. J. C)

49. CMS Collaboration, Search for supersymmetry in the multijet and missing transverse momentum final state in pp collisions at 13 TeV. Phys. Lett. B **758**, 152 (2016). doi:10.1016/j.physletb.2016.05.002. arXiv:1602.06581

50. CMS Collaboration, Search for new physics with the M_{T2} variable in all-jets final states produced in pp collisions at $\sqrt{s} = 13$ TeV. JHEP **10**, 006 (2016). doi:10.1007/JHEP10(2016)006

51. P.J. Fox, R. Harnik, R. Primulando, C.-T. Yu, Taking a razor to dark matter parameter space at the LHC. Phys. Rev. D **86**, 015010 (2012). doi:10.1103/PhysRevD.86.015010. arXiv:1203.1662

52. O. Buchmueller, S.A. Malik, C. McCabe, B. Penning, Constraining dark matter interactions with pseudoscalar and scalar mediators using collider searches for multijets plus missing transverse energy. Phys. Rev. Lett. **115**, 181802 (2015). doi:10.1103/PhysRevLett.115.181802. arXiv:1505.07826

53. L. Randall, D. Tucker-Smith, Dijet searches for supersymmetry at the Large Hadron Collider. Phys. Rev. Lett. **101**, 221803 (2008). doi:10.1103/PhysRevLett.101.221803. arXiv:0806.1049

54. CMS Collaboration, The CMS experiment at the CERN LHC. JINST **3**, S08004 (2008). doi:10.1088/1748-0221/3/08/S08004

55. J. Alwall et al., The automated computation of tree-level and next-to-leading order differential cross sections, and their matching to parton shower simulations. JHEP **07**, 079 (2014). doi:10.1007/JHEP07(2014)079. arXiv:1405.0301

56. S. Alioli, P. Nason, C. Oleari, E. Re, A general framework for implementing NLO calculations in shower Monte Carlo programs: the POWHEG BOX. JHEP **06**, 043 (2010). doi:10.1007/JHEP06(2010)043. arXiv:1002.2581

57. E. Re, Single-top Wt-channel production matched with parton showers using the POWHEG method. Eur. Phys. J. C **71**, 1547 (2011). doi:10.1140/epjc/s10052-011-1547-z. arXiv:1009.2450

58. R. Gavin, Y. Li, F. Petriello, S. Quackenbush, W physics at the LHC with FEWZ 2.1. Comput. Phys. Commun. **184**, 209 (2013). doi:10.1016/j.cpc.2012.09.005. arXiv:1201.5896

59. R. Gavin, Y. Li, F. Petriello, S. Quackenbush, FEWZ 2.0: a code for hadronic Z production at next-to-next-to-leading order. Comput. Phys. Commun. **182**, 2388 (2011). doi:10.1016/j.cpc.2011.06.008. arXiv:1011.3540

60. T. Melia, P. Nason, R. Rontsch, G. Zanderighi, W^+W^-, WZ and ZZ production in the POWHEG BOX. JHEP **11**, 078 (2011). doi:10.1007/JHEP11(2011)078. arXiv:1107.5051

61. M. Czakon, A. Mitov, Top++: a program for the calculation of the top-pair cross-section at hadron colliders. Comput. Phys. Commun. **185**, 2930 (2014). doi:10.1016/j.cpc.2014.06.021. arXiv:1112.5675

62. S. Alioli, P. Nason, C. Oleari, E. Re, NLO single-top production matched with shower in POWHEG: s- and t-channel contributions. JHEP **09**, 111 (2009). doi:10.1088/1126-6708/2009/09/111. arXiv:0907.4076

63. GEANT4 Collaboration, GEANT4—a simulation toolkit. Nucl. Instrum. Methods A **506**, 250 (2003). doi:10.1016/S0168-9002(03)01368-8

64. T. Sjöstrand et al., An introduction to PYTHIA 8.2. Comput. Phys. Commun. **191**, 159 (2015). doi:10.1016/j.cpc.2015.01.024. arXiv:1410.3012

65. W. Beenakker, R. Höpker, M. Spira, P.M. Zerwas, Squark and gluino production at hadron colliders. Nucl. Phys. B **492**, 51 (1997). doi:10.1016/S0550-3213(97)80027-2. arXiv:hep-ph/9610490

66. A. Kulesza, L. Motyka, Threshold resummation for squark-antisquark and gluino-pair production at the LHC. Phys. Rev. Lett. **102**, 111802 (2009). doi:10.1103/PhysRevLett.102.111802. arXiv:0807.2405

67. A. Kulesza, L. Motyka, Soft gluon resummation for the production of gluino-gluino and squark-antisquark pairs at the LHC. Phys. Rev. D **80**, 095004 (2009). doi:10.1103/PhysRevD.80.095004. arXiv:0905.4749

68. W. Beenakker et al., Soft-gluon resummation for squark and gluino hadroproduction. JHEP **09**, 041 (2009). doi:10.1088/1126-6708/2009/12/041. arXiv:0909.4418

69. W. Beenakker et al., Squark and gluino hadroproduction. Int. J. Mod. Phys. A **26**, 2637 (2011). doi:10.1142/S0217751X11053560. arXiv:1105.1110

70. P.M. Nadolsky et al., Implications of CTEQ global analysis for collider observables. Phys. Rev. D **78**, 013004 (2008). doi:10.1103/PhysRevD.78.013004. arXiv:0802.0007

71. A.D. Martin, W.J. Stirling, R.S. Thorne, G. Watt, Parton distributions for the LHC. Eur. Phys. J. C **63**, 189 (2009). doi:10.1140/epjc/s10052-009-1072-5. arXiv:0901.0002

72. CMS Collaboration, The fast simulation of the CMS detector at LHC. J. Phys. Conf. Ser. **331**, 032049 (2011). doi:10.1088/1742-6596/331/3/032049

73. NNPDF Collaboration, Parton distributions for the LHC Run II. JHEP **04**, 040 (2015). doi:10.1007/JHEP04(2015)040. arXiv:1410.8849

74. CMS Collaboration, Event generator tunes obtained from underlying event and multiparton scattering measurements. Eur. Phys. J. C **76**, 155 (2016). doi:10.1140/epjc/s10052-016-3988-x. arXiv:1512.00815

75. CMS Collaboration, Particle-flow event reconstruction in CMS and performance for jets, taus, and E_T^{miss}. CMS Physics Analysis Summary CMS-PAS-PFT-09-001 (2009)

76. CMS Collaboration, Commissioning of the particle-flow event with the first LHC collisions recorded in the CMS detector. CMS Physics Analysis Summary CMS-PAS-PFT-10-001 (2010)

77. CMS Collaboration, Performance of photon reconstruction and identification with the CMS detector in proton–proton collisions at $\sqrt{s} = 8$ TeV. JINST **10**, P08010 (2015). doi:10.1088/1748-0221/10/08/P08010. arXiv:1502.02702

78. CMS Collaboration, Performance of electron reconstruction and selection with the CMS detector in proton–proton collisions at $\sqrt{s} = 8$ TeV. JINST **10**, P06005 (2015). doi:10.1088/1748-0221/10/06/P06005. arXiv:1502.02701

79. CMS Collaboration, Performance of CMS muon reconstruction in pp collision events at $\sqrt{s} = 7$ TeV. JINST **7**, P10002 (2012). doi:10.1088/1748-0221/7/10/P10002. arXiv:1206.4071

80. M. Cacciari, G.P. Salam, G. Soyez, The anti-k_t jet clustering algorithm. JHEP **04**, 063 (2008). doi:10.1088/1126-6708/2008/04/063. arXiv:0802.1189

81. M. Cacciari, G.P. Salam, Pileup subtraction using jet areas. Phys. Lett. B **659**, 119 (2008). doi:10.1016/j.physletb.2007.09.077. arXiv:0707.1378

82. CMS Collaboration, Determination of jet energy calibration and transverse momentum resolution in CMS. JINST **6**, P11002 (2011). doi:10.1088/1748-0221/6/11/P11002. arXiv:1107.4277

83. CMS Collaboration, Identification of b-quark jets with the CMS experiment. J. Instrum. **8**, P04013 (2013). doi:10.1088/1748-0221/8/04/P04013

84. CMS Collaboration, Identification of b quark jets at the CMS Experiment in the LHC Run 2. CMS Physics Analysis Summary CMS-PAS-BTV-15-001 (2016)

85. CMS Collaboration, Missing transverse energy performance of the CMS detector. JINST **6**, P09001 (2011). doi:10.1088/1748-0221/6/09/P09001. arXiv:1106.5048

86. CMS Collaboration, Identification and filtering of uncharacteristic noise in the CMS hadron calorimeter. JINST **5**, T03014 (2010). doi:10.1088/1748-0221/5/03/T03014. arXiv:0911.4881

87. Z. Bern et al., Driving missing data at next-to-leading order. Phys. Rev. D **84**, 114002 (2011). doi:10.1103/PhysRevD.84.114002. arXiv:1106.1423

88. ATLAS Collaboration, Measurement of the inelastic proton–proton cross section at $\sqrt{s} = 13$ TeV with the ATLAS Detector at the LHC (2016). arXiv:1606.02625 (Submitted to Phys. Rev. Lett.)

89. CMS Collaboration, Measurement of the differential cross section for top quark pair production in pp collisions at $\sqrt{s} = 8$ TeV. Eur. Phys. J. C **75**, 542 (2015). doi:10.1140/epjc/s10052-015-3709-x. arXiv:1505.04480

90. J.S. Conway, Incorporating nuisance parameters in likelihoods for multisource spectra, in *PHYSTAT 2011 Workshop on Statistical Issues Related to Discovery Claims in Search Experiments and Unfolding*, ed. by H.B. Prosper, L. Lyons, p. 115. CERN (2011). doi:10.5170/CERN-2011-006.115

91. J.K. Lindsey, *Parametric Statistical Inference* (Oxford University Press, Oxford, UK, 1996) (ISBN 0-19-852359-9)

92. J. Alwall, P. Schuster, N. Toro, Simplified models for a first characterization of new physics at the LHC. Phys. Rev. D **79**, 075020 (2009). doi:10.1103/PhysRevD.79.075020. arXiv:0810.3921

93. J. Alwall, M.-P. Le, M. Lisanti, J.G. Wacker, Model-independent jets plus missing energy searches. Phys. Rev. D **79**, 015005 (2009). doi:10.1103/PhysRevD.79.015005. arXiv:0809.3264

94. D. Alves et al., Simplified models for LHC new physics searches. J. Phys. G **39**, 105005 (2012). doi:10.1088/0954-3899/39/10/105005. arXiv:1105.2838

95. G. Cowan, K. Cranmer, E. Gross, O. Vitells, Asymptotic formulae for likelihood-based tests of new physics. Eur. Phys. J. C **71**, 1554 (2011). doi:10.1140/epjc/s10052-011-1554-0. arXiv:1007.1727 [Erratum: doi:10.1140/epjc/s10052-013-2501-z]

96. ATLAS and CMS Collaborations, and LHC Higgs Combination Group, Procedure for the LHC Higgs boson search combination in Summer 2011. Technical Report CMS-NOTE-2011-005 ATL-PHYS-PUB-2011-11, CERN, Geneva (2011)

97. T. Junk, Confidence level computation for combining searches with small statistics. Nucl. Instrum. Methods A **434**, 435 (1999). doi:10.1016/S0168-9002(99)00498-2. arXiv:hep-ex/9902006

98. A.L. Read, Presentation of search results: the CL_s technique. J. Phys. G **28**, 2693 (2002). doi:10.1088/0954-3899/28/10/313

99. CMS Collaboration, CMS luminosity measurement for the 2015 data taking period. CMS Physics Analysis Summary CMS-PAS-LUM-15-001 (2016)

100. CMS Collaboration, Search for top-squark pair production in the single-lepton final state in pp collisions at $\sqrt{s} = 8$ TeV. Eur. Phys. J. C **73**, 2677 (2013). doi:10.1140/epjc/s10052-013-2677-2

CMS Collaboration

Yerevan Physics Institute, Yerevan, Armenia
V. Khachatryan, A. M. Sirunyan, A. Tumasyan

Institut für Hochenergiephysik, Vienna, Austria
W. Adam, E. Asilar, T. Bergauer, J. Brandstetter, E. Brondolin, M. Dragicevic, J. Erö, M. Flechl, M. Friedl, R. Frühwirth[1],
V. M. Ghete, C. Hartl, N. Hörmann, J. Hrubec, M. Jeitler[1], A. König, I. Krätschmer, D. Liko, T. Matsushita, I. Mikulec,
D. Rabady, N. Rad, B. Rahbaran, H. Rohringer, J. Schieck[1], J. Strauss, W. Waltenberger, C.-E. Wulz[1]

Institute for Nuclear Problems, Minsk, Belarus
O. Dvornikov, V. Makarenko, V. Zykunov

National Centre for Particle and High Energy Physics, Minsk, Belarus
V. Mossolov, N. Shumeiko, J. Suarez Gonzalez

Universiteit Antwerpen, Antwerpen, Belgium
S. Alderweireldt, E. A. De Wolf, X. Janssen, J. Lauwers, M. Van De Klundert, H. Van Haevermaet, P. Van Mechelen,
N. Van Remortel, A. Van Spilbeeck

Vrije Universiteit Brussel, Brussel, Belgium
S. Abu Zeid, F. Blekman, J. D'Hondt, N. Daci, I. De Bruyn, K. Deroover, S. Lowette, S. Moortgat, L. Moreels,
A. Olbrechts, Q. Python, S. Tavernier, W. Van Doninck, P. Van Mulders, I. Van Parijs

Université Libre de Bruxelles, Bruxelles, Belgium
H. Brun, B. Clerbaux, G. De Lentdecker, H. Delannoy, G. Fasanella, L. Favart, R. Goldouzian, A. Grebenyuk,
G. Karapostoli, T. Lenzi, A. Léonard, J. Luetic, T. Maerschalk, A. Marinov, A. Randle-conde, T. Seva, C. Vander Velde,
P. Vanlaer, D. Vannerom, R. Yonamine, F. Zenoni, F. Zhang[2]

Ghent University, Ghent, Belgium
A. Cimmino, T. Cornelis, D. Dobur, A. Fagot, G. Garcia, M. Gul, I. Khvastunov, D. Poyraz, S. Salva, R. Schöfbeck,
A. Sharma, M. Tytgat, W. Van Driessche, E. Yazgan, N. Zaganidis

Université Catholique de Louvain, Louvain-la-Neuve, Belgium
H. Bakhshiansohi, C. Beluffi[3], O. Bondu, S. Brochet, G. Bruno, A. Caudron, S. De Visscher, C. Delaere, M. Delcourt,
B. Francois, A. Giammanco, A. Jafari, P. Jez, M. Komm, G. Krintiras, V. Lemaitre, A. Magitteri, A. Mertens, M. Musich,
C. Nuttens, K. Piotrzkowski, L. Quertenmont, M. Selvaggi, M. Vidal Marono, S. Wertz

Université de Mons, Mons, Belgium
N. Beliy

Centro Brasileiro de Pesquisas Fisicas, Rio de Janeiro, Brazil
W. L. Aldá Júnior, F. L. Alves, G. A. Alves, L. Brito, C. Hensel, A. Moraes, M. E. Pol, P. Rebello Teles

Universidade do Estado do Rio de Janeiro, Rio de Janeiro, Brazil
E. Belchior Batista Das Chagas, W. Carvalho, J. Chinellato[4], A. Custódio, E. M. Da Costa, G. G. Da Silveira[5],
D. De Jesus Damiao, C. De Oliveira Martins, S. Fonseca De Souza, L. M. Huertas Guativa, H. Malbouisson,
D. Matos Figueiredo, C. Mora Herrera, L. Mundim, H. Nogima, W. L. Prado Da Silva, A. Santoro, A. Sznajder,
E. J. Tonelli Manganote[4], A. Vilela Pereira

Universidade Estadual Paulista[a], Universidade Federal do ABC[b], São Paulo, Brazil
S. Ahuja[a], C. A. Bernardes[b], S. Dogra[a], T. R. Fernandez Perez Tomei[a], E. M. Gregores[b], P. G. Mercadante[b], C. S. Moon[a],
S. F. Novaes[a], Sandra S. Padula[a], D. Romero Abad[b], J. C. Ruiz Vargas

Institute for Nuclear Research and Nuclear Energy, Sofia, Bulgaria
A. Aleksandrov, R. Hadjiiska, P. Iaydjiev, M. Rodozov, S. Stoykova, G. Sultanov, M. Vutova

University of Sofia, Sofia, Bulgaria
A. Dimitrov, I. Glushkov, L. Litov, B. Pavlov, P. Petkov

Beihang University, Beijing, China
W. Fang[6]

Institute of High Energy Physics, Beijing, China
M. Ahmad, J. G. Bian, G. M. Chen, H. S. Chen, M. Chen, Y. Chen[7], T. Cheng, C. H. Jiang, D. Leggat, Z. Liu, F. Romeo, S. M. Shaheen, A. Spiezia, J. Tao, C. Wang, Z. Wang, H. Zhang, J. Zhao

State Key Laboratory of Nuclear Physics and Technology, Peking University, Beijing, China
Y. Ban, G. Chen, Q. Li, S. Liu, Y. Mao, S. J. Qian, D. Wang, Z. Xu

Universidad de Los Andes, Bogota, Colombia
C. Avila, A. Cabrera, L. F. Chaparro Sierra, C. Florez, J. P. Gomez, C. F. González Hernández, J. D. Ruiz Alvarez, J. C. Sanabria

Faculty of Electrical Engineering, Mechanical Engineering and Naval Architecture, University of Split, Split, Croatia
N. Godinovic, D. Lelas, I. Puljak, P. M. Ribeiro Cipriano, T. Sculac

University of Split, Faculty of Science, Split, Croatia
Z. Antunovic, M. Kovac

Institute Rudjer Boskovic, Zagreb, Croatia
V. Brigljevic, D. Ferencek, K. Kadija, S. Micanovic, L. Sudic, T. Susa

University of Cyprus, Nicosia, Cyprus
A. Attikis, G. Mavromanolakis, J. Mousa, C. Nicolaou, F. Ptochos, P. A. Razis, H. Rykaczewski, D. Tsiakkouri

Charles University, Prague, Czech Republic
M. Finger[8], M. Finger Jr.[8]

Universidad San Francisco de Quito, Quito, Ecuador
E. Carrera Jarrin

Academy of Scientific Research and Technology of the Arab Republic of Egypt, Egyptian Network of High Energy Physics, Cairo, Egypt
E. El-khateeb[9], S. Elgammal[10], A. Mohamed[11]

National Institute of Chemical Physics and Biophysics, Tallinn, Estonia
B. Calpas, M. Kadastik, M. Murumaa, L. Perrini, M. Raidal, A. Tiko, C. Veelken

Department of Physics, University of Helsinki, Helsinki, Finland
P. Eerola, J. Pekkanen, M. Voutilainen

Helsinki Institute of Physics, Helsinki, Finland
J. Härkönen, T. Järvinen, V. Karimäki, R. Kinnunen, T. Lampén, K. Lassila-Perini, S. Lehti, T. Lindén, P. Luukka, J. Tuominiemi, E. Tuovinen, L. Wendland

Lappeenranta University of Technology, Lappeenranta, Finland
J. Talvitie, T. Tuuva

IRFU, CEA, Université Paris-Saclay, Gif-sur-Yvette, France
M. Besancon, F. Couderc, M. Dejardin, D. Denegri, B. Fabbro, J. L. Faure, C. Favaro, F. Ferri, S. Ganjour, S. Ghosh, A. Givernaud, P. Gras, G. Hamel de Monchenault, P. Jarry, I. Kucher, E. Locci, M. Machet, J. Malcles, J. Rander, A. Rosowsky, M. Titov, A. Zghiche

Laboratoire Leprince-Ringuet, Ecole Polytechnique, IN2P3-CNRS, Palaiseau, France
A. Abdulsalam, I. Antropov, S. Baffioni, F. Beaudette, P. Busson, L. Cadamuro, E. Chapon, C. Charlot, O. Davignon, R. Granier de Cassagnac, M. Jo, S. Lisniak, P. Miné, M. Nguyen, C. Ochando, G. Ortona, P. Paganini, P. Pigard, S. Regnard, R. Salerno, Y. Sirois, T. Strebler, Y. Yilmaz, A. Zabi

Institut Pluridisciplinaire Hubert Curien, Université de Strasbourg, Université de Haute Alsace Mulhouse, CNRS/IN2P3, Strasbourg, France

J.-L. Agram[12], J. Andrea, A. Aubin, D. Bloch, J.-M. Brom, M. Buttignol, E. C. Chabert, N. Chanon, C. Collard, E. Conte[12], X. Coubez, J.-C. Fontaine[12], D. Gelé, U. Goerlach, A.-C. Le Bihan, K. Skovpen, P. Van Hove

Centre de Calcul de l'Institut National de Physique Nucleaire et de Physique des Particules, CNRS/IN2P3, Villeurbanne, France

S. Gadrat

Université de Lyon, Université Claude Bernard Lyon 1, CNRS-IN2P3, Institut de Physique Nucléaire de Lyon, Villeurbanne, France

S. Beauceron, C. Bernet, G. Boudoul, E. Bouvier, C. A. Carrillo Montoya, R. Chierici, D. Contardo, B. Courbon, P. Depasse, H. El Mamouni, J. Fan, J. Fay, S. Gascon, M. Gouzevitch, G. Grenier, B. Ille, F. Lagarde, I. B. Laktineh, M. Lethuillier, L. Mirabito, A. L. Pequegnot, S. Perries, A. Popov[13], D. Sabes, V. Sordini, M. Vander Donckt, P. Verdier, S. Viret

Georgian Technical University, Tbilisi, Georgia

T. Toriashvili[14]

Tbilisi State University, Tbilisi, Georgia

Z. Tsamalaidze[8]

RWTH Aachen University, I. Physikalisches Institut, Aachen, Germany

C. Autermann, S. Beranek, L. Feld, A. Heister, M. K. Kiesel, K. Klein, M. Lipinski, A. Ostapchuk, M. Preuten, F. Raupach, S. Schael, C. Schomakers, J. Schulz, T. Verlage, H. Weber, V. Zhukov[13]

RWTH Aachen University, III. Physikalisches Institut A, Aachen, Germany

A. Albert, M. Brodski, E. Dietz-Laursonn, D. Duchardt, M. Endres, M. Erdmann, S. Erdweg, T. Esch, R. Fischer, A. Güth, M. Hamer, T. Hebbeker, C. Heidemann, K. Hoepfner, S. Knutzen, M. Merschmeyer, A. Meyer, P. Millet, S. Mukherjee, M. Olschewski, K. Padeken, T. Pook, M. Radziej, H. Reithler, M. Rieger, F. Scheuch, L. Sonnenschein, D. Teyssier, S. Thüer

RWTH Aachen University, III. Physikalisches Institut B, Aachen, Germany

V. Cherepanov, G. Flügge, F. Hoehle, B. Kargoll, T. Kress, A. Künsken, J. Lingemann, T. Müller, A. Nehrkorn, A. Nowack, I. M. Nugent, C. Pistone, O. Pooth, A. Stahl[15]

Deutsches Elektronen-Synchrotron, Hamburg, Germany

M. Aldaya Martin, T. Arndt, C. Asawatangtrakuldee, K. Beernaert, O. Behnke, U. Behrens, A. A. Bin Anuar, K. Borras[16], A. Campbell, P. Connor, C. Contreras-Campana, F. Costanza, C. Diez Pardos, G. Dolinska, G. Eckerlin, D. Eckstein, T. Eichhorn, E. Eren, E. Gallo[17], J. Garay Garcia, A. Geiser, A. Gizhko, J. M. Grados Luyando, P. Gunnellini, A. Harb, J. Hauk, M. Hempel[18], H. Jung, A. Kalogeropoulos, O. Karacheban[18], M. Kasemann, J. Keaveney, C. Kleinwort, I. Korol, D. Krücker, W. Lange, A. Lelek, J. Leonard, K. Lipka, A. Lobanov, W. Lohmann[18], R. Mankel, I.-A. Melzer-Pellmann, A. B. Meyer, G. Mittag, J. Mnich, A. Mussgiller, E. Ntomari, D. Pitzl, R. Placakyte, A. Raspereza, B. Roland, M. Ö. Sahin, P. Saxena, T. Schoerner-Sadenius, C. Seitz, S. Spannagel, N. Stefaniuk, G. P. Van Onsem, R. Walsh, C. Wissing

University of Hamburg, Hamburg, Germany

V. Blobel, M. Centis Vignali, A. R. Draeger, T. Dreyer, E. Garutti, D. Gonzalez, J. Haller, M. Hoffmann, A. Junkes, R. Klanner, R. Kogler, N. Kovalchuk, T. Lapsien, T. Lenz, I. Marchesini, D. Marconi, M. Meyer, M. Niedziela, D. Nowatschin, F. Pantaleo[15], T. Peiffer, A. Perieanu, J. Poehlsen, C. Sander, C. Scharf, P. Schleper, A. Schmidt, S. Schumann, J. Schwandt, H. Stadie, G. Steinbrück, F. M. Stober, M. Stöver, H. Tholen, D. Troendle, E. Usai, L. Vanelderen, A. Vanhoefer, B. Vormwald

Institut für Experimentelle Kernphysik, Karlsruhe, Germany

M. Akbiyik, C. Barth, S. Baur, C. Baus, J. Berger, E. Butz, R. Caspart, T. Chwalek, F. Colombo, W. De Boer, A. Dierlamm, S. Fink, B. Freund, R. Friese, M. Giffels, A. Gilbert, P. Goldenzweig, D. Haitz, F. Hartmann[15], S. M. Heindl, U. Husemann, I. Katkov[13], S. Kudella, P. Lobelle Pardo, H. Mildner, M. U. Mozer, Th. Müller, M. Plagge, G. Quast, K. Rabbertz, S. Röcker, F. Roscher, M. Schröder, I. Shvetsov, G. Sieber, H. J. Simonis, R. Ulrich, J. Wagner-Kuhr, S. Wayand, M. Weber, T. Weiler, S. Williamson, C. Wöhrmann, R. Wolf

Institute of Nuclear and Particle Physics (INPP), NCSR Demokritos, Aghia Paraskevi, Greece
G. Anagnostou, G. Daskalakis, T. Geralis, V. A. Giakoumopoulou, A. Kyriakis, D. Loukas, I. Topsis-Giotis

National and Kapodistrian University of Athens, Athens, Greece
S. Kesisoglou, A. Panagiotou, N. Saoulidou, E. Tziaferi

University of Ioánnina, Ioánnina, Greece
I. Evangelou, G. Flouris, C. Foudas, P. Kokkas, N. Loukas, N. Manthos, I. Papadopoulos, E. Paradas

MTA-ELTE Lendület CMS Particle and Nuclear Physics Group, Eötvös Loránd University, Budapest, Hungary
N. Filipovic

Wigner Research Centre for Physics, Budapest, Hungary
G. Bencze, C. Hajdu, P. Hidas, D. Horvath[19], F. Sikler, V. Veszpremi, G. Vesztergombi[20], A. J. Zsigmond

Institute of Nuclear Research ATOMKI, Debrecen, Hungary
N. Beni, S. Czellar, J. Karancsi[21], A. Makovec, J. Molnar, Z. Szillasi

University of Debrecen, Debrecen, Hungary
M. Bartók[20], P. Raics, Z. L. Trocsanyi, B. Ujvari

National Institute of Science Education and Research, Bhubaneswar, India
S. Bahinipati, S. Choudhury[22], P. Mal, K. Mandal, A. Nayak[23], D. K. Sahoo, N. Sahoo, S. K. Swain

Panjab University, Chandigarh, India
S. Bansal, S. B. Beri, V. Bhatnagar, R. Chawla, U. Bhawandeep, A. K. Kalsi, A. Kaur, M. Kaur, R. Kumar, P. Kumari, A. Mehta, M. Mittal, J. B. Singh, G. Walia

University of Delhi, Delhi, India
Ashok Kumar, A. Bhardwaj, B. C. Choudhary, R. B. Garg, S. Keshri, S. Malhotra, M. Naimuddin, N. Nishu, K. Ranjan, R. Sharma, V. Sharma

Saha Institute of Nuclear Physics, Kolkata, India
R. Bhattacharya, S. Bhattacharya, K. Chatterjee, S. Dey, S. Dutt, S. Dutta, S. Ghosh, N. Majumdar, A. Modak, K. Mondal, S. Mukhopadhyay, S. Nandan, A. Purohit, A. Roy, D. Roy, S. Roy Chowdhury, S. Sarkar, M. Sharan, S. Thakur

Indian Institute of Technology Madras, Madras, India
P. K. Behera

Bhabha Atomic Research Centre, Mumbai, India
R. Chudasama, D. Dutta, V. Jha, V. Kumar, A. K. Mohanty[15], P. K. Netrakanti, L. M. Pant, P. Shukla, A. Topkar

Tata Institute of Fundamental Research-A, Mumbai, India
T. Aziz, S. Dugad, G. Kole, B. Mahakud, S. Mitra, G. B. Mohanty, B. Parida, N. Sur, B. Sutar

Tata Institute of Fundamental Research-B, Mumbai, India
S. Banerjee, S. Bhowmik[24], R. K. Dewanjee, S. Ganguly, M. Guchait, Sa. Jain, S. Kumar, M. Maity[24], G. Majumder, K. Mazumdar, T. Sarkar[24], N. Wickramage[25]

Indian Institute of Science Education and Research (IISER), Pune, India
S. Chauhan, S. Dube, V. Hegde, A. Kapoor, K. Kothekar, S. Pandey, A. Rane, S. Sharma

Institute for Research in Fundamental Sciences (IPM), Tehran, Iran
H. Behnamian, S. Chenarani[26], E. Eskandari Tadavani, S. M. Etesami[26], A. Fahim[27], M. Khakzad, M. Mohammadi Najafabadi, M. Naseri, S. Paktinat Mehdiabadi[28], F. Rezaei Hosseinabadi, B. Safarzadeh[29], M. Zeinali

University College Dublin, Dublin, Ireland
M. Felcini, M. Grunewald

INFN Sezione di Bari^a, Università di Bari^b, Politecnico di Bari^c, Bari, Italy

M. Abbrescia^{a,b}, C. Calabria^{a,b}, C. Caputo^{a,b}, A. Colaleo^a, D. Creanza^{a,c}, L. Cristella^{a,b}, N. De Filippis^{a,c}, M. De Palma^{a,b}, L. Fiore^a, G. Iaselli^{a,c}, G. Maggi^{a,c}, M. Maggi^a, G. Miniello^{a,b}, S. My^{a,b}, S. Nuzzo^{a,b}, A. Pompili^{a,b}, G. Pugliese^{a,c}, R. Radogna^{a,b}, A. Ranieri^a, G. Selvaggi^{a,b}, L. Silvestris^{a,15}, R. Venditti^{a,b}, P. Verwilligen^a

INFN Sezione di Bologna^a, Università di Bologna^b, Bologna, Italy

G. Abbiendi^a, C. Battilana, D. Bonacorsi^{a,b}, S. Braibant-Giacomelli^{a,b}, L. Brigliadori^{a,b}, R. Campanini^{a,b}, P. Capiluppi^{a,b}, A. Castro^{a,b}, F. R. Cavallo^a, S. S. Chhibra^{a,b}, G. Codispoti^{a,b}, M. Cuffiani^{a,b}, G. M. Dallavalle^a, F. Fabbri^a, A. Fanfani^{a,b}, D. Fasanella^{a,b}, P. Giacomelli^a, C. Grandi^a, L. Guiducci^{a,b}, S. Marcellini^a, G. Masetti^a, A. Montanari^a, F. L. Navarria^{a,b}, A. Perrotta^a, A. M. Rossi^{a,b}, T. Rovelli^{a,b}, G. P. Siroli^{a,b}, N. Tosi^{a,b,15}

INFN Sezione di Catania^a, Università di Catania^b, Catania, Italy

S. Albergo^{a,b}, M. Chiorboli^{a,b}, S. Costa^{a,b}, A. Di Mattia^a, F. Giordano^{a,b}, R. Potenza^{a,b}, A. Tricomi^{a,b}, C. Tuve^{a,b}

INFN Sezione di Firenze^a, Università di Firenze^b, Florence, Italy

G. Barbagli^a, V. Ciulli^{a,b}, C. Civinini^a, R. D'Alessandro^{a,b}, E. Focardi^{a,b}, V. Gori^{a,b}, P. Lenzi^{a,b}, M. Meschini^a, S. Paoletti^a, G. Sguazzoni^a, L. Viliani^{a,b,15}

INFN Laboratori Nazionali di Frascati, Frascati, Italy

L. Benussi, S. Bianco, F. Fabbri, D. Piccolo, F. Primavera^{15}

INFN Sezione di Genova^a, Università di Genova^b, Genoa, Italy

V. Calvelli^{a,b}, F. Ferro^a, M. Lo Vetere^{a,b}, M. R. Monge^{a,b}, E. Robutti^a, S. Tosi^{a,b}

INFN Sezione di Milano-Bicocca^a, Università di Milano-Bicocca^b, Milan, Italy

L. Brianza^{15}, M. E. Dinardo^{a,b}, S. Fiorendi^{a,b,15}, S. Gennai^a, A. Ghezzi^{a,b}, P. Govoni^{a,b}, M. Malberti, S. Malvezzi^a, R. A. Manzoni^{a,b,15}, D. Menasce^a, L. Moroni^a, M. Paganoni^{a,b}, D. Pedrini^a, S. Pigazzini, S. Ragazzi^{a,b}, T. Tabarelli de Fatis^{a,b}

INFN Sezione di Napoli^a, Università di Napoli 'Federico II'^{b}, Napoli, Italy, Università della Basilicata^c, Potenza, Italy, Università G. Marconi^d, Rome, Italy

S. Buontempo^a, N. Cavallo^{a,c}, G. De Nardo, S. Di Guida^{a,d,15}, M. Esposito^{a,b}, F. Fabozzi^{a,c}, F. Fienga^{a,b}, A. O. M. Iorio^{a,b}, G. Lanza^a, L. Lista^a, S. Meola^{a,d,15}, P. Paolucci^{a,15}, C. Sciacca^{a,b}, F. Thyssen

INFN Sezione di Padova^a, Università di Padova^b Padova Italy, Università di Trento^c, Trento, Italy

P. Azzi^{a,15}, N. Bacchetta^a, L. Benato^{a,b}, D. Bisello^{a,b}, A. Boletti^{a,b}, R. Carlin^{a,b}, A. Carvalho Antunes De Oliveira^{a,b}, P. Checchia^a, M. Dall'Osso^{a,b}, P. De Castro Manzano^a, T. Dorigo^a, U. Dosselli^a, F. Gasparini^{a,b}, U. Gasparini^{a,b}, A. Gozzelino^a, S. Lacaprara^a, M. Margoni^{a,b}, A. T. Meneguzzo^{a,b}, J. Pazzini^{a,b}, N. Pozzobon^{a,b}, P. Ronchese^{a,b}, F. Simonetto^{a,b}, E. Torassa^a, M. Zanetti, P. Zotto^{a,b}, G. Zumerle^{a,b}

INFN Sezione di Pavia^a, Università di Pavia^b, Pavia, Italy

A. Braghieri^a, A. Magnani^{a,b}, P. Montagna^{a,b}, S. P. Ratti^{a,b}, V. Re^a, C. Riccardi^{a,b}, P. Salvini^a, I. Vai^{a,b}, P. Vitulo^{a,b}

INFN Sezione di Perugia^a, Università di Perugia^b, Perugia, Italy

L. Alunni Solestizi^{a,b}, G. M. Bilei^a, D. Ciangottini^{a,b}, L. Fanò^{a,b}, P. Lariccia^{a,b}, R. Leonardi^{a,b}, G. Mantovani^{a,b}, M. Menichelli^a, A. Saha^a, A. Santocchia^{a,b}

INFN Sezione di Pisa^a, Università di Pisa^b, Scuola Normale Superiore di Pisa^c, Pisa, Italy

K. Androsov^{a,30}, P. Azzurri^{a,15}, G. Bagliesi^a, J. Bernardini^a, T. Boccali^a, R. Castaldi^a, M. A. Ciocci^{a,30}, R. Dell'Orso^a, S. Donato^{a,c}, G. Fedi, A. Giassi^a, M. T. Grippo^{a,30}, F. Ligabue^{a,c}, T. Lomtadze^a, L. Martini^{a,b}, A. Messineo^{a,b}, F. Palla^a, A. Rizzi^{a,b}, A. Savoy-Navarro^{a,31}, P. Spagnolo^a, R. Tenchini^a, G. Tonelli^{a,b}, A. Venturi^a, P. G. Verdini^a

INFN Sezione di Roma^a, Università di Roma^b, Rome, Italy

L. Barone^{a,b}, F. Cavallari^a, M. Cipriani^{a,b}, D. Del Re^{a,b,15}, M. Diemoz^a, S. Gelli^{a,b}, E. Longo^{a,b}, F. Margaroli^{a,b}, B. Marzocchi^{a,b}, P. Meridiani^a, G. Organtini^{a,b}, R. Paramatti^a, F. Preiato^{a,b}, S. Rahatlou^{a,b}, C. Rovelli^a, F. Santanastasio^{a,b}

INFN Sezione di Torino[a], Università di Torino[b], Turin, Italy, Università del Piemonte Orientale[c], Novara, Italy
N. Amapane[a,b], R. Arcidiacono[a,c,15], S. Argiro[a,b], M. Arneodo[a,c], N. Bartosik[a], R. Bellan[a,b], C. Biino[a], N. Cartiglia[a], F. Cenna[a,b], M. Costa[a,b], R. Covarelli[a,b], A. Degano[a,b], N. Demaria[a], L. Finco[a,b], B. Kiani[a,b], C. Mariotti[a], S. Maselli[a], E. Migliore[a,b], V. Monaco[a,b], E. Monteil[a,b], M. M. Obertino[a,b], L. Pacher[a,b], N. Pastrone[a], M. Pelliccioni[a], G. L. Pinna Angioni[a,b], F. Ravera[a,b], A. Romero[a,b], M. Ruspa[a,c], R. Sacchi[a,b], K. Shchelina[a,b], V. Sola[a], A. Solano[a,b], A. Staiano[a], P. Traczyk[a,b]

INFN Sezione di Trieste[a], Università di Trieste[b], Trieste, Italy
S. Belforte[a], M. Casarsa[a], F. Cossutti[a], G. Della Ricca[a,b], A. Zanetti[a]

Kyungpook National University, Taegu, Korea
D. H. Kim, G. N. Kim, M. S. Kim, S. Lee, S. W. Lee, Y. D. Oh, S. Sekmen, D. C. Son, Y. C. Yang

Chonbuk National University, Jeonju, Korea
A. Lee

Institute for Universe and Elementary Particles, Chonnam National University, Kwangju, Korea
H. Kim

Hanyang University, Seoul, Korea
J. A. Brochero Cifuentes, T. J. Kim

Korea University, Seoul, Korea
S. Cho, S. Choi, Y. Go, D. Gyun, S. Ha, B. Hong, Y. Jo, Y. Kim, B. Lee, K. Lee, K. S. Lee, S. Lee, J. Lim, S. K. Park, Y. Roh

Seoul National University, Seoul, Korea
J. Almond, J. Kim, H. Lee, S. B. Oh, B. C. Radburn-Smith, S. H. Seo, U. K. Yang, H. D. Yoo, G. B. Yu

University of Seoul, Seoul, Korea
M. Choi, H. Kim, J. H. Kim, J. S. H. Lee, I. C. Park, G. Ryu, M. S. Ryu

Sungkyunkwan University, Suwon, Korea
Y. Choi, J. Goh, C. Hwang, J. Lee, I. Yu

Vilnius University, Vilnius, Lithuania
V. Dudenas, A. Juodagalvis, J. Vaitkus

National Centre for Particle Physics, Universiti Malaya, Kuala Lumpur, Malaysia
I. Ahmed, Z. A. Ibrahim, J. R. Komaragiri, M. A. B. Md Ali[32], F. Mohamad Idris[33], W. A. T. Wan Abdullah, M. N. Yusli, Z. Zolkapli

Centro de Investigacion y de Estudios Avanzados del IPN, Mexico City, Mexico
H. Castilla-Valdez, E. De La Cruz-Burelo, I. Heredia-De La Cruz[34], A. Hernandez-Almada, R. Lopez-Fernandez, R. Magaña Villalba, J. Mejia Guisao, A. Sanchez-Hernandez

Universidad Iberoamericana, Mexico City, Mexico
S. Carrillo Moreno, C. Oropeza Barrera, F. Vazquez Valencia

Benemerita Universidad Autonoma de Puebla, Puebla, Mexico
S. Carpinteyro, I. Pedraza, H. A. Salazar Ibarguen, C. Uribe Estrada

Universidad Autónoma de San Luis Potosí, San Luis Potosí, Mexico
A. Morelos Pineda

University of Auckland, Auckland, New Zealand
D. Krofcheck

University of Canterbury, Christchurch, New Zealand
P. H. Butler

National Centre for Physics, Quaid-I-Azam University, Islamabad, Pakistan
A. Ahmad, M. Ahmad, Q. Hassan, H. R. Hoorani, W. A. Khan, A. Saddique, M. A. Shah, M. Shoaib, M. Waqas

National Centre for Nuclear Research, Swierk, Poland
H. Bialkowska, M. Bluj, B. Boimska, T. Frueboes, M. Górski, M. Kazana, K. Nawrocki, K. Romanowska-Rybinska, M. Szleper, P. Zalewski

Institute of Experimental Physics, Faculty of Physics, University of Warsaw, Warsaw, Poland
K. Bunkowski, A. Byszuk[35], K. Doroba, A. Kalinowski, M. Konecki, J. Krolikowski, M. Misiura, M. Olszewski, M. Walczak

Laboratório de Instrumentação e Física Experimental de Partículas, Lisbon, Portugal
P. Bargassa, C. Beirão Da Cruz E Silva, A. Di Francesco, P. Faccioli, P. G. Ferreira Parracho, M. Gallinaro, J. Hollar, N. Leonardo, L. Lloret Iglesias, M. V. Nemallapudi, J. Rodrigues Antunes, J. Seixas, O. Toldaiev, D. Vadruccio, J. Varela, P. Vischia

Joint Institute for Nuclear Research, Dubna, Russia
S. Afanasiev, P. Bunin, M. Gavrilenko, I. Golutvin, I. Gorbunov, A. Kamenev, V. Karjavin, A. Lanev, A. Malakhov, V. Matveev[36,37], V. Palichik, V. Perelygin, S. Shmatov, S. Shulha, N. Skatchkov, V. Smirnov, N. Voytishin, A. Zarubin

Petersburg Nuclear Physics Institute, Gatchina (St. Petersburg), Russia
L. Chtchipounov, V. Golovtsov, Y. Ivanov, V. Kim[38], E. Kuznetsova[39], V. Murzin, V. Oreshkin, V. Sulimov, A. Vorobyev

Institute for Nuclear Research, Moscow, Russia
Yu. Andreev, A. Dermenev, S. Gninenko, N. Golubev, A. Karneyeu, M. Kirsanov, N. Krasnikov, A. Pashenkov, D. Tlisov, A. Toropin

Institute for Theoretical and Experimental Physics, Moscow, Russia
V. Epshteyn, V. Gavrilov, N. Lychkovskaya, V. Popov, I. Pozdnyakov, G. Safronov, A. Spiridonov, M. Toms, E. Vlasov, A. Zhokin

Moscow Institute of Physics and Technology, Moscow, Russia
A. Bylinkin[37]

National Research Nuclear University 'Moscow Engineering Physics Institute' (MEPhI), Moscow, Russia
M. Chadeeva[40], V. Rusinov, E. Tarkovskii

P.N. Lebedev Physical Institute, Moscow, Russia
V. Andreev, M. Azarkin[37], I. Dremin[37], M. Kirakosyan, A. Leonidov[37], S. V. Rusakov, A. Terkulov

Skobeltsyn Institute of Nuclear Physics, Lomonosov Moscow State University, Moscow, Russia
A. Baskakov, A. Belyaev, E. Boos, M. Dubinin[41], L. Dudko, A. Ershov, A. Gribushin, V. Klyukhin, O. Kodolova, I. Lokhtin, I. Miagkov, S. Obraztsov, S. Petrushanko, V. Savrin, A. Snigirev

Novosibirsk State University (NSU), Novosibirsk, Russia
V. Blinov[42], Y. Skovpen[42], D. Shtol[42]

State Research Center of Russian Federation, Institute for High Energy Physics, Protvino, Russia
I. Azhgirey, I. Bayshev, S. Bitioukov, D. Elumakhov, V. Kachanov, A. Kalinin, D. Konstantinov, V. Krychkine, V. Petrov, R. Ryutin, A. Sobol, S. Troshin, N. Tyurin, A. Uzunian, A. Volkov

Faculty of Physics and Vinca Institute of Nuclear Sciences, University of Belgrade, Belgrade, Serbia
P. Adzic[43], P. Cirkovic, D. Devetak, M. Dordevic, J. Milosevic, V. Rekovic

Centro de Investigaciones Energéticas Medioambientales y Tecnológicas (CIEMAT), Madrid, Spain

J. Alcaraz Maestre, M. Barrio Luna, E. Calvo, M. Cerrada, M. Chamizo Llatas, N. Colino, B. De La Cruz, A. Delgado Peris, A. Escalante Del Valle, C. Fernandez Bedoya, J. P. Fernández Ramos, J. Flix, M. C. Fouz, P. Garcia-Abia, O. Gonzalez Lopez, S. Goy Lopez, J. M. Hernandez, M. I. Josa, E. Navarro De Martino, A. Pérez-Calero Yzquierdo, J. Puerta Pelayo, A. Quintario Olmeda, I. Redondo, L. Romero, M. S. Soares

Universidad Autónoma de Madrid, Madrid, Spain

J. F. de Trocóniz, M. Missiroli, D. Moran

Universidad de Oviedo, Oviedo, Spain

J. Cuevas, J. Fernandez Menendez, I. Gonzalez Caballero, J. R. González Fernández, E. Palencia Cortezon, S. Sanchez Cruz, I. Suárez Andrés, J. M. Vizan Garcia

Instituto de Física de Cantabria (IFCA), CSIC-Universidad de Cantabria, Santander, Spain

I. J. Cabrillo, A. Calderon, J. R. Castiñeiras De Saa, E. Curras, M. Fernandez, J. Garcia-Ferrero, G. Gomez, A. Lopez Virto, J. Marco, C. Martinez Rivero, F. Matorras, J. Piedra Gomez, T. Rodrigo, A. Ruiz-Jimeno, L. Scodellaro, N. Trevisani, I. Vila, R. Vilar Cortabitarte

CERN, European Organization for Nuclear Research, Geneva, Switzerland

D. Abbaneo, E. Auffray, G. Auzinger, M. Bachtis, P. Baillon, A. H. Ball, D. Barney, P. Bloch, A. Bocci, A. Bonato, C. Botta, T. Camporesi, R. Castello, M. Cepeda, G. Cerminara, M. D'Alfonso, D. d'Enterria, A. Dabrowski, V. Daponte, A. David, M. De Gruttola, A. De Roeck, E. Di Marco[44], M. Dobson, B. Dorney, T. du Pree, D. Duggan, M. Dünser, N. Dupont, A. Elliott-Peisert, S. Fartoukh, G. Franzoni, J. Fulcher, W. Funk, D. Gigi, K. Gill, M. Girone, F. Glege, D. Gulhan, S. Gundacker, M. Guthoff, J. Hammer, P. Harris, J. Hegeman, V. Innocente, P. Janot, J. Kieseler, H. Kirschenmann, V. Knünz, A. Kornmayer[15], M. J. Kortelainen, K. Kousouris, M. Krammer[1], C. Lange, P. Lecoq, C. Lourenço, M. T. Lucchini, L. Malgeri, M. Mannelli, A. Martelli, F. Meijers, J. A. Merlin, S. Mersi, E. Meschi, P. Milenovic[45], F. Moortgat, S. Morovic, M. Mulders, H. Neugebauer, S. Orfanelli, L. Orsini, L. Pape, E. Perez, M. Peruzzi, A. Petrilli, G. Petrucciani, A. Pfeiffer, M. Pierini, A. Racz, T. Reis, G. Rolandi[46], M. Rovere, M. Ruan, H. Sakulin, J. B. Sauvan, C. Schäfer, C. Schwick, M. Seidel, A. Sharma, P. Silva, P. Sphicas[47], J. Steggemann, M. Stoye, Y. Takahashi, M. Tosi, D. Treille, A. Triossi, A. Tsirou, V. Veckalns[48], G. I. Veres[20], M. Verweij, N. Wardle, H. K. Wöhri, A. Zagozdzinska[35], W. D. Zeuner

Paul Scherrer Institut, Villigen, Switzerland

W. Bertl, K. Deiters, W. Erdmann, R. Horisberger, Q. Ingram, H. C. Kaestli, D. Kotlinski, U. Langenegger, T. Rohe

Institute for Particle Physics, ETH Zurich, Zurich, Switzerland

F. Bachmair, L. Bäni, L. Bianchini, B. Casal, G. Dissertori, M. Dittmar, M. Donegà, C. Grab, C. Heidegger, D. Hits, J. Hoss, G. Kasieczka, P. Lecomte[†], W. Lustermann, B. Mangano, M. Marionneau, P. Martinez Ruiz del Arbol, M. Masciovecchio, M. T. Meinhard, D. Meister, F. Micheli, P. Musella, F. Nessi-Tedaldi, F. Pandolfi, J. Pata, F. Pauss, G. Perrin, L. Perrozzi, M. Quittnat, M. Rossini, M. Schönenberger, A. Starodumov[49], V. R. Tavolaro, K. Theofilatos, R. Wallny

Universität Zürich, Zurich, Switzerland

T. K. Aarrestad, C. Amsler[50], L. Caminada, M. F. Canelli, A. De Cosa, C. Galloni, A. Hinzmann, T. Hreus, B. Kilminster, J. Ngadiuba, D. Pinna, G. Rauco, P. Robmann, D. Salerno, Y. Yang, A. Zucchetta

National Central University, Chung-Li, Taiwan

V. Candelise, T. H. Doan, Sh. Jain, R. Khurana, M. Konyushikhin, C. M. Kuo, W. Lin, Y. J. Lu, A. Pozdnyakov, S. S. Yu

National Taiwan University (NTU), Taipei, Taiwan

Arun Kumar, P. Chang, Y. H. Chang, Y. W. Chang, Y. Chao, K. F. Chen, P. H. Chen, C. Dietz, F. Fiori, W.-S. Hou, Y. Hsiung, Y. F. Liu, R.-S. Lu, M. Miñano Moya, E. Paganis, A. Psallidas, J. F. Tsai, Y. M. Tzeng

Department of Physics, Faculty of Science, Chulalongkorn University, Bangkok, Thailand

B. Asavapibhop, G. Singh, N. Srimanobhas, N. Suwonjandee

Cukurova University, Adana, Turkey

A. Adiguzel, S. Cerci[51], S. Damarseckin, Z. S. Demiroglu, C. Dozen, I. Dumanoglu, S. Girgis, G. Gokbulut, Y. Guler, I. Hos, E. E. Kangal[52], O. Kara, A. Kayis Topaksu, U. Kiminsu, M. Oglakci, G. Onengut[53], K. Ozdemir[54], D. Sunar Cerci[51], H. Topakli[55], S. Turkcapar, I. S. Zorbakir, C. Zorbilmez

Physics Department, Middle East Technical University, Ankara, Turkey

B. Bilin, S. Bilmis, B. Isildak[56], G. Karapinar[57], M. Yalvac, M. Zeyrek

Bogazici University, Istanbul, Turkey

E. Gülmez, M. Kaya[58], O. Kaya[59], E. A. Yetkin[60], T. Yetkin[61]

Istanbul Technical University, Istanbul, Turkey

A. Cakir, K. Cankocak, S. Sen[62]

Institute for Scintillation Materials of National Academy of Science of Ukraine, Kharkov, Ukraine

B. Grynyov

National Scientific Center, Kharkov Institute of Physics and Technology, Kharkov, Ukraine

L. Levchuk, P. Sorokin

University of Bristol, Bristol, UK

R. Aggleton, F. Ball, L. Beck, J. J. Brooke, D. Burns, E. Clement, D. Cussans, H. Flacher, J. Goldstein, M. Grimes, G. P. Heath, H. F. Heath, J. Jacob, L. Kreczko, C. Lucas, D. M. Newbold[63], S. Paramesvaran, A. Poll, T. Sakuma, S. Seif El Nasr-storey, D. Smith, V. J. Smith

Rutherford Appleton Laboratory, Didcot, UK

K. W. Bell, A. Belyaev[64], C. Brew, R. M. Brown, L. Calligaris, D. Cieri, D. J. A. Cockerill, J. A. Coughlan, K. Harder, S. Harper, E. Olaiya, D. Petyt, C. H. Shepherd-Themistocleous, A. Thea, I. R. Tomalin, T. Williams

Imperial College, London, UK

M. Baber, R. Bainbridge, O. Buchmuller, A. Bundock, D. Burton, S. Casasso, M. Citron, D. Colling, L. Corpe, P. Dauncey, G. Davies, A. De Wit, M. Della Negra, R. Di Maria, P. Dunne, A. Elwood, D. Futyan, Y. Haddad, G. Hall, G. Iles, T. James, R. Lane, C. Laner, R. Lucas[63], L. Lyons, A.-M. Magnan, S. Malik, L. Mastrolorenzo, J. Nash, A. Nikitenko[49], J. Pela, B. Penning, M. Pesaresi, D. M. Raymond, A. Richards, A. Rose, C. Seez, S. Summers, A. Tapper, K. Uchida, M. Vazquez Acosta[65], T. Virdee[15], J. Wright, S. C. Zenz

Brunel University, Uxbridge, UK

J. E. Cole, P. R. Hobson, A. Khan, P. Kyberd, D. Leslie, I. D. Reid, P. Symonds, L. Teodorescu, M. Turner

Baylor University, Waco, USA

A. Borzou, K. Call, J. Dittmann, K. Hatakeyama, H. Liu, N. Pastika

The University of Alabama, Tuscaloosa, USA

O. Charaf, S. I. Cooper, C. Henderson, P. Rumerio, C. West

Boston University, Boston, USA

D. Arcaro, A. Avetisyan, T. Bose, D. Gastler, D. Rankin, C. Richardson, J. Rohlf, L. Sulak, D. Zou

Brown University, Providence, USA

G. Benelli, E. Berry, D. Cutts, A. Garabedian, J. Hakala, U. Heintz, J. M. Hogan, O. Jesus, K. H. M. Kwok, E. Laird, G. Landsberg, Z. Mao, M. Narain, S. Piperov, S. Sagir, E. Spencer, R. Syarif

University of California, Davis, Davis, USA

R. Breedon, G. Breto, D. Burns, M. Calderon De La Barca Sanchez, S. Chauhan, M. Chertok, J. Conway, R. Conway, P. T. Cox, R. Erbacher, C. Flores, G. Funk, M. Gardner, W. Ko, R. Lander, C. Mclean, M. Mulhearn, D. Pellett, J. Pilot, S. Shalhout, J. Smith, M. Squires, D. Stolp, M. Tripathi, S. Wilbur, R. Yohay

University of California, Los Angeles, USA

C. Bravo, R. Cousins, A. Dasgupta, P. Everaerts, A. Florent, J. Hauser, M. Ignatenko, N. Mccoll, D. Saltzberg, C. Schnaible, E. Takasugi, V. Valuev, M. Weber

University of California, Riverside, Riverside, USA
K. Burt, R. Clare, J. Ellison, J. W. Gary, S. M. A. Ghiasi Shirazi, G. Hanson, J. Heilman, P. Jandir, E. Kennedy, F. Lacroix, O. R. Long, M. Olmedo Negrete, M. I. Paneva, A. Shrinivas, W. Si, H. Wei, S. Wimpenny, B. R. Yates

University of California, San Diego, La Jolla, USA
J. G. Branson, G. B. Cerati, S. Cittolin, M. Derdzinski, R. Gerosa, A. Holzner, D. Klein, V. Krutelyov, J. Letts, I. Macneill, D. Olivito, S. Padhi, M. Pieri, M. Sani, V. Sharma, S. Simon, M. Tadel, A. Vartak, S. Wasserbaech[66], C. Welke, J. Wood, F. Würthwein, A. Yagil, G. Zevi Della Porta

Department of Physics, University of California, Santa Barbara, Santa Barbara, USA
N. Amin, R. Bhandari, J. Bradmiller-Feld, C. Campagnari, A. Dishaw, V. Dutta, K. Flowers, M. Franco Sevilla, P. Geffert, C. George, F. Golf, L. Gouskos, J. Gran, R. Heller, J. Incandela, S. D. Mullin, A. Ovcharova, H. Qu, J. Richman, D. Stuart, I. Suarez, J. Yoo

California Institute of Technology, Pasadena, USA
D. Anderson, A. Apresyan, J. Benda vid, A. Bornheim, J. Bunn, Y. Chen, J. Duarte, J. M. Lawhorn, A. Mott, H. B. Newman, C. Pena, M. Spiropulu, J. R. Vlimant, S. Xie, R. Y. Zhu

Carnegie Mellon University, Pittsburgh, USA
M. B. Andrews, V. Azzolini, T. Ferguson, M. Paulini, J. Russ, M. Sun, H. Vogel, I. Vorobiev, M. Weinberg

University of Colorado Boulder, Boulder, USA
J. P. Cumalat, W. T. Ford, F. Jensen, A. Johnson, M. Krohn, T. Mulholland, K. Stenson, S. R. Wagner

Cornell University, Ithaca, USA
J. Alexander, J. Chaves, J. Chu, S. Dittmer, K. Mcdermott, N. Mirman, G. Nicolas Kaufman, J. R. Patterson, A. Rinkevicius, A. Ryd, L. Skinnari, L. Soffi, S. M. Tan, Z. Tao, J. Thom, J. Tucker, P. Wittich, M. Zientek

Fairfield University, Fairfield, USA
D. Winn

Fermi National Accelerator Laboratory, Batavia, USA
S. Abdullin, M. Albrow, G. Apollinari, S. Banerjee, L. A. T. Bauerdick, A. Beretvas, J. Berryhill, P. C. Bhat, G. Bolla, K. Burkett, J. N. Butler, H. W. K. Cheung, F. Chlebana, S. Cihangir†, M. Cremonesi, V. D. Elvira, I. Fisk, J. Freeman, E. Gottschalk, L. Gray, D. Green, S. Grünendahl, O. Gutsche, D. Hare, R. M. Harris, S. Hasegawa, J. Hirschauer, Z. Hu, B. Jayatilaka, S. Jindariani, M. Johnson, U. Joshi, B. Klima, B. Kreis, S. Lammel, J. Linacre, D. Lincoln, R. Lipton, M. Liu, T. Liu, R. Lopes De Sá, J. Lykken, K. Maeshima, N. Magini, J. M. Marraffino, S. Maruyama, D. Mason, P. McBride, P. Merkel, S. Mrenna, S. Nahn, C. Newman-Holmes†, V. O'Dell, K. Pedro, O. Prokofyev, G. Rakness, L. Ristori, E. Sexton-Kennedy, A. Soha, W. J. Spalding, L. Spiegel, S. Stoynev, J. Strait, N. Strobbe, L. Taylor, S. Tkaczyk, N. V. Tran, L. Uplegger, E. W. Vaandering, C. Vernieri, M. Verzocchi, R. Vidal, M. Wang, H. A. Weber, A. Whitbeck, Y. Wu

University of Florida, Gainesville, USA
D. Acosta, P. Avery, P. Bortignon, D. Bourilkov, A. Brinkerhoff, A. Carnes, M. Carver, D. Curry, S. Das, R. D. Field, I. K. Furic, J. Konigsberg, A. Korytov, J. F. Low, P. Ma, K. Matchev, H. Mei, G. Mitselmakher, D. Rank, L. Shchutska, D. Sperka, L. Thomas, J. Wang, S. Wang, J. Yelton

Florida International University, Miami, USA
S. Linn, P. Markowitz, G. Martinez, J. L. Rodriguez

Florida State University, Tallahassee, USA
A. Ackert, J. R. Adams, T. Adams, A. Askew, S. Bein, B. Diamond, S. Hagopian, V. Hagopian, K. F. Johnson, A. Khatiwada, H. Prosper, A. Santra

Florida Institute of Technology, Melbourne, USA
M. M. Baarmand, V. Bhopatkar, S. Colafranceschi, M. Hohlmann, D. Noonan, T. Roy, F. Yumiceva

University of Illinois at Chicago (UIC), Chicago, USA

M. R. Adams, L. Apanasevich, D. Berry, R. R. Betts, I. Bucinskaite, R. Cavanaugh, O. Evdokimov, L. Gauthier, C. E. Gerber, D. J. Hofman, K. Jung, P. Kurt, C. O'Brien, I. D. Sandoval Gonzalez, P. Turner, N. Varelas, H. Wang, Z. Wu, M. Zakaria, J. Zhang

The University of Iowa, Iowa City, USA

B. Bilki[67], W. Clarida, K. Dilsiz, S. Durgut, R. P. Gandrajula, M. Haytmyradov, V. Khristenko, J.-P. Merlo, H. Mermerkaya[68], A. Mestvirishvili, A. Moeller, J. Nachtman, H. Ogul, Y. Onel, F. Ozok[69], A. Penzo, C. Snyder, E. Tiras, J. Wetzel, K. Yi

Johns Hopkins University, Baltimore, USA

I. Anderson, B. Blumenfeld, A. Cocoros, N. Eminizer, D. Fehling, L. Feng, A. V. Gritsan, P. Maksimovic, C. Martin, M. Osherson, J. Roskes, U. Sarica, M. Swartz, M. Xiao, Y. Xin, C. You

The University of Kansas, Lawrence, USA

A. Al-bataineh, P. Baringer, A. Bean, S. Boren, J. Bowen, C. Bruner, J. Castle, L. Forthomme, R. P. Kenny III, S. Khalil, A. Kropivnitskaya, D. Majumder, W. Mcbrayer, M. Murray, S. Sanders, R. Stringer, J. D. Tapia Takaki, Q. Wang

Kansas State University, Manhattan, USA

A. Ivanov, K. Kaadze, Y. Maravin, A. Mohammadi, L. K. Saini, N. Skhirtladze, S. Toda

Lawrence Livermore National Laboratory, Livermore, USA

F. Rebassoo, D. Wright

University of Maryland, College Park, USA

C. Anelli, A. Baden, O. Baron, A. Belloni, B. Calvert, S. C. Eno, C. Ferraioli, J. A. Gomez, N. J. Hadley, S. Jabeen, R. G. Kellogg, T. Kolberg, J. Kunkle, Y. Lu, A. C. Mignerey, F. Ricci-Tam, Y. H. Shin, A. Skuja, M. B. Tonjes, S. C. Tonwar

Massachusetts Institute of Technology, Cambridge, USA

D. Abercrombie, B. Allen, A. Apyan, R. Barbieri, A. Baty, R. Bi, K. Bierwagen, S. Brandt, W. Busza, I. A. Cali, Z. Demiragli, L. Di Matteo, G. Gomez Ceballos, M. Goncharov, D. Hsu, Y. Iiyama, G. M. Innocenti, M. Klute, D. Kovalskyi, K. Krajczar, Y. S. Lai, Y.-J. Lee, A. Levin, P. D. Luckey, B. Maier, A. C. Marini, C. Mcginn, C. Mironov, S. Narayanan, X. Niu, C. Paus, C. Roland, G. Roland, J. Salfeld-Nebgen, G. S. F. Stephans, K. Sumorok, K. Tatar, M. Varma, D. Velicanu, J. Veverka, J. Wang, T. W. Wang, B. Wyslouch, M. Yang, V. Zhukova

University of Minnesota, Minneapolis, USA

A. C. Benvenuti, R. M. Chatterjee, A. Evans, A. Finkel, A. Gude, P. Hansen, S. Kalafut, S. C. Kao, Y. Kubota, Z. Lesko, J. Mans, S. Nourbakhsh, N. Ruckstuhl, R. Rusack, N. Tambe, J. Turkewitz

University of Mississippi, Oxford, USA

J. G. Acosta, S. Oliveros

University of Nebraska-Lincoln, Lincoln, USA

E. Avdeeva, R. Bartek[70], K. Bloom, D. R. Claes, A. Dominguez[70], C. Fangmeier, R. Gonzalez Suarez, R. Kamalieddin, I. Kravchenko, A. Malta Rodrigues, F. Meier, J. Monroy, J. E. Siado, G. R. Snow, B. Stieger

State University of New York at Buffalo, Buffalo, USA

M. Alyari, J. Dolen, J. George, A. Godshalk, C. Harrington, I. Iashvili, J. Kaisen, A. Kharchilava, A. Kumar, A. Parker, S. Rappoccio, B. Roozbahani

Northeastern University, Boston, USA

G. Alverson, E. Barberis, A. Hortiangtham, A. Massironi, D. M. Morse, D. Nash, T. Orimoto, R. Teixeira De Lima, D. Trocino, R.-J. Wang, D. Wood

Northwestern University, Evanston, USA

S. Bhattacharya, K. A. Hahn, A. Kubik, A. Kumar, N. Mucia, N. Odell, B. Pollack, M. H. Schmitt, K. Sung, M. Trovato, M. Velasco

University of Notre Dame, Notre Dame, USA

N. Dev, M. Hildreth, K. Hurtado Anampa, C. Jessop, D. J. Karmgard, N. Kellams, K. Lannon, N. Marinelli, F. Meng, C. Mueller, Y. Musienko[36], M. Planer, A. Reinsvold, R. Ruchti, G. Smith, S. Taroni, M. Wayne, M. Wolf, A. Woodard

The Ohio State University, Columbus, USA

J. Alimena, L. Antonelli, J. Brinson, B. Bylsma, L. S. Durkin, S. Flowers, B. Francis, A. Hart, C. Hill, R. Hughes, W. Ji, B. Liu, W. Luo, D. Puigh, B. L. Winer, H. W. Wulsin

Princeton University, Princeton, USA

S. Cooperstein, O. Driga, P. Elmer, J. Hardenbrook, P. Hebda, D. Lange, J. Luo, D. Marlow, J. Mc Donald, T. Medvedeva, K. Mei, M. Mooney, J. Olsen, C. Palmer, P. Piroué, D. Stickland, A. Svyatkovskiy, C. Tully, A. Zuranski

University of Puerto Rico, Mayaguez, USA

S. Malik

Purdue University, West Lafayette, USA

A. Barker, V. E. Barnes, S. Folgueras, L. Gutay, M. K. Jha, M. Jones, A. W. Jung, D. H. Miller, N. Neumeister, J. F. Schulte, X. Shi, J. Sun, F. Wang, W. Xie, L. Xu

Purdue University Calumet, Hammond, USA

N. Parashar, J. Stupak

Rice University, Houston, USA

A. Adair, B. Akgun, Z. Chen, K. M. Ecklund, F. J. M. Geurts, M. Guilbaud, W. Li, B. Michlin, M. Northup, B. P. Padley, R. Redjimi, J. Roberts, J. Rorie, Z. Tu, J. Zabel

University of Rochester, Rochester, USA

B. Betchart, A. Bodek, P. de Barbaro, R. Demina, Y. T. Duh, T. Ferbel, M. Galanti, A. Garcia-Bellido, J. Han, O. Hindrichs, A. Khukhunaishvili, K. H. Lo, P. Tan, M. Verzetti

Rutgers, The State University of New Jersey, Piscataway, USA

A. Agapitos, J. P. Chou, E. Contreras-Campana, Y. Gershtein, T. A. Gómez Espinosa, E. Halkiadakis, M. Heindl, D. Hidas, E. Hughes, S. Kaplan, R. Kunnawalkam Elayavalli, S. Kyriacou, A. Lath, K. Nash, H. Saka, S. Salur, S. Schnetzer, D. Sheffield, S. Somalwar, R. Stone, S. Thomas, P. Thomassen, M. Walker

University of Tennessee, Knoxville, USA

A. G. Delannoy, M. Foerster, J. Heideman, G. Riley, K. Rose, S. Spanier, K. Thapa

Texas A&M University, College Station, USA

O. Bouhali[71], A. Celik, M. Dalchenko, M. De Mattia, A. Delgado, S. Dildick, R. Eusebi, J. Gilmore, T. Huang, E. Juska, T. Kamon[72], R. Mueller, Y. Pakhotin, R. Patel, A. Perloff, L. Perniè, D. Rathjens, A. Rose, A. Safonov, A. Tatarinov, K. A. Ulmer

Texas Tech University, Lubbock, USA

N. Akchurin, C. Cowden, J. Damgov, F. De Guio, C. Dragoiu, P. R. Dudero, J. Faulkner, E. Gurpinar, S. Kunori, K. Lamichhane, S. W. Lee, T. Libeiro, T. Peltola, S. Undleeb, I. Volobouev, Z. Wang

Vanderbilt University, Nashville, USA

S. Greene, A. Gurrola, R. Janjam, W. Johns, C. Maguire, A. Melo, H. Ni, P. Sheldon, S. Tuo, J. Velkovska, Q. Xu

University of Virginia, Charlottesville, USA

M. W. Arenton, P. Barria, B. Cox, J. Goodell, R. Hirosky, A. Ledovskoy, H. Li, C. Neu, T. Sinthuprasith, X. Sun, Y. Wang, E. Wolfe, F. Xia

Wayne State University, Detroit, USA

C. Clarke, R. Harr, P. E. Karchin, J. Sturdy

University of Wisconsin-Madison, Madison, WI, USA

D. A. Belknap, C. Caillol, S. Dasu, L. Dodd, S. Duric, B. Gomber, M. Grothe, M. Herndon, A. Hervé, P. Klabbers, A. Lanaro, A. Levine, K. Long, R. Loveless, I. Ojalvo, T. Perry, G. A. Pierro, G. Polese, T. Ruggles, A. Savin, N. Smith, W. H. Smith, D. Taylor, N. Woods

† **Deceased**

1: Also at Vienna University of Technology, Vienna, Austria
2: Also at State Key Laboratory of Nuclear Physics and Technology, Peking University, Beijing, China
3: Also at Institut Pluridisciplinaire Hubert Curien, Université de Strasbourg, Université de Haute Alsace Mulhouse, CNRS/IN2P3, Strasbourg, France
4: Also at Universidade Estadual de Campinas, Campinas, Brazil
5: Also at Universidade Federal de Pelotas, Pelotas, Brazil
6: Also at Université Libre de Bruxelles, Bruxelles, Belgium
7: Also at Deutsches Elektronen-Synchrotron, Hamburg, Germany
8: Also at Joint Institute for Nuclear Research, Dubna, Russia
9: Now at Ain Shams University, Cairo, Egypt
10: Now at British University in Egypt, Cairo, Egypt
11: Also at Zewail City of Science and Technology, Zewail, Egypt
12: Also at Université de Haute Alsace, Mulhouse, France
13: Also at Skobeltsyn Institute of Nuclear Physics, Lomonosov Moscow State University, Moscow, Russia
14: Also at Tbilisi State University, Tbilisi, Georgia
15: Also at CERN, European Organization for Nuclear Research, Geneva, Switzerland
16: Also at RWTH Aachen University, III. Physikalisches Institut A, Aachen, Germany
17: Also at University of Hamburg, Hamburg, Germany
18: Also at Brandenburg University of Technology, Cottbus, Germany
19: Also at Institute of Nuclear Research ATOMKI, Debrecen, Hungary
20: Also at MTA-ELTE Lendület CMS Particle and Nuclear Physics Group, Eötvös Loránd University, Budapest, Hungary
21: Also at University of Debrecen, Debrecen, Hungary
22: Also at Indian Institute of Science Education and Research, Bhopal, India
23: Also at Institute of Physics, Bhubaneswar, India
24: Also at University of Visva-Bharati, Santiniketan, India
25: Also at University of Ruhuna, Matara, Sri Lanka
26: Also at Isfahan University of Technology, Isfahan, Iran
27: Also at University of Tehran, Department of Engineering Science, Tehran, Iran
28: Also at Yazd University, Yazd, Iran
29: Also at Plasma Physics Research Center, Science and Research Branch, Islamic Azad University, Tehran, Iran
30: Also at Università degli Studi di Siena, Siena, Italy
31: Also at Purdue University, West Lafayette, USA
32: Also at International Islamic University of Malaysia, Kuala Lumpur, Malaysia
33: Also at Malaysian Nuclear Agency, MOSTI, Kajang, Malaysia
34: Also at Consejo Nacional de Ciencia y Tecnología, Mexico city, Mexico
35: Also at Warsaw University of Technology, Institute of Electronic Systems, Warsaw, Poland
36: Also at Institute for Nuclear Research, Moscow, Russia
37: Now at National Research Nuclear University 'Moscow Engineering Physics Institute' (MEPhI), Moscow, Russia
38: Also at St. Petersburg State Polytechnical University, St. Petersburg, Russia
39: Also at University of Florida, Gainesville, USA
40: Also at P.N. Lebedev Physical Institute, Moscow, Russia
41: Also at California Institute of Technology, Pasadena, USA
42: Also at Budker Institute of Nuclear Physics, Novosibirsk, Russia
43: Also at Faculty of Physics, University of Belgrade, Belgrade, Serbia
44: Also at INFN Sezione di Roma; Università di Roma, Rome, Italy
45: Also at University of Belgrade, Faculty of Physics and Vinca Institute of Nuclear Sciences, Belgrade, Serbia
46: Also at Scuola Normale e Sezione dell'INFN, Pisa, Italy

47: Also at National and Kapodistrian University of Athens, Athens, Greece
48: Also at Riga Technical University, Riga, Latvia
49: Also at Institute for Theoretical and Experimental Physics, Moscow, Russia
50: Also at Albert Einstein Center for Fundamental Physics, Bern, Switzerland
51: Also at Adiyaman University, Adiyaman, Turkey
52: Also at Mersin University, Mersin, Turkey
53: Also at Cag University, Mersin, Turkey
54: Also at Piri Reis University, Istanbul, Turkey
55: Also at Gaziosmanpasa University, Tokat, Turkey
56: Also at Ozyegin University, Istanbul, Turkey
57: Also at Izmir Institute of Technology, Izmir, Turkey
58: Also at Marmara University, Istanbul, Turkey
59: Also at Kafkas University, Kars, Turkey
60: Also at Istanbul Bilgi University, Istanbul, Turkey
61: Also at Yildiz Technical University, Istanbul, Turkey
62: Also at Hacettepe University, Ankara, Turkey
63: Also at Rutherford Appleton Laboratory, Didcot, UK
64: Also at School of Physics and Astronomy, University of Southampton, Southampton, UK
65: Also at Instituto de Astrofísica de Canarias, La Laguna, Spain
66: Also at Utah Valley University, Orem, USA
67: Also at Argonne National Laboratory, Argonne, USA
68: Also at Erzincan University, Erzincan, Turkey
69: Also at Mimar Sinan University, Istanbul, Istanbul, Turkey
70: Now at The Catholic University of America, Washington, USA
71: Also at Texas A&M University at Qatar, Doha, Qatar
72: Also at Kyungpook National University, Taegu, Korea